UNIVERSITÀ DEL PIEMONTE ORIENTALE

Dipartimento di scienze e innovazione tecnologica

(DISIT)

A safe by design approach for carbon nanomaterial biotechnological applications

PhD in "Chemistry and Biology"

Energy, environmental and food sciences

SDS: BIO/07

XXXIV cycle 2018/2022

Supervisor

Prof. Francesco Dondero

PhD Student

Candida Lorusso

PhD Program Coordinator

Prof. Gian Cesare Tron

Table of Contents

Chapter 1

Introduction

Nanotechnology

In the last twenty years, nanomaterials (NMs) have become a really interesting subject of research. There has been a rapid development of this new class of materials used for nanotechnology because they have a large number of applications that can be used in several fields such as construction, medicine and agriculture, biotechnology.
Nanotechnology mainly promotes innovation and development in many application areas, academic and commercial research and development.

The importance of nanotechnologies development in Europe has also been underlined by projects such as the EU Framework Program for Research and Innovation Horizon 2020 (2014-2020), which recognized nanotechnologies as key to technological growth. Moreover, the global market for nanotechnologies is expected to exceed $ 125 billion by 2024. In European research and innovation programs, nanotechnology is now a priority to achieve the objectives of global challenges and competitiveness of the European industry, such as the digitalization (Coileain, 2021).

Having defined the meaning of these new technologies, it is important to determine what they actually are. There is no single definition of nanotechnology, but the Irish Nanotechnology Commercialisation Framework (2010) defines it as "the purposeful engineering of matter at scales of less than 100 nanometers to achieve size-dependent properties and functions". The properties that materials develop thanks to their size are one of the most interesting features that have led to NMs being used in many applications. Their small size allows them to acquire some interesting physical and mechanical properties, such as electrical and thermal conductivity, hardness, tensile strength, chemical stability, transparency or wavelength-dependent responses to light. It is important to note that NMs are not just engineered materials. In fact, there are NMs that have been formed naturally, such as volcanic ash, or that have been formed by human activities, such as the combustion of fuels or the degradation of plastics. They can have different forms (sheets, wives or fibers), and these properties are very important to define their behavior. The enumerated properties of NMs make them very interesting in many application areas, starting with information and communication technologies. In the last decades, thanks to nanoelectronics, computers have been developed more and more towards nanoscale. Semiconductors in nano-dimensions made it possible to obtain more powerful machines in a smaller space and with lower power requirements. This was an essential component for digital innovation. Today, the challenges have not yet been overcome, because the semiconductor market represents a large part of the market, on a global scale we are talking about 440 billion euros. In Europe, it is currently still relatively small (10%), but is expected to grow to 20%

by 2030. The rise in this sector of the economy is driving investment in new materials and approaches such as NMs. For example, in order to have smaller and faster computer chip is important to improve flexible electronics thanks to materials such as graphene or carbon nanotubes. Another important application for these materials is manufacturing, especially in the context of the digitalization of industry, but also with their use in new production technologies. An important impetus came from NMs, for example, in 3D printer technology. Indeed, their use improves quality and expands the variety of materials that can be used in this new technology. Electrically conductive NMs could be used to print cheap circuits, sensors or batteries. But not only that, they could also be used in nanomedicine by using cells as printing materials, as it is possible to combine them with magnetic nanoparticles, making it possible to replicate and simulate a tissue with the conditions in the body. Nanotechnology in medicine is a really large area of interest, encompassing a wide range of applications; so much so that in Europe the "European Technology Platform on Nanotechnology (ETPN)" has been established, an independent association of 125 members from 25 European member states, drawn from universities, industry, public institutions and representatives of the European Commission, who want to address the application of nanotechnology in medicine. NMs and nanoparticles (NPs) in this particular application area have the important property of being smaller than human cells, of being able to get close to viruses or biological molecules, which allows them to circulate in the body and penetrate most cells when they are smaller than 50 nm, and to move in and out of blood vessels when they are smaller than 20 nm; this

property allows a long list of applications. Especially in diagnostics, NMs are used in rapid and sensitive medical tests and diagnostic tools; they allow automation, faster turnaround, and low cost. Some interesting examples include early screening of Alzheimer's disease with a simple blood test and the recent similar test to screen for the COVID -19 pandemic. In the latter test, COVID -19 antibodies link the surface of gold or magnetic NPs, producing a color change. The second application is nano-therapy. NPs can be used to target cells or tissues, which could make it possible to reduce the amount of drug or duration of treatment or avoid damage to cells that are not the target. The use of nanotechnology has been a major innovation for diabetes therapy, making it possible to replace injections with oral medications. Research aims to develop a new approach with real-time monitoring of insulin levels to release drugs into the body at any time thanks to nanotechnology. Another important therapeutic area is cancer therapy. Pancreatic cancer, for example, is very aggressive and the survival rate of patients is very low, but thanks to treatment with iron NP, which is selectively taken up by cancer cells, the drugs are more efficient. A third application is imaging. Thanks to their ability to penetrate into the cells, NPs allow to improve the images produced by different techniques such as ultrasound, magnetic resonance imaging and position emission tomography (PET). They provide greater sensitivity and, for example, reduce the amount of radioactive material required for PET. Basic NPs are used in the new generation of vaccines; in fact, they are a safe way to stabilize mRNA vaccines; an example is the Moderna and Pfizer COVID -19 mRNA vaccine, in which lipid NPs are used for stabilization. To conclude the summary on medical uses,

it is important to talk about regenerative medicine. As stated earlier, it is possible to recreate tissues using the technique. They can be used not only for research, but also for repairing injuries and damaged organs. An example of this application is the treatment of osteoarthritis; thanks to 3D printing, a biological implant is produced using graphene to facilitate the repair of nerve injuries (Coileain, 2021). Another important application area for nanotechnology is the agri-food industry. Since the world population is expected to grow to over 9 billion people by 2050, it is very important to develop technologies capable of meeting the large food demand, but in the most sustainable way possible (Sharma, et al., 2021). Nanotechnology and NMs fit into this view of things. Nanotechnology could be useful in agriculture and food processing, and indeed this area of interest is growing very rapidly. Nanotechnology is used in many areas of production. First in food production where it is used for the production of pesticides and herbicides or fertilizers, for sensors in agrochemistry, but also for animal diagnostics, plant genetic engineering or animal nutrition. In food processing it is used for cleaning equipment, encapsulating flavors, for antimicrobial packaging; with sensors for food contamination. And finally, to increase the nutritional value of food (Coileain, 2021; He et al., 2019; Kim et al., 2018; Kwak et al., 2017; Handford et al., 2014). Some interesting arguments could be the nano-pesticides, which have many advantages compared to the classical pesticides; they improve efficiency and reduce toxicity at the same dosage. There are two different forms of nano-pesticides: Nano-pesticides, which have a size of < 100 nm and have the function of pesticides themselves, or nano-pesticide formulations, in which the

NMs only have the function of carriers for the effective pesticides. NMs have unique properties, such as large surface area, tenable pore size with high loading capacity, many of them are biocompatible, low cost, and can release pesticides in a controlled manner. In addition, in many cases NMs reduce insecticide residues, make them more bioavailable, and improve their photostability and water solubility; it is also possible to regulate their release. An example is the use of graphene oxide spiked with copper selenide NPs so that it becomes hydrophobic and can easily combine with chlorpyrifos, making it possible to activate the pesticide only when it arrives in the intestines of domestic animals, where it is released thanks to alkaline conditions (Sharma, et al., 2021). A similar approach is used for fertilizers. The use of NMs allows nutrients to remain in the soil longer and be less easily washed out. These properties are very important because the use of fertilizers has a very low efficiency, so an excess of fertilizers leads to a distortion of the soil ecosystem due to leaching or immobilization of fertilizers in the soil. This damage to the soil ecosystem is a major problem because while the soil takes a million years to establish the proper balance, the damage occurs in 100 years of pollution (Sharma, et al., 2021). Increasing the nutrient content of food is a sector of great interest. It is possible to use NMs to add super nutrients, vitamins, or preservatives and colorants to foods; an example is milk, where milk proteins are used to combine NPs with vitamins or other dietary supplements. For animals and plants, an optimal use of nanotechnology is for sensors (Coileain, 2021; El-Salam and El-Shibiny, 2012). The various properties of NMs, such as optics, electricity, surface area, and

porosity, are useful for sensors. There are two types of sensors: electrochemical sensors and luminescence sensors.

So far, only positive characteristics of nanotechnology are listed, it is described as a great avant-garde in many fields of application; but the possible risks associated with it are not yet considered. The safety of NMs is a fundamental argument in the debate, so much so that scientists and regulators have been working for the last two decades to define a guide for toxicological assessments and analytical methods to determine their behaviour and describe a regulatory domain. In 2019, the annual Global Summit on Regulatory Science (GSRS) conference was held in Italy in exactly this direction. The focus of the meeting was on nanotechnology, in particular the benefits of regulations, medical devices or drugs, and the safety of NMs and emerging pollutants such as nanoplastics. A platform for global collaboration was created to share information and define a common line for regulation, thanks in part to the presence of 200 participants from more than 30 countries such as the United States, Canada, Argentina, Chile, China, Japan, Singapore, Korea, India, Australia, New Zealand, Egypt, and the European Union (Allan, et al., 2021).

In the use of nanomaterials in medicine, the definition of risk and potential toxicity for short- and long-term exposure becomes an important issue. Examples include carbon nanotubes that can damage DNA due to their shape and size, or some NMs that have been shown to be long-lived in the human body, such as gold nanoparticles, or even silver nanoparticles or plastic NPs that can pass through the placenta and enter the brain during pregnancy. Therefore, it is important to

control the use of some NMs in patients to prevent harmless concentrations from causing health problems. The situation is similar with NMs in food applications. Among the NMs used as additives to lighten and colour foods are titanium oxide and iron oxide; the former, long considered safe, has been found to accumulate in the human body, and it is not possible to rule out its toxicity / interference to genes; Therefore, today, any engineered NM-product must first undergo a risk assessment and be approved by the European Food Safety Authority (EFSA) before it can be marketed, and the presence of nanomaterials must be indicated in the list of ingredients (Coileain, 2021; Hardy et al., 2018).

However, nanotechnology is a young and expanding technology, so it may be difficult to regulate. Regarding European regulation, the European Chemicals Agency (ECHA) uses European chemicals legislation (REACH EC 190/2006) for safety regulations of chemicals in general and thus also for nanochemicals, with the introduction of some specific information on nanoproducts in 2018, although standardised test methods are not always available. Food legislation has been implemented by EFSA, as already indicated; they take care of biohazard control, animal health, contaminants, food additives, plant protection and health. They also conduct assessments to look at environmental risks and the impact on ecosystem biodiversity (Allan, et al., 2021).

Carbon nanotubes

One of the first materials to raise doubts about possible risks to human health from long-term exposure is carbon nanotubes (CNTs).

CNTs were discovered by Iijima (1991) and belong to the fullerene family. They consist of hexagonal layers composed of carbon atoms forming a cylindrical structure. They are divided into two types of CNTs: Single-Wallet (SWCNT), when they have only one sheet, or Multi-Wallet (MWCNT), when they have two or more sheets; the different orientation of each sheet about any tubular axis defines the helicity of the CNT. Over time, they have shown such interesting electrical and mechanical properties that they have had a great attraction to many industrial applications: automotive, electrical, electronics, sporting goods manufacturing, renewable energy, pharmaceuticals. It has been confirmed that the conductivity of CNTs is related to their diameter and helicity, both in theorerical andexperimental studies.

The synthesis of these materials starts with a small production in the laboratory and goes up to tonnes of MWNTs produced per year. Mass production of MWCNTs is underway thanks to the 94% chemical vapour synthesis technique, which makes it possible to obtain large quantities and high purity material. The production of SWCNTs is still expensive.

Therefore, today CNT synthesis achieves good results because it is inexpensive, can be produced on a large scale, and the materials obtained are high quality products. As mentioned above, the most commonly used synthesis method has been chemical vapour deposition

(CVD), although it is important to remember that there are two other production methods, but they are not as advantageous. The first is electrical arc discharge. In this method, two graphite rods are used as electrodes, under a voltage of 20 V and a current of less than 100 A, under a pressure of 500 Torr of helium or argon; the gas pressure determines the purity and the gain of the reaction. In the case of SWCNTs, graphite is perforated and covered with a mixture of metal catalyst and graphite powder (Ebbesen and Ajayan, 1992). The second method is laser ablation. In this method, pieces of graphite placed in a quartz tube in a temperature-controlled furnace are vaporized by laser irradiation in an inert atmosphere. In the case of SWCNTs, an additional amount of catalyst to the graphite is required (Guo et al., 1995). The last and most useful method is chemical vapor deposition. In this case, the reaction starts with a volatile precursor that produces solid and volatile products through a chemical reaction (Joseyacaman et al., 1993); compared to the first two methods, this one is cheaper, more controllable, the products are purer, and the reaction is more profitable. After obtaining CNTs from any of these three methods, it is sometimes necessary to purify the materials, using processes such as filtration, flocculation, chromatography, and centrifugation. For SWCNTs, density gradient ultracentrifugation is also used (Bandow et al., 1998; Duesberg et al., 1999; Ebbesen et al., 1994; Hiura et al., 1995; Bonard et al., 1997; Arnold et al., 2006); to understand what the purity level of CNTs is, scanning electron microscopy (SEM) and transmission electron microscopy (TEM) are used.

After describing CNT synthesis and purification, it is important to define the unique properties of CNTs, as these are critical to their

success. CNTs are flexible and elastic. These properties are linked to their size and purity; depending on chirality and diameter, they can be metallic or semiconducting. These specific properties, together with the typical high aspect ratio of NMs, make them very attractive for many applications, thanks also to the large number of companies synthesising them. CNTs are used in many different products: starting with electronic devices such as microscopes (atomic force microscope (AFM) and scanning tunnelling microscopy (STM)), in which they are used for the tips of scanning probe microscopes, the functionalized CNTs enable the imaging of polymeric and biological materials; in electron microscopy, they are used to make electron guns; they are used in flat panel displays, X-ray sources, or microwave amplifiers; they also perform well in individual field-effect transistors, photoluminescence, and electroluminescence. Another interesting application arises from the discovery that SWCNT films have conductivity equivalent to that of the established indium tin oxide (ITO), but are mechanically stronger, less expensive, and more abundant on Earth. All these properties make them a more environmentally friendly solution for many products such as touch screens, photovoltaics and display bus bars. Other applications include supercapacitors, Li batteries, solar cells, fuel cells and sensors. For Li batteries, a significant increase in performance of up to 10 times compared to the same weight of a classical lithium battery has been demonstrated, and the small size of CNTs makes it possible to produce smaller and more powerful batteries. CNTs also appear to be good storage for hydrogen. In view of its future use as environmentally friendly energy, this particular application is very important. Another

application of this material is biomedical products and techniques. They could be used to cross the plasma membrane and transport molecules or contrast agents. In addition, thanks to their electrical, thermal and optical properties, they could be used to achieve strong electromagnetic stimulation and thus sensitive detection in various imaginary techniques. The possibility of functionalizing CNTs also allows them to be used in tissue regeneration, for example for bone structures, vascular stents or neuron regeneration. In the latter case, the high electrical conductivity of CNTs enables the construction of an efficient network for signal transmission. Finally, the combination of CNTs and DNA confers some unique properties in terms of electrochemical activity, physical quality, biocompatibility and size, which allow the development of biosensors capable of continuously monitoring clinical analytes (e.g. glucose or antibodies) and used in clinical chemistry, food industry and environmental science (Donaldson, et al., 2012; Francis & Devasena, 2017).

As for the study of toxicity of CNTs, the main reason leading to an evaluation of their potential toxicity is their similarity to asbestos fibers. Due to the potential pathogenicity of fibers, a fibre pathogenicity paradigm (FPP) has been defined over the years, which evaluates pathological effects thanks to some typical characteristics; therefore, the FPP was used in the first approach to understand the potential toxicity of CNTs.

It is important to first define what type of disease is caused by asbestos fibers: Asbestosis is bilateral interstitial fibrosis with accumulation of fibrous tissue in the interstitial space of the lung, leading to problems

of gas diffusion and expansion and constriction of the lung; bronchial carcinoma is a malignant cancer arising from cells covering the bronchi; Mesothelioma is a tumour that originates from the mesothelium; pleural fibrosis is an accumulation of fibrous tissue in the pleura that leads to fluid accumulation in the pleural space; finally, pleural plaques are a formation of fibrous lesions (Fig.1). To better understand the development of mesothelioma, it is important to describe the anatomic area of interest. The pleura is a serous membrane that lines the lungs. It is divided into the visceral pleura, which covers the parenchyma of the lung, and the parietal pleura, which covers the thoracic cavity and has a monolayer of mesothelial cells; between these two parts is a pleural fluid, which is important to prevent contact and damage between the two parts. The pleural fluid is also connected to numerous lymphatic vessels thanks to the lymphatic stomata. (Donaldson, et al., 2013)

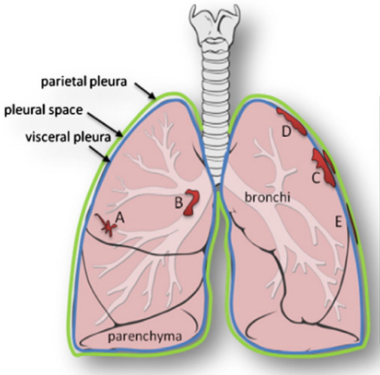

Label	Pathology	Site
A	Asbestosis	Parenchyma
B	Bronchogenic carcinoma (lung cancer)	Bronchi
C	Mesothelioma	Pleurae
D	Pleural fibrosis	Pleurae
E	Pleural plaque	Parietal pleura

Fig.1 Pathologies caused by fibers (Donaldson, et al., 2013).

For the first time, an association between asbestos exposure and progression of mesothelioma was confirmed in 1960 (Wagner, et al., 1960); since that article, numerous research efforts have been conducted to understand the mechanism of action of fibers and to define FPP. This paradigm begins with defining the central role of diameter in fibre pathogenicity. Fibres that are 1 μm or less in diameter are defined respirable, allowing them to be deposited over ciliated cells. The second important parameter is length. Fibers longer than 8 μm have been found to be associated with carcinogenesis. In vivo and vitro studies, exposure to long asbestos fibers has been shown to result in fibrosis, tumors, proinflammatory and genotoxic activity (Adamson, et al., 1991; Davis, et al., 1986; Donaldson, et al., 1992; Hill, et al., 1995; Donaldson & Golyasnya, 1995).

The toxicity of long fibers was explained by their longer residence time than short fibers. Because of their length, macrophages are unable to fully engulf them, resulting in frustrated phagocytosis that triggers an inflammatory process; in addition, long fibers inhibit macrophage locomotion (Poland et al, 2011; Schinwald et al., 2012). The last point of the paradigm is biopersistence. It consists in the ability not to be damaged or to change in the tissue. Biopersistence plays an important role in the excretion and then toxicity of the fibers. It has been observed that the intensity of the effect in the lung and pleura is directly related to the rate of dissolution of the fibers, i.e., the faster the dissolution, the less the accumulation and the less acute the effects (Mcconnell, et al., 1999). A description of FPP can be found in Fig. 2 (Donaldson, et al., 2013).

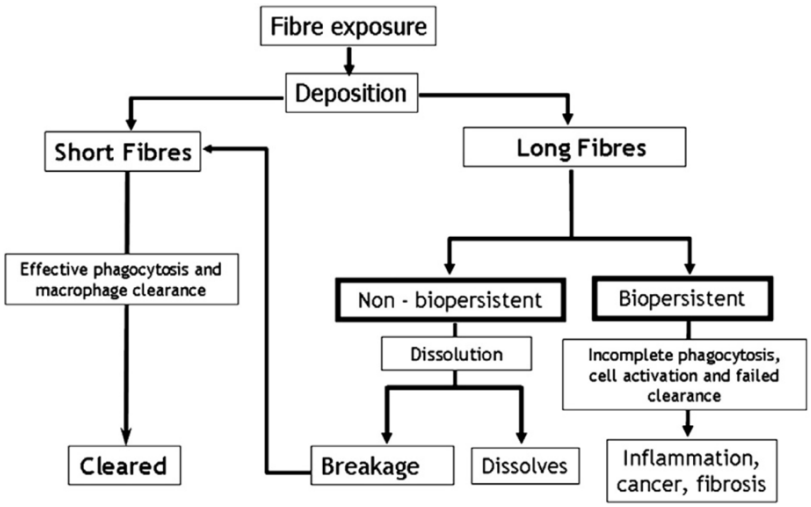

Fig.2 Schematization of FPP to obtain inflammation, cancer and fibrosis (Donaldson, et al., 2013)

After defining the features that cause pathogenetic states in fibers, it was important to understand whether this paradigm could also apply to nanofibers. This prompted the researchers to conduct experiments to study the behavior of different types of CNTs. Long and short CNTs, asbestos fibers, and carbon black NPs were directly injected intra-pleurally into mice. The results showed length-dependent pathogenicity, with long CNTs eliciting an inflammatory response and granuloma formation very similar to that of asbestos fibers (Murphy, et al., 2011). Another level of similarity between asbestos fibers and nanofibers that needs to be evaluated is the molecular mechanisms. Thanks to vitro models, it is possible to understand the molecular mechanisms that drive mesothelial cells to convert into tumorigenic cells. Exposure to asbestos fibers triggers signaling cascades involving mitogen-activated protein kinase (MAPK) and nuclear factor kappa B

(NF-kB) (Zanella, et al., 1996; Shukla, et al., 1999). In addition, as a result of binding of fibers to cellular receptors or generation of oxidative stress, numerous transcription factors (such as activator protein-1) are activated, triggering proliferation and pro-inflammatory responses. When exposed to CNTs, the molecular responses were found to be very similar, with activation of transcription factors associated with a pro-inflammatory response and activation of the MAPK pathway (Pacurari, et al., 2008). The same results were obtained in vivo studies showing that mesothelial cells in the presence of CNTs are exposed to constant stimulation by inflammatory factors that trigger activation of pro-oncogenic signaling pathways. In addition, exposure to MWCNTs in vivo models showed alterations in the proteins p53 and caspase-3, which are associated with apoptosis and MMP-2 and MMP-9. All of these proteins are part of the cancer response pathway of chronic inflammation (Park, et al., 201; Bremnes, et al., 2011).

All these studies suggest that nanofibers can pose an asbestos-like hazard if they are long enough and biopersistent. Thus, it can be said that fibers or nanofibers longer than 5-8 μm, less than 1 μm in diameter, and biopersistent can pose a risk of asbestos-like disease. (Donaldson, et al., 2013)

The profile of CNTs described by Donaldson, et al., (2013) is certainly exhaustive, so much so that they also analyzed the direct release of free radicals by both types of fibers. Indeed, it seems that asbestos fibers release reactive oxygen species directly or through an inflammatory process. It seems that the release of radicals in asbestos is related to the iron incorporated in its crystalline structure, just as the pro-

inflammatory reactions in CNTs could be due to contamination by metals.

However, it is important to keep in mind that NMs are unique materials. CNTs are heterogeneous in terms of structure, impurities, and physicochemical properties, so over time many researchers have studied the effects of different types of CNTs and under different conditions. Experimental tests have been performed in vivo, in vitro, on gene expression and genotoxicity; so it is important to define what kind of results are obtained.

In vivo tests can be cited Poland, et al. (2008), in which mice were exposed by intraperitoneal injection to four samples of MWCNTs selected to simulate the behavior of asbestos fibers; two of these CNTs are longer than 20 μm and the other two form tangled aggregates, using a positive control (long fiber amosite) and a negative control (carbon black, i.e. amorphous carbon). The results show that only long CNTs and amosite produce inflammation and granuloma. They also show images of frustrated phagocytosis with both amosite and long CNTs. Lam, et al. (2004) exposed mice to three different types of SWCNTs by intratracheal instillation, one rich in iron impurities, one purified with acid, and one 'CarboLex CNTs' containing nickel and yttrium impurities, carbon black, and quartz particles. After 7 days of exposure, mice exposed to CNTs developed epithelioid granulomas and interstitial inflammation in direct proportion to the exposure dose. CNTs were found to be more toxic than carbon black and quartz. Mice exposed to SWCNTs by aspiration from the pharynx experienced rapidly progressive fibrosis, acute inflammation, granulomas, and alveolar wall insufficiency, in addition to pathological lesions,

respiratory insufficiency, and a decrease in bacterial clearance (Shvedova, et al., 2005). Another study reported that rats exposed to MWCNTs or ground MWCNTs suspended in saline showed lung lesions with collagen-rich granulomas after two months. In addition, the rats showed immunosuppression after 14 days of exposure to high dose (Muller, et al., 2005). SWCNTs were tested in mice also in the presence of allergens (Inoue, et al., 2010) and reported an increase in T-helper cytokines and chemokines, moreover they have a supportive activity for the formation of allergen-specific IgG1 and IgE compared to animals exposed to allergens only. They also cause the increase of oxidative stress biomarkers in the presence of the allergen. In conclusion Francis, et al., (2015), it was shown how a single exposure to MWCNTs causes inflammation, epithelial cell damage and cell lysis in rats, which was confirmed by an increase in TNF-α, IL -4, LDH, blood cell count and activity of ALP (Francis & Devesena, 2017). In conclusion, many results of in vivo exposure seem to confirm reactions associated with oxidative stress, granulomas and the formation of pathological lesions.

As for the experimental tests in vitro on mesothelial cells, the results have shown that exposure to SWCNTs leads to a change in cell survival and a decrease in proliferation. Other studies indicated cytotoxicity in different mesothelial cells, from normal mesothelial cells to malignant mesothelioma cells and finally in large SV40 T antigen transformed mesothelial cells (Met5A). Even though in this last case a different degree of dispersion of CNTs produced a different degree of cytotoxicity, well dispersed material proved to be less toxic to cells than CNT agglomerates (Kaiser, et al., 2007; Tabet, et al., 2008; Wick,

et al., 2007). Another interesting aspect at the cellular level is the possibility that CNTs interact with the cell surface. Thanks to the interaction with the membrane receptors, the CNTs could be taken up into the cells, although this ability could vary when using different dispersion media for the CNTs modifying their surface. For example, in macrophages, the scavenger receptor MARCO appears to be involved in the interaction with MWCNTs (Thakur, et al., 2009; Hirano, et al., 2008; Jaurand, et al., 2009). Over time, many different cell types have been used to test the potential cytotoxicity of CNTs. Human pneumocytes A549 have been used to test NPs of titanium oxide and MWCNTs. Both NPs and CNTs showed the ability to penetrate into the cells, and the length and metallic impurity of the second type of impurities did not seem to affect their toxicity (Simon-Deckers, et al., 2008). Other studies confirmed the ability of CNTs to penetrate cells. They penetrate the cell membrane of rat macrophages (NR8383) and alter physiology and cellular functions. In addition, this study demonstrated an increase in ROS and a decrease in mitochondrial membrane potential in both macrophages and human A549 lung cells. In the same study, purified CNTs exhibited few or none of these effects, so it appears that the metal content may make the difference in cytotoxicity (Pulskamp, et al., 2007). Another point confirmed with testes on different cell lines was the variation in cytotoxicity depending on the degree of dispersion of the particles. Indeed, CNTs were found to be less toxic in dispersed form than in agglomerated form. In fact, a truly agglomerated form of CNTs (voluminous, rigid and solid) showed higher toxicity than asbestos fibers (Wick, et al., 2007). The ability of CNTs to cross the plasma

membrane has been demonstrated in several studies. Pantarotto, et al. (2003) observed in human fibroblast 3T6 and mouse 3T3 cells that CNTs can cross the plasma membrane and accumulate in the cytoplasm or enter the nucleus. Functionalized CNTs showed no toxicity at concentrations less than 10 μM. In keratinocytes (HaCaT), an increase in oxidative stress was observed, in the first case with a loss of cell viability caused by the activation of the transcription factor NF-kB, in the second case with a change in the ultrastructure and morphology of the cells, a loss of their integrity and apoptosis induced in some of them (Manna, et al., 2005). Modification of the CNT surface by functionalization could significantly improve the toxicity of CNTs. SWCNTs functionalized with streptavidin showed low cytotoxicity in HL60 cells, but cells functionalized with biotin-streptavidin stimulated death. In contrast, increased toxicity was observed with MWCNTs functionalized with carbonyl, carboxyl, and hydroxyl groups. Similarly, geometric conformation appears to play a role in toxicity. Comparison of SWCNTs with MWCNTs (10-20 nm diameter) and C60 fullerene revealed that SWCNTs exhibited higher toxicity than MWCNTs and C60 fullerene showed no toxicity (Shi Kam, et al., 2004; Fenoglio, et al., 2006; Jia, et al., 2005). To conclude this compilation, we can evaluate the results of tests that aimed to determine the effect at the molecular level. MWCNTs altered the expression of several proteins, caused GSH depletion, the formation of ROS with lipid peroxidation and protein release. In human skin fibroblasts, they activated genes involved in cellular transport, metabolism, cell cycle regulation, and stress responses. Their toxicity is associated with the activation of p38- ERK-MAPK (Monteiro-

Riviere & Inman, 2005; Yang, et al., 2008; Ding, et al., 2005; Francis & Devesena, 2017).

Finally, in vivo and in vitro tests suggest the possibility of genotoxicity after exposure to CNTs. Mutation of the oncogene K-Ras was observed in mice exposed to SWCNTs, while MWCNTs caused chromosomal aberrations (Shvedova, et al., 2008; Muller, et al., 2008). Genotoxicity was also observed by micronucleus testing, both in rat epithelial cells and in human epithelial cells exposed to MWCNTs, with chromosome breaks and chromosome loss also observed in the latter case (Muller, et al., 2008; Muller, et al., 2008).

Given all the information on CNTs, it seems crucial to accurately define and classify the toxicity of these materials, primarily because, as mentioned earlier, their physical properties place them among the fibrous materials, and finally because their use leads to severe human exposure in a variety of ways, from skin to ingestion to inhalation. Starting from the firm point that literature data have shown potential toxicity in a large number of experimental tests, given the viability of CNTs as a result of a large number of applications, it becomes relevant to use an approach that, starting from the concept of "safe by design", systematically evaluates the toxicity of a single material on a case-by-case basis, using an approach based on different levels.

Graphene

In recent years, another NMs has attracted great interest: graphene (G). This is a planar layer of carbon atoms that can be single-layered, bilayered, or multilayered. A single-layer graphene (SLG) consists of a two-dimensional hexagonal layer of carbon atoms (Fig. 3A). Two-layer and few-layer graphene (FLG) have the same basic organization but more layers of the same two-dimensional sheet. Graphene has a hybridized sp2 bond with three stronger and stiffer σ bonds in the plane and π orbitals perpendicular to the plane, which control the interaction between the different graphene layers (Fig. 3B).

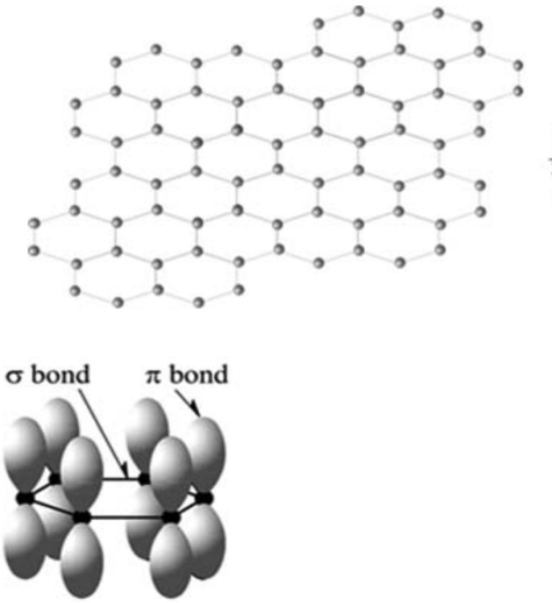

Fig.3 Graphene structure. (A)Two-dimensional hexagonal graphene sheet; (B)Schematic representation of graphene sheet in the plane. (Choi et al., 2010)

The best technique for observing and understanding G structure is transmission electron microscopy (TEM). However, this is a destructive technique in which samples are lost, so it is not always suitable. A good alternative for structural analysis could be Raman spectroscopy, which can provide information about graphene layers. Graphene has a number of interesting properties, some of which can be varied with the variation of the G structure. SLG has a unique electronic structure that gives it some unusual properties that make it suitable for electronic applications. But not only that, SLG is capable of adsorbing gas molecules that change the local carrier concentration, modifying the resistance. Thanks to this property, microscale gas sensors are created to detect adsorption and desorption of single molecules or gasses (CO, H_2O, NH_3, NO_2) (Shedin, et al., 2007). An interesting application of the gas adsorption capability of G, used in both SLG and bilayer graphene, is the adsorption of atomic hydrogen (H_2), resulting in a truly high transparency to light in the ultraviolet to infrared range, enabling its use in solar cell applications. In the case of FLG, the higher the layers, the stronger the metallic property. It has a very large surface area, roughly comparable to SLG, which allows it to adsorb gas. FLG can also be well functionalized, both covalently and non-covalently. However, functionalization by covalent modification seems to change the electronic structure of graphene. Therefore, to avoid this effect, a non-covalent modification is sometimes preferred to make G water-soluble. Another commonly used modification of G is decoration with metallic NPs. This type of modification makes it more useful for electronic, optical, and biotechnological applications. FLG was often decorated with Pt, Ag, or Au NPs in a one-step

chemical process. The chemical modification also resulted in a change in the magnetic properties of G. FLGs are also used in Li batteries as part of the electrode interconnect.

Graphene was discovered by Novoselov, et al., (2004), who was the first to demonstrate the reproducible synthesis of G by exfoliation. There are numerous methods to produce G. The first was exfoliation, Novoselov, et al., (2004) starting from a highly oriented pyrolytic graphite of 1mm, dry printing was performed in an oxygen plasma. This was applied to photoresist and beaked, from which a graphene sheet was peeled off. This sheet, dissolved in acetone and transferred to a Si substrate, proved to be SLG or FLG. Thanks to some later modifications, the method showed good quality suitable for industrial production. Stankovich, et al., (2005) realized the exfoliation in the liquid phase. They used the hydrophobicity of graphite to exfoliate it in aqueous solution using ultrasound and tried to reduce it in hydrazine hydrate at 100°C for 24 hours. The graphene obtained from this exfoliation was not completely reduced and some oxygen remained in the structure. The second method for synthesizing G is relatively new and is thermal chemical vapor deposition (CVD). In CVD, G is produced from camphor, which is first vaporized at 180 °C and then pyrolyzed at 700 to 850 °C, using argon as the carrier gas. It is cooled to room temperature and forms FLG plates on a Ni foil support (Somani et al., 2006). Recent results from these techniques have confirmed the production of good quality graphene on a centimeter-sized substrate, which can be transferred to many other substrates such as Si, glass, and polydimnethylsiloxane (PDMS). These improvements enable the use of G in photovoltaics and flexible electronics. Plasma-

enhanced chemical vapor deposition (PECVD) is another option for G synthesis. The first research group to talk about this technique was Obraztsov, et al., (2003). In their study they used Si chips, Ni, W, Mo and some other metal plates as substrate and a gas mixture of CH_4 and H_2 with gas pressure between 10 and 150 Torr. However, the first to describe the synthesis of SLG and FLG using this technique were (Wang, et al., 2004a) and (Wang, et al., 2004b). The simplicity of the described procedure interested the whole scientific community, so it was used in many laboratories. Over the years, some variations have been applied, up to microwave PECVD (Malesevic, et al., 2008). Another popular technique to produce graphene is thermal decomposition of SiC. When H_2 is nicked into the surface of 6H-SiC, which is heated to a temperature between 1250 and 1450 °C for a short time, graphene is formed. One of the latest techniques is 'unpacking CNTs', in which MWCNTs were used as the starting material. First, MWCNTs are opened longitudinally by intercalation of Li and ammonia, and then exfoliated in acid and coarse heating. In another approach, MWCNTs are opened by multistep chemical treatment, including exfoliation by H_2SO_4, $KMnO_4$, and H_2O_2 in concentrated form.

Defined mechanisms of G-synthesis become important to describe in what kind of product these nanomaterials could be found.

The capability of graphene-based sensors relies on the change in electrical conductivity of G due to its association with molecules on its surfaces. The change in conductivity of graphene is related to the change in charge carrier concentration caused by the molecules adsorbed on it, which can act as acceptor or donor. The great ability of

G like sensors was related to several points: first, it is a two-dimensional material, so the entire amount of carbon atoms on its surface is exposed, allowing it to connect molecules; second, it is highly conductive but has low Johnson noise (which is electrical noise due to thermal motion emanating from the charge carriers when the electrical conductor is in equilibrium and any voltage is applied), which means that a small change in the amount of charge carriers can cause a large change in electrical conductivity. With a single graphene dispositive, it is possible to analyze four different samples with low-resistance electrical contacts. Graphene has been shown to have good sensing properties for various types of molecules such as NO_2, NH_3, H_2O, and CO. Moreover, its sensing properties are fully recoverable after use, vacuum drying at 150 °C or short-term application of UV radiation (Schedin, et al., 2007). Another molecule that can be analyzed with graphene sensors is dinitrotoluene (DNT), a volatile compound of explosives. The detection of DNT was similar to that of NO2, with a similar mechanism. In addition to gas detection (Shan, et al., 2009), G demonstrated the ability to realize biosensors with glucose molecules. They realized an electrochemical biosensor composed of graphene protected with polyethylenimine and functionalized with glucose oxidase. G-biosensors also seem to be more suitable than CNTs for the detection of catecholamine neurotransmitters such as dopamine and serotonin. Li, et al., (2009) has developed a sensor based on Nafion graphene for the detection of cadmium by anodic stripping voltammetry.

Another possible application of G is in field effect transistors (FET), for this application it must be in the quasi-one-dimensional form with

narrow widths and atomically smooth edges. Thanks to its incredible thermal, chemical and mechanical stability, its high transparency and its atomic layer thickness, graphene is the best candidate for an alternative to ITO for transparent conducting electrode applications. ITO Graphene is indeed used for liquid crystal displays, apartment panel displays, touch panels and solar cells, but it is very expensive and limited, making graphene the perfect substitute. Graphene is perfect for photovoltaic applications due to its high mobility in hole transport, large surface area and insensitivity to oxygen and water. Graphene is also used to replace graphite as an anode in lithium-ion batteries due to its superior electrical conductivity, large surface area, and chemical tolerance (Choi, et al., 2010).

The applications in which G is used are not limited to the more well-known ones. In recent years, its use has been greatly expanded and touches a wide range of areas of interest. Srivastava, et al., (2014) realized an immobilization of the enzyme β-amylase on graphene sheets. This enzyme is essential for the production of maltose. Maltose is used in pharmaceutical dosage thanks to its good thermal stability, low viscosity and colorlessness. The enzyme β-amylase is highly specific to catalyze an efficient reaction, but it is not stable and difficult to recover and reuse; therefore, Srivastava, et al., (2014) decided to try to make it more stable using graphene. Thanks to the immobilization on functionalized graphene, the enzyme obtained more stability and showed better activity in the alkaline pH range compared to the soluble enzyme, a significant improvement in high temperature tolerance by maintaining an activity of 29% at 80 °C and finally an activity of 60%

after 120 days at +4 °C, while the soluble enzyme had only a residual activity of 20%.

Another interesting application for G is the decontamination of wastewater. G could be used to adsorb contaminants due to its delocalized π-electron system, which strongly interacts with contaminants; but also due to its high specific surface area, which creates a large number of sorption sites, good regeneration and reusability capacity (Wang, et al., 2013; Yuan, et al., 2013; Sun & Chang, 2008). There are many examples of its use for adsorption of pollutants. Al-Khateeb, et al., (2014) showed the removal of aspirin, acetaminophen and caffeine. The graphene oxide was used for the adsorption of tetracycline, naphthalene, 2-naphthol, 1-naphthylamine, tylosin, beta blockers, diclofenac and sulfamethoxazole (Gao, et al., 2012; Ji, et al., 2013; Ghadim, et al., 2013; Kyzas, et al., 2015; Nam, et al., 2015; Sophia, et al., 2016). In addition, the negative surface area of graphene oxide and reduced graphene oxide enables the removal of cations such as heavy metals, not to mention graphene-coated biochar is used to remove polyaromatic hydrocarbons and increases the basal ability of uncoated biochar by 20-fold (Zhang, et al., 2012). The adsorption capacity of grafene has also been tested for pesticides. It has been shown that between graphene oxide and graphene nanosheet, the second one has a higher ability to bind pesticides such as malathion, endosulfan, and chlorpyrifos. In the same way, Fe3O4/reduced graphene oxide showed the ability to remove five types of pesticides (ametryn, prometryn, simazine, simeton and atrazine (Maliyekkal, et al., 2013; Buruah, et al., 2017; Nupearachchi, et al., 2017).

So far, only graphene applications have been addressed, but the use of this material in such a large number of products, makes it possible to come into contact with the human body through various routes, such as inhalation, dermal adsorption, and ingestion (Oberdorster, et al., 2005; Stone, et al., 2017). Although the toxicity of graphene was studied later, a lot of research has been conducted in recent years, also thanks to the EU Graphene Flagship project (https://graphene-flagship.eu/). The toxicity of graphene has been studied in immune cells. Russier , et al., (2013) observed the effects of graphene oxide (GO) of different sizes on mouse primary macrophages and obtained a dose-dependent toxicity. GO of smaller size is internalized more efficiently than the largest, which has a significant effect on cell viability. Other authors found a different type of response, Ma, et al., (2015) observed a stronger adsorption of large GO to the membrane of macrophages compared to smaller ones and a strong activation of the NF-kB pathway. Different forms of GO were also analyzed, Li, et al., (2018) evaluated pristine, reduced GO (rGO), hydrogenated GO (hGO) on mouse lung macrophages and epithelial cells. THP-1 and BEAS-2B exposed to hGO exhibited lipid peroxidation and cell death. In addition, exposure to hGO elicited inflammatory responses in the lung more than others. Cheng, et al., (2012) tested GO in RAW264.7 and observed the formation of vacuoles for small GO but without cell death, with increasing concentration, the number of vacuoles increased and cytotoxicity increased significantly. The central role in the inflammatory responses was played by NF-kB. It is known that graphene is able to link biological molecules, so many studies have been conducted to understand how the coating could alter toxicity. It

seems that graphene coating with complement factor H reduces more then 90% of complement activation, i.e. inflammatory response, while coating with BSA reduces only by 40% (Belling, et al., 2016). Not all results agree, as some studies report a reduction in cytotoxicity in macrophages after GO coating with PEG, while other studies suggest that a strong cytokine response is stimulated (Matesanz, et al., 2013; Luo, et al., 2017).

Graphene was used in vivo tests exposing animals by inhalation to determine pulmonary toxicity. Exposure from 6 hours to 28 days showed no lung damage. The same type of study with larger graphene showed the same situation of absence of inflammatory response, but materials were also found in mediastinal nodules, indicating displacement of graphene. Using the same type of experimental approach, original graphene and functionalized graphene were tested. In this case, an inflammatory response with activation of neutrophils was observed, which was more pronounced with functionalized graphene (Shin, et al., 2015; Kim, et al., 2016; Lee, et al., 2017). Different forms of GO are also evaluated for pulmonary toxicology, GO, rGO, hGO, with the latter producing the highest amount of carbon radicals and ROS, while rGO produces the lowest. Exposure to hGO causes more lung damage (Li, et al, 2018). Thanks to its unique physicochemical properties such as high conductivity, transparency, and flexibility, graphene is also a good candidate for developing functional brain implants, neurotherapies, and reconstructing functional neuron and glial cell networks, so it is very important to study its toxicity in the central nervous system. An example in this

direction is the experiment conducted by Rauti, et al., (2016), in which flakes of GO of different sizes were tested on neuronal and glial cells. Large GO showed cytotoxicity in both cell types. However, while the large GO did not affect neuronal activity, the smaller ones specifically affected neuronal synapses without affecting cell viability. Interestingly, only the excitatory synapses were damaged, not the inhibitory ones.

Considering the information on graphene toxicity that can be found in the literature, it can be concluded that, as with all NMs, there is a wide range of variability in graphene that determines its toxicity. Since research on graphene toxicity started later than for other materials, it is particularly important to collect data in different study models, to promote the use of high-throughput screening (transcriptomics, proteomics, metabolomics), and to process these data in a safe-by-design manner, with a collaborative network, the use of QSAR models, and information sharing. In this way, it may be possible to create a toxicity assessment model for future forms (Fadeel, et al., 2018).

In Vitro models of NMs toxicity: the mesothelial cell model system

In determining a model for a toxicity study, one of the most important issues is determining the best in vitro model for the study. The case of NM is complex because of its variable form and properties due to different exposure parameters (functionalization, dispersion, medium,

etc.), so the toxicity of NM is generally evaluated by epidemiology, in vivo assays, and cell-based in vitro assays. In epidemiological studies, the conditions are generally complex, so it can be difficult to interpret the data. In addition, new NMs are constantly being introduced to the market, making it difficult to obtain sufficient data on materials that have just been developed. Animal models require more time for testing and are not suitable for high-throughput screening, not to mention ethical issues. Therefore, defining a good in vitro model becomes an important issue when evaluating a toxicity model (Cao, et al., 2020). In defining a good in vitro model, it is important that it can describe reality as accurately as possible. First, it is important to determine the correct cellular lineage for each toxicological test. For NMs tests, many different cell lines are used to determine toxicity. First, the different response of cancer cell lines and normal cell lines was evaluated. Cancer cell lines are commonly used for NMs toxicity testing for several reasons. First, they are easier to culture and more available than normal cells, and second, they are considered a good model for this type of study. However, the use of cancer cell lines does not always prove to be a good choice because they react differently than normal cells due to their different gene expression patterns and their different proliferation characteristics. An example of this is the evaluation of the toxicity of NPs with anticancer properties. One example is ZnO NPs used as anticancer agents. Several studies reported that ZnO NPs in different forms (NPs, quantum dots, flower-like nanostructures) decreased cellular viability and activated the apoptosis pathway, but only in cancer cells, not in normal cells (Moratin, et al., 2017; Paino, et al., 2016; Roshini, et al., 2017). Moreover, Michalkova, et al., (2020)

reported that anodic TiO2 nanotubes induce membrane degradation and apoptosis or necrosis, but in a more effective manner in cancer cells than in normal cells. Therefore, using cancer cell lines to test NMs may not be a good choice if these materials could have specific effects on them. In any case, when using normal cells for testing, other parameters must be considered to define the proper study model. First of all, some authors have shown that when comparing cancer and normal cells, the second cell sometimes shows more toxic effects after exposure to NMs, which might be related to a different uptake of the compounds by the cells. For example, A549 (human lung carcinoma cells) and 16HBE (immortalized human bronchial epithelial cells) exposed to SiO2 showed cytotoxicity only in 16HBE. This was explained by the fact that A549 expressed a high level of ABC transporters that export NPs from cells (Li, et al., 2019). Another point to be defined is the endpoint to be evaluated. Ursini, et al., (2014) has shown that when BEAS-2B cells (human immortalized bronchial cells) and A549 were exposed to TiO2- NP, the first cell showed a decrease in viability and more membrane damage than the second cell, but only A549 showed DNA damage and inflammatory responses. Therefore, when a cell line is selected to test NMs, it is important to evaluate the properties of the NMs and, if possible, use different cell types to compare the effect and understand the mechanisms of action of the material (Cao, et al., 2020). Several studies have shown that not only the choice of cell model can influence the outcome of NM exposure tests, but also other relevant parameters, such as the possible formation of a protein corona around the NM. Thanks to their high aspect ratio and the high energy on their surface, NMs could bind biological

molecules to themselves and thus completely change the effect of NMs. A soft and a hard corona can form around the NPs. The first one is not stable and the proteins have low affinity to the surface, the second one is more stable because it has a stronger connection due to the higher affinity of the proteins to the surface of the NPs (Winzen, et al., 2015; Liu, et al., 2020). This corona alters the interaction of NPs with cells. For example, Duan, et al., (2015) found that graphene oxide adsorbed with bovine serum albumin decreased its interaction with the cell membrane and thus its cytotoxicity. Miclaus, et al., (2016) exposed J774 mouse macrophages to PVP-coated silver NP and observed that Ag ions formed a protein corona due to the presence of bovine albumin in the cell culture medium, resulting in the formation of Ag2S crystals and a decrease in cytotoxicity and inflammatory responses. The formation of a corona does not always lead to a decrease in toxicity (Zhang, et al., 2019). In fact, MWCNTs with a corona of BSA or IgG were observed to increase their internalization and thus their inflammatory responses. Also, Long, et al., (2018) confirmed that the BSA corona in MWCNTs enhanced internalization and inflammatory responses, while decreasing cytotoxicity and oxidative stress compared to non-coated MWCNTs. The increased uptake of NPs after corona formation was explained by the fact that the change in CNT conformation triggers an endocytosis process via receptors, which in some cases increases toxicity (Barbalinardo, et al., 2018). The cell types selected for study are critical in determining whether the protein corona could increase or decrease toxicity (Cheng, et al., 2015). Indeed, corona has been shown to inhibit the internalization of Au NPs in phagocytic cells significantly more than in non-phagocytic cells.

Having established the importance of individualizing the cell type and precisely defining the microenvironment of the cells in order to understand how the NPs actually interact with the cell culture, it became important for some researchers to create as realistic a physiological environment as possible for the tests. For example, Fede , et al., (2015) studied the toxicity of Au NPs in HUVECs cells using a microfluidic device and compared flow conditions with static conditions. The result showed that the sedimentation of NPs decreased under flowing conditions and so did the cytotoxicity. Another example is the study by Chortarea, et al., (2017), in which human bronchial tissue from healthy and asthmatic patients was exposed to MWCNTs using the air-liquid interference cell exposure system. This showed that the tissue cells from the asthmatic patients exhibited more significant inflammatory and oxidative stress responses. However, this type of in vitro model is too tied to the presence of donors and therefore more difficult to implement, which is why the use of 3D models or organoid models is recommended in some cases. The 3D spheroid models have cells that secrete an extracellular matrix similar to the conditions in vivo. The cell organization alters the responses to NPs. Chia, et al., (2015) observed that genotoxicity and inflammatory responses to ZnO NPs were more evident in 2D cultures than in 3D cultures. It seems that more or less compact culture induces different responses. In an experiment by Sambale, et al., (2015), 3D spheroids from two different cell types (A549; NIH-3T3) exposed to ZnO NPs were compared to their 2D culture and it was observed that in the first case the spheroids were more sensitive than the 2D culture, while in the second case the toxicity effect was comparable between 3D and 2D culture. This effect

was related to the organization of the cells in the spheroids, which formed a loose aggregate in the first case and a compact aggregate in the second case. Organoids are formed from self-organizing stem cells and can mimic the architecture, functionality, and genetic signature of the original tissue in vivo. One example is the use of a 3D human brain organoid to test the exposure of MWCNTs that exposed different markers of the cortical layers. It was found that a high concentration of MWCNTs decreased the production of NO, which induced the production of ROS and altered the nNOS-Kruppel like factor pathway. The production of nNOS proteins was reduced in both the outer layer and inner layer of the organoid (Jiang, et al., 2020; Cao, et al., 2020).

Meanwhile, general reference was made to the approach used in the study of NMs.

In our case, the first model we faced concerns the study of CNTs. Most literature data on the effect of CNTs in the in vitro model concern lung epithelial cells. MWCNTs have been shown to cause a dose-dependent decrease in cell viability in epithelial cell models (Srivastava, et al., 2011). A549 and BEAS-2B epithelial cells exposed to SWCNTs showed cytotoxicity after 72 hours, and in lung epithelial cells, cell proliferation slowed after prolonged exposure (Herzog, et al., 2007). As just underlined, the degree of dispersion in the biological medium used for exposure is of great importance in defining the model of CNT studies. A relevant physiological dispersant is pulmonary surfactant (DPPC), which is used for dispersion of CNTs. SWCNTs dispersed in DPPC were used to expose BEAS-2B cells. Low concentrations stimulated their proliferation, while higher concentrations inhibited

proliferation; the same cells exposed to SWCNTs that were not dispersed in surfactant did not alter cell viability (Wang, et al., 2010). The use of surfactant, like sonication, allows CNTs to disperse, which increases their uptake and toxicity (Donaldson, et al., 2012). The situation is different when the dispersion medium is based on a culture medium, i.e., contains serum. The serum can improve the dispersion of CNTs, but it can also coat and alter them.

C6 glioma cells

Another area of interest in the behavior of NPs concerns the brain. The main reasons for this interest are two, the first related to the increasing use of NMs in medicine, in particular the discovery that NPs can be used as carriers of drugs for brain pathologies, the second related to the discovery that NPs can enter the human body in various ways and also accumulate in the brain. For example, the use of NMs has been introduced for glioblastoma therapy. Classical glioblastoma chemotherapy reached its limits because the drugs could not work well due to the blood-brain barrier (BBB) (Banks, 2016). The BBB is a physiological barrier to the central nervous system consisting of a continuous layer of endothelial cells connected to tight junctions supported by pericytes and astrocytes (Neuwel, et al., 2011). The BBB limits the passage of macromolecules, so for good drug delivery, the integrity of the tight junction could be temporarily destroyed or intracranial injection into the brain could be used, but these types of

methods can be difficult to control and could cause medical damage if used chronically, so NPs have begun to be used to deliver drugs across the BBB. Recently, many NPs have been used to improve drug therapy via the BBB, including natural polymers, such as protein-based polymers, which have attracted great interest due to their low-cost production and low toxicity (Wong, et al., 2012; Xie, et al., 2019; Saraiva, et al., 2016; Michael, et al., 2018;Fu, et al., 2019). Zhang, et al., (2021), for example, developed a curcumin-loaded zein NP (CUR -ZpD-G23) for therapy against glioblastoma cells. They observed that C6 glioma cells realized excellent uptake of CUR -ZpD-G23 and it invaded 3D tumor spheroids. Functionalized NPs exhibited dose-dependent cytotoxicity in C6 glioma cells and inhibited cell migration and colony formation. Moreover, they increased the production of ROS and induced apoptosis in C6 glioma cells. Another interesting example of using NMs as brain cancer therapy was reported by You, et al., (2019), who functionalized MWCNTs with a cell-penetrating peptide and a cancer target to obtain a good anti-cancer therapy. They achieved a good system that can overcome the BBB and improve selectivity for targeting the brain, and tested it in a HBMEC/C6 co-culture model. In addition, they showed that functionalized MWCNTs produced cytotoxicity in C6 glioma cells but little cytotoxicity in other cell types; they demonstrated that functionalized MWCNTs enter cells via endocytosis. These functionalized CNTs are also capable of penetrating C6 tumor spheroids, reducing their volume and inhibiting their growth. They were also able to treat an in situ tumor (orthoptic brain glioma) by decreasing the growth index of the tumor volume over

time. Finally, they showed no effect on the normal organs of mice exposed to the functionalized MWCNTs.

As for the potential risks posed by the daily contact of the human body with NPs, it attracted interest when it began to be understood that NPs contained in consumer products can be ingested, inhaled, or touch the skin and penetrate thanks to their small size. One example of NMs that are considered a potential risk is metal-containing NPs. Some studies suggest that they can cross the BBB and accumulate in the central nervous system, interacting with glial cells and neurons, potentially causing neurotoxicity (Lovisolo, et al., 2018). A large number of studies have been conducted to evaluate the toxicity of metal-containing NPs in various brain cell lines. Huang, et al., (2015) tested Ag NPs in astrocytes (ALT), BV2 and N2a cells and found signals of neuroinflammation, significant secretion of IL -1βin BV2 cells, induction of gene expression pathways for inflammatory responses and oxidative stress (CXCL13; GSS). Huerta-Garcia, et al., (2014) showed the effects of TiO2 NPs on C6 and U373 cells. They exhibited severe oxidative stress in both glial cell lines, with alteration of cellular redox state and lipid peroxidation, as well as increase in the expression of glutathione peroxidase, catalase, and superoxide dismutase genes. In addition, NPs caused morphological changes and damage in mitochondria with a decrease in mitochondrial membrane potential. Salazar-Garcia, et al., (2015) exposed astrocytes and C6 cells to Ag-NP and obtained a decrease in proliferation due to the induction of apoptosis. Marquez-Ramirez, et al., (2012) noted dose-dependent cytotoxicity in C6 cells and U373 cells exposed to TiO2-NP, with inhibition of cell proliferation and induction of programmatic cell

death (apoptosis) and morphological changes. Wang, et al., (2014) tested ZnO NPs in primary astrocytes and achieved apoptosis by generating ROS, activating caspase 3, decreasing mitochondrial membrane potential, phosphorylating JNK, ERK and p38 MAPK.
Therefore, given the great interest in nanomedicine and how easily NPs can enter the human body, it is important to evaluate alternative study models. When talking about NMs that can be inhaled, it is important to consider that it has been shown that some NMs can enter the central nervous system via the olfactory or trigeminal nerves after intranasal instillation (Liu, et al., 2009; Chang, et al., 2021).

Safe-by-design

Safe-by-Design (SbD) is not a complete new concept that, however, has emerged in various productive fields and defines the safety measures to prevent accidents, diseases and environmental damage during the design or production process. In the field of nanotechnology, it is a relatively new concept, because in order to apply this type of method, it is necessary to know what properties make NMs more or less safe. At the moment, an SbD-based approach to NM study results is attracting a lot of interest, because everything related to the study of NMs and their toxicity is at an early stage of definition. There are inconsistencies between the data on their potential applications and the data on their toxicity, but not only that, because the wide variability in the parameters used to test toxicity leads to

answers that are not always comparable. Moreover, nanotechnology is a field that is continuously and rapidly expanding, so a unified approach to safety assessment is needed. Nanomaterials are characterized by specific properties, such as magnetic, optical, chemical, and electrical properties, which make them suitable for a wide range of applications. These properties are based on their physicochemical characteristics such as composition, size, shape, and surface area. Moreover, they can change depending on the matrix in which they are incorporated or through interaction with other molecules. On the other hand, they can affect human health or pollute the environment during their life cycle. Thus, the implementation of a SbD model will allow to relate the properties of NMs to their effects in vitro and vivo. SbD model structures are being implemented in some European projects (NANoREG and ProSafe initiatives). They have created a structure for organizing a nanomaterial safety assessment project that includes several steps (Fig. 4). They started by collecting data on material, process, and product information. These data are organized in a database that contains all the characteristics that allow classification of the experimental data, such as study model, type of material, concentration, evaluated endpoint, etc. To obtain good modeling, more possible quantitative experimental data for a given endpoint and more possible exposure scenarios are needed. All the data obtained from the literature, exposure and toxicity model, material characterization and quantitative structure-activity relationships (QSARs) form the safety dossier, which becomes a safety profile after evaluation by decision makers and regulatory authorities. The greatest strength of this approach is sharing. There are two approaches to

sharing: the first involves sharing data among the components of the project; the second involves sharing data on an external platform that is used as a common database, an "Internet forum," or a free source of information (Kraegeloh, et al., 2018).

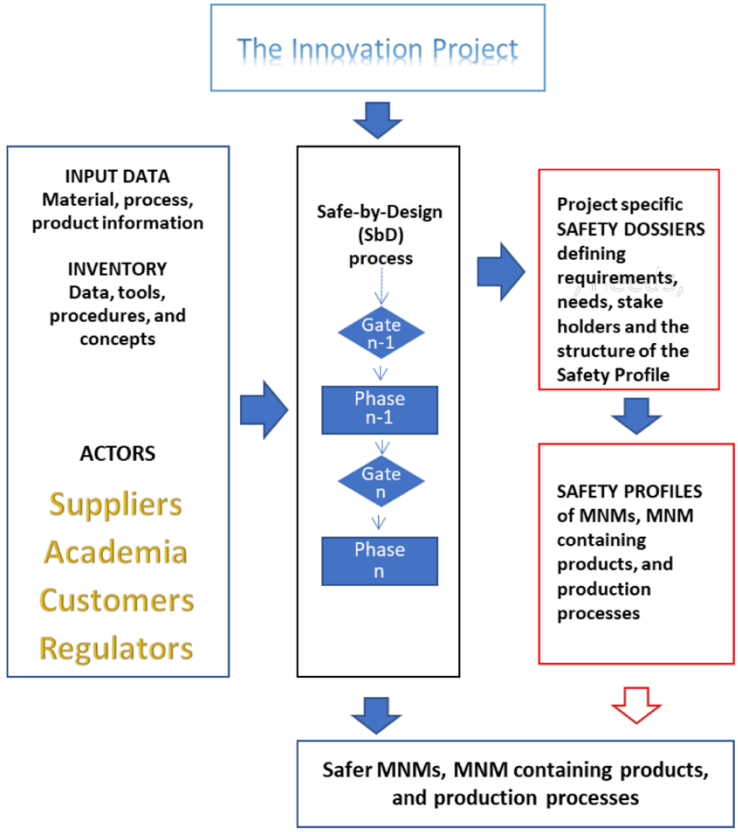

Fig.4 Model of SbD structure (Kraegeloh, et al., 2018).

Getting specific now, we will refer to two cases in which the study of NMs was performed with an SbD system. One certainly interesting case is the evaluation of NMs in the field of nanomedicine. As all known nanomedicine has generated a lot of interest in the last decades, with a lot of publications on the argument. Likewise, it is known that

NMs can produce toxicity, so researchers started to approach the argument with a SbD method. Yan, et al., (2019) explained exactly this approach in their review. They explained that the high surface free energy makes NMs reactive toward biomolecules. These interactions lead to changes in the properties of NMs and have nanotoxicological effects. Yan, et al., (2019) is based on the use of nano-informatics, which allows data from NMs studies to be analyzed using computational algorithms to identify important parameters for research. Several computational models have been implemented, but the large volume and controversial content of the data make interpretation difficult (Roca, et al., 2012; Maojo, et al., 2012). Another tool used in their SbD approach is QSARs, a computational method that can evaluate the quantitative correlation between the physicochemical properties of NMs and a range of biological effects. It has been used to predict the toxicity of materials, but the success of this method is based on a large amount of biological data archived with a large amount of modeling to study (Paramasivam, et al., 2014). Interesting information was provided by Yan, et al., (2019) the current strategy used for nanomedicine in the SbD approach. After defining that the most important property for toxicology is high surface free energy, they described different methods to cover/vary the surface area of NMs. The methods used include: insertion of the toxic NP into amphipathic lipids, polymers, silica, ZnS, or other biocompatible materials (coating and encapsulation) (Guerrero-Martinez, et al., 2010); covalent attachment of organic molecules, polymers, or biomolecules to the surface of NMs (loading); covalent attachment of probe molecules and targeting ligands to the surface of NMs, allowing

the NPs to be used more efficiently for drug delivery (grafting) (Presolski & Pumera, 2016); introduction of a small percentage of impurity atoms to modulate the surface properties (doping) (Yu, et al., 2002). Thanks to the SbD approach, other parameters have also been defined that can be varied for safety and efficiency. Namely, they regulate the size and structure of NMs. The smaller product is degraded faster, while a large dimension determines the accumulation in lungs, liver and spleen; but too fast excretion is not good either, because it reduces the possibility to reach the target. Another property that affects toxicity is biopersistence. NMs can be divided into soft nanostructures, which include organic molecules, polymers, and biomolecules (liposomes, protein NPs, etc.) that have good biocompatibility and are easily degradable, and hard nanostructures, such as metal-, metal oxide-, and carbon-based NMs that are persistent and can accumulate in the body (Akagi, et al., 2006; Shvedova, et al., 2014). Biopersistence produces toxicity, therefore, modification of NMs with specific functional groups can reduce their biopersistence and thus their toxicity. An example of this is the functionalization of CNTs with coumarin and catechin moieties, which allows for higher biodegradation rates (Sureshbabu, et al., 2015).

Another study based on SbD method was conducted by Guo, et al., (2021). They showed how it is possible to analyze graphene-based materials using this type of method. They collected information about graphene structural properties, toxicity, uptake and biodistribution. They showed how it is possible to use a computational approach to evaluate the potential risk by relating physicochemical properties to biological behavior and effects. For graphs, a program for molecular

dynamics (MD) simulations was used. In this way, it was possible to assume the behavior of different graphene forms in contact with cell membranes. Cheng, et al., (2016) realized MD simulations and observed that graphene oxide (GO) sheets had a different behavior compared to pristine graphene, GO, in fact, thanks to the hydrophilic surface was adsorbed on the surface of the lipid polar head group and thus inserted into the membrane, lipid changed its orientation, resulting with membrane damage and cell death. In contrast, pristine graphene penetrates the membrane thanks to its hydrophobic properties (Li, et al., 2013). An additional technology also described in this study is the QSAR method or other machine learning based on this approach that could be used to correlate the toxicity of NMs with their structural properties. The key factor for a possible predictive methodology seems to be the use of omics data (Afantitis, et al., 2020). An alternative to the QSAR method is the read-across and grouping method. It can be used when the data set is large enough or when the data set has gaps that need to be filled. The method is based on the assumption that similar technical NMs might have similar toxic behavior (Kuseva, et al., 2019). This methodology was just used for MWCNTs, Varsou, et al., (2019) realized two read-across to predict protein binding and cytotoxicity of functionalized MWCNTs, and put on a web service platform in a project structured on SbD. Based on the same concept, (Arts, et al., 2015) realized a database on carbon NMs. Thanks to the application of the DF4nanoGrouping framework (Fig.5), which classifies them into "biopersistent NMs with high aspect ratio", "passive NMs" and "active NMs", these groups could be used to develop a read-across model to determine their toxicity.

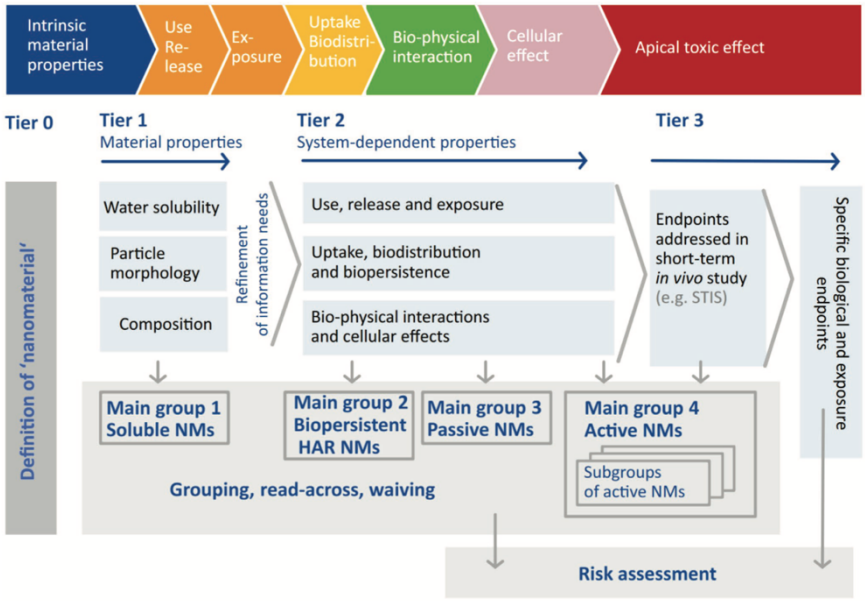

Fig.5 DF4nanoGrouping framework classifying structure (Guo, et al., 2021).

To arrive at *safe-by-design* approach application is important to structure the upstream research. One of the most common methods applied at research that want to support the *safe-by-design* approach is the use of an adverse outcome pathway (AOP) framework. AOPs permit to organize existing knowledge about an adverse health effect that start with a molecular initiating event (MIE) that generates key events (KEs) at different biological organization levels, which drive to an adverse outcome (AO). The AOP definition permits to individuate the causally connected KEs and so individuate the best models for the study (Barosova, et al., 2020). During the time different AOP are defined and are use like model in specific study. One of the most common AOP used described the mechanism of pulmonary fibrosis

and it was developed as a part of the Organisation for Economic Co-operation and Development (OECD) AOP Development Effort overseen by the Extended Advisory Group on Molecular Screening and Toxicogenomics. The mechanism was well described in Fig.6.

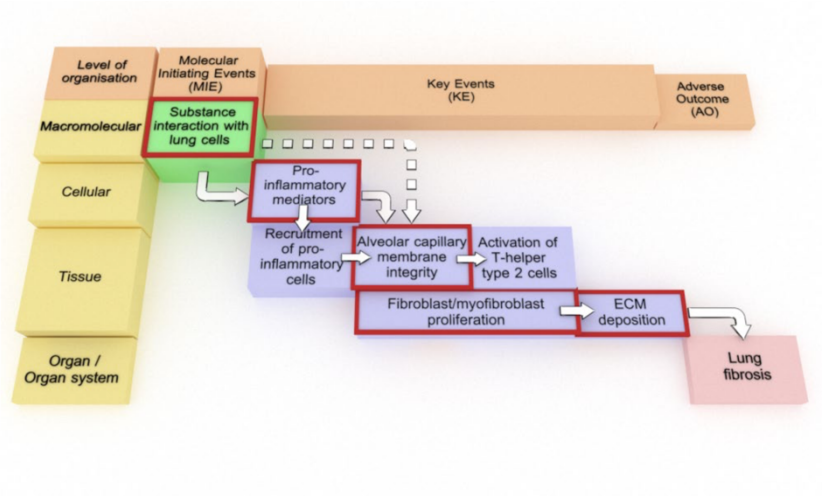

Fig.6 Adverse outcome pathway (AOP) framework: pulmonary fibrosis. (Barosova, et al., 2020)

Essentially, when a substance came in contact with the cellular membrane were released some maker of danger, part of inflammatory response (KE1). The inflammatory responses is based also on the release of pro-inflammatory cytokine, their release precedes the loss of integrity in alveolar barrier (KE2). This damage is repaired thanks to proliferation and migration of epithelial cells and differentiation of fibroblast into myofibroblasts (KE3), which produce extracellular matrix elements in order to repair the damage. Into normal condition damage was repaired, but if dose of exposition was so high or time of exposition so long the inflammatory process continue and there was an

excessive deposition of extracellular matrix with generation of pulmonary fibrosis (AO) (Barosova, et al., 2020).

Bibliography

Adamson, I. Y., Letourneau, H. I. & Bowden, D. H., 1991. Comparison of alveolar and interstitial macrophages in fibroblast stimulation after silica and long or short asbestos.. *Lab.Invest.,* Volume 64, pp. 339-344.

Afantitis, A. et al., 2020. NanoSolveIT Project: Driving nanoinformatics research to develop innovative and integrated tools for in silico nanosafety assessment. *Computational and Structural Biotechnology Journal,* Volume 18, pp. 583-602.

Akagi, T. et al., 2006. Hydrolytic and Enzymatic Degradation of Nanoparticles Based on Amphiphilic Poly(γ-glutamic acid)-graft-l-Phenylalanine Copolymers. *Biomacromolecules,* 7(1), pp. 297-303.

Al-Khateeb, L. A., Almotiry, S. & Salam, M. A., 2014. Adsorption of pharmaceutical pollutants onto graphene nanoplatelets. *Chemical Engineering Journal,* 15 7, Volume 248, pp. 191-199.

Allan, et al., 2021. Regulatory landscape of nanotechnology and nanoplastics from a global perspective. *Regulatory Toxicology and Pharmacology,* 19 02, Volume 121, pp. 1-18.

Arts, J. H. E. et al., 2015. A decision-making framework for the grouping and testing of nanomaterials (DF4nanoGrouping). *Regulatory Toxicology and Pharmacology ,* 71(2), pp. S1-S27.

Banks, W. A., 2016. From blood–brain barrier to blood–brain interface: new opportunities for CNS drug delivery. *Nature Reviews Drug Discovery ,* Volume 15, pp. 275-292.

Barbalinardo, M., Caicci, F., Cavallini, M. & Gentili, D., 2018. Protein corona mediated uptake and cytotoxicity of silver nanoparticles in mouse embryonic fibroblast. *Nano Micro Small,* 14(34), p. e1801219.

Barosova, H. et al., 2020. Use of EpiAlveolar Lung Model to Predict Fibrotic Potential of Multiwalled Carbon Nanotubes. *ACS Nano,* Volume 14, pp. 3941-3956.

Belling, J. N. et al., 2016. Immune Properties of Graphene Oxide Enabled by Surface-Bound Complement Factor H. *ACS Nano,* Volume 10, pp. 10161-10172.

Bremnes, R. M. et al., 2011. The Role of Tumor-Infiltrating Immune Cells and Chronic Inflammation at the Tumor Site on Cancer Development, Progression, and Prognosis: Emphasis on Non-small Cell Lung Cancer. *Journal of Thoracic Oncology,* 4, 6(4), pp. 824-833.

Broaddus, V. C. & Jaurand, M. C., 2002. Asbestos !bres and their interaction with mesothelial cells in vitro and in vivo.. *Mesothelioma,* Volume London: Taylor and Francis, pp. 273-294.

Buruah, P. K., Sharma, B., Hussain, N. & Das, M. R., 2017. Magnetically recoverable Fe3O4/graphene nanocomposite towards efficient removal of triazine pesticides from aqueous solution: Investigation of the adsorption phenomenon and specific ion effect. *Chemosphere,* 2, Volume 168, pp. 1058-1067.

Cao, Y., Li, S. & Chen, J., 2020. Modeling better in vitro models for the prediction of nanoparticle toxicity: a review. *Toxicology Mechanisms and Methods,* 12 10, 31(1), pp. 1-17.

Chang, X. et al., 2021. Neurotoxicity of metal-containing nanoparticles and implications in glial cells. *Journal of Applied Toxicology,* Volume 41, pp. 65-81.

Cheng, G. Y. et al., 2012. Simultaneous Induction of Autophagy and Toll-like Receptor Signaling Pathways by Graphene Oxide.. *Biomaterials,* Volume 33, pp. 6559-6569.

Cheng, J. et al., 2016. Interaction of Graphene and its Oxide with Lipid Membrane: A Molecular Dynamics Simulation Study. *The Journal of Physical Chemistry C,* 120(11), pp. 6225-6231.

Cheng, X. et al., 2015. Protein corona influences cellular uptake of gold nanopar- ticles by phagocytic and nonphagocytic cells in a size-dependent manner. *ACS Applied Materials & Interfaces,* 7(37), pp. 20568-20575.

Chia, S. L., Tay, C. Y., Setyawati, M. I. & Leong, D. T., 2015. Biomimicry 3D gastro- intestinal spheroid platform for the assessment of toxicity and inflam- matory effects of zinc oxide nanoparticles.. *Micro Nano Small,* 11(6), pp. 702-712.

Choi, W., Lahiri, I., Seelaboyina, R. & Kang, Y. S., 2010. Synthesis of Graphene and Its Applications: A Review. *Solid State and Material Science,* Volume 35, pp. 52-71.

Chortarea, S. et al., 2017. Human asthmatic bronchial cells are more sus- ceptible to subchronic repeated exposures of aerosolized carbon nanotubes at occupationally relevant doses than healthy cells. *ACS Nano,* 11(8), pp. 7615-7625.

Coileain, O., 2021. The influence, risks and opportunities of a rising technology. *Library & Research Service,* 15 06, Volume Nanotechnology, pp. 1-30.

Davis, J. G. et al., 1986. The pathogenicity of long versus short fiber samples of amosite asbestos administered to rats by inhalation and intraperitoneal injection. *Br. J. Exp. Pathol.,* Volume 67, pp. 415-430.

Davoren, M. et al., 2007. In vitro toxicity evaluation of single walled carbon nanotubes on human A549 lung cells. *Toxicology in Vitro,* 21(3), pp. 438-448.

Ding, L. et al., 2005. Molecular Characterization of the Cytotoxic Mechanism of Multiwall Carbon Nanotubes and Nano-Onions on Human Skin Fibroblast. *Nano Letters,* 29 10, 5(12), pp. 2448-2464.

Donaldson, K. & Golyasnya, N., 1995. Cytogenetic and pathogenic effects of long and short amosite asbestos. *J. Pathol.,* Volume 177, pp. 303-307.

Donaldson, K. et al., 1992. Asbestos-stimulated tumor-necrosis-factor release from alveolar macrophages depends on fiber length and opsonization. *J. Pathol.,* Volume 168, pp. 243-248.

Donaldson, K. et al., 2013. Pulmonary toxicity of carbon nanotubes and asbestos — Similarities and differences. *Advanced Drug Delivery Reviews ,* 27 7, Volume 65, pp. 2078-2086.

Donaldson, K., Poland, C. A., Duffin, R. & Bonner, J., 2012. *The toxicology of carbon nanotubes.* New York: Cambridge University Press.

Duan, G. et al., 2015. Protein corona mitigates the cytotoxicity of graphene oxide by reducing its physical interaction with cell membrane. *Nanoscale,* 7(37), pp. 15214-15224.

Fadeel, B. et al., 2018. Safety Assessment of Graphene-Based www.acsnano.org Materials: Focus on Human Health and the Environment. *ACS Nano,* Volume 12, pp. 10582-10620.

Fede , C. et al., 2015. Evaluation of gold nanoparticles toxicity towards human endothelial cells under static and flow conditions. *Microvascular Research,* Volume 97, pp. 147-155.

Fenoglio, I. et al., 2006. Reactivity of carbon nanotubes: Free radical generation or scavenging activity?. *Free Radical Biology and Medicine,* 1 4, 40(7), pp. 1227-1233.

Francis & Devasena, 2017. Toxicity of carbon nanotubes: A review. *Toxicology and Industrial Health,* 13 11, 34(3), pp. 200-210.

Francis, A. P. & Devesena, T., 2017. Toxicity of carbon nanotubes: A review. *Toxicology and Industrial Health,* 13 11, 34(3), pp. 200-210.
Francis, A. P. et al., 2015. One time nose-only inhalation of MWCNTs: Exploring the mechanism of toxicity by intermittent sacrifice in Wistar rats. *Toxicology Reports,* Volume 2, pp. 111-120.

Fu, S. et al., 2019. Dual-Modified Novel Biomimetic Nanocarriers Improve Targeting and Therapeutic Efficacy in Glioma. *ACS Applied Materials & Interfaces,* 11(2), pp. 1841-1854.

Gao, Y. et al., 2012. Adsorption and removal of tetracycline antibiotics from aqueous solution by graphene oxide Author links open overlay panel. *Journal of Colloid and Interface Science,* 15 2, Volume 368, pp. 540-546.

Ghadim, E. E. et al., 2013. Adsorption Properties of Tetracycline onto Graphene Oxide: Equilibrium, Kinetic and Thermodynamic Studies. *Plos one,* 26 11, 8(11), p. e79254.

Guerrero-Martinez, A., Pérez-Juste, J. & Liz-Marzan, L. M., 2010. Recent Progress on Silica Coating of Nanoparticles and Related Nanomaterials. *Advanced Materials ,* 22(11), pp. 1182-1195.

Guo, Z. et al., 2021. Surface Functionalization of Graphene-Based Materials: Biological Behavior, Toxicology, and Safe-By-Design Aspects. *Advanced Biology,* Volume 5, p. 2100637.

Herzog, E. et al., 2007. A new approach to the toxicity testing of carbon-based nanomaterials—The clonogenic assay. *Toxicology Letters,* 174(1-3), pp. 49-60.

Hill, I. M., Beswick, P. H. & Donaldson, K., 1995. Differential release of superoxide anions by macrophages treated with long and short-fiber amosite asbestos is a consequence of differential affinity for opsoninv. *Occup. Environ. Med.,* Volume 52, pp. 92-96.

Hirano, S., Fujitani, Y., Furuyama, A. & Kanno, S., 2010. Uptake and cytotoxic effects of multi-walled carbon nanotubes in human bronchial epithelial cells. *Toxicology and Applied Pharmacology,* 249(1), pp. 8-15.

Hirano, S., Kanno, S. & Furuyama, A., 2008. Multi-walled carbon nanotubes injure the plasma membrane of macrophages. *Toxicology and Applied Pharmacology,* 15 10, 232(2), pp. 244-251.

Huang, C. L. et al., 2015. Silver nanoparticles affect on gene expression of inflammatory and neurodegenerative responses in mouse brain neural cells.. *Environment Research,* Volume 136, pp. 253-263.

Huerta-Garcia, E. et al., 2014. Titanium dioxide nanoparticles induce strong oxidative stress and mitochondrial damage in glial cells.. *Free Radical Biology and Medicine,* Volume 73, pp. 84-94.

Iijima, S., 1991. Helical microtubules of graphitic carbon. *Nature ,* 7 11, Volume 354, pp. 56-58.

Inoue, K. et al., 2010. Repeated pulmonary exposure to single-walled carbon nanotubes exacerbates allergic inflammation of the airway: Possible role of oxidative stress. *Free Radical Biology and Medicine ,* 1 4, 48(7), pp. 924-934.

Jaurand, M. F., Renier, A. & Daubriac, J., 2009. Mesothelioma: Do asbestos and carbon nanotubes pose the same health risk?. *Particle and Fibre Toxicology,* 12 6, Volume 6, pp. 1-14.

Ji, L. et al., 2013. Graphene Nanosheets and Graphite Oxide as Promising Adsorbents for Removal of Organic Contaminants from Aqueous Solution. *Journal of Environmental Quality,* 1 1, 42(1), pp. 191-198.

Jia, G. et al., 2005. Cytotoxicity of Carbon Nanomaterials: Single-Wall Nanotube, Multi-Wall Nanotube, and Fullerene. *Environmental Science & Technology,* 7 1, 39(5), pp. 1378-1383.

Jiang, Y. et al., 2020. Multi-walled carbon nano- tubes decrease neuronal NO synthase in 3D brain organoids. *Science of The Total Environment,* Volume 748, p. 141384.

Kaiser, J. et al., 2007. Single walled carbon nanotubes (SWCNT) affect cell physiology and cell architecture. *Journal of Materials Science: Materials in Medicine,* 8 11, Volume 19, pp. 1523-1527.

Kim, J. K. et al., 2016. 28-Day Inhalation Toxicity of Graphene Nanoplatelets in Sprague-Dawley Rats. *Nanotoxicology,* Volume 10, pp. 891-901.

Kraegeloh, A., Suarerz-Merino, B., Sluijters, T. & Micheletti, C., 2018. Implementation of Safe-by-Design for Nanomaterial Development and

Safe Innovation: Why We Need a Comprehensive Approach. *nanomaterials,* Volume 8, p. 239.

Kuseva, C. et al., 2019. The implementation of RAAF in the OECD QSAR Toolbox. *Regulatory Toxicology and Pharmacology,* Volume 105, pp. 51-61.

Kyzas, G. Z. et al., 2015. Removal of beta-blockers from aqueous media by adsorption onto graphene oxide. *Science of The Total Environment,* 15 12, Volume 537, pp. 411-420.

Lam, C., James, J. T., McCluskey, R. & Hunter, L., 2004. Pulmonary Toxicity of Single-Wall Carbon Nanotubes in Mice 7 and 90 Days After Intratracheal Instillation. *Toxicological Sciences,* 1 1, Volume 77, pp. 126-134.

Lee, J. K. et al., 2017. The Role of Surface Functionalization on the Pulmonary Inflammogenicity and Trans- location into Mediastinal Lymph Nodes of Graphene Nanoplatelets in Rats. *Arch. Toxicology,* Volume 91, pp. 667-676.

Li, J. et al., 2019. Evaluation of in vitro toxicity of silica nanoparticles (NPs) to lung cells: Influence of cell types and pulmonary surfactant component DPPC. *Ecotoxicology and Environmental Safety,* 30 12, Volume 186, p. 109779.

Li, J., Guo, S., Zhai, Y. & Wang, E., 2009. Nafion–graphene nanocomposite film as enhanced sensing platform for ultrasensitive determination of cadmium. *Electrochemistry Communications,* 5, 11(5), pp. 1085-1088.

Li, R. et al., 2018. Surface Oxidation of Graphene Oxide Determines Membrane Damage, Lipid Peroxidation, and Cytotoxicity in Macrophages in a Pulmonary Toxicity Model.. *ACS Nano,* Volume 12, pp. 1390-1402.

Li, R. et al., 2018. Surface Oxidation of Graphene Oxide Determines Membrane Damage, Lipid Peroxidation, and Cytotoxicity in Macrophages in a Pulmonary Toxicity Model. *ACS Nano,* Volume 12, pp. 1390-1402.

Li, Y. et al., 2013. Graphene microsheets enter cells through spontaneous membrane penetration at edge asperities and corner sites. *PNAS,* 110(30), pp. 12295-12300.

Liu, J., Tang, M. & Ding, J., 2020. The interaction between nanoparticles-pro- tein corona complex and cells and its toxic effect on cells.. *Chemosphere,* Volume 245, p. 125624.

Liu, Y. et al., 2009. Potential Health Impact on Mice after Nasal Instillation of Nano-Sized Copper Particles and Their Translocation in Mice. *American Scientific Publishers,* 9(11), pp. 6335-6343.

Lohcharoenkal, W. et al., 2013. Chronic Exposure to Carbon Nanotubes Induces Invasion of Human Mesothelial Cells through Matrix Metalloproteinase-2. *ACS Nano,* 7(9), pp. 7711-7723.

Long, J. et al., 2018. nternalization, cytotox- icity, oxidative stress and inflammation of multi-walled carbon nano- tubes in human endothelial cells: influence of pre-incubation with bovine serum albumin. *Royal Society of Chemistry,* 8(17), pp. 9253-9260.

Lovisolo, D., Dionisi, M., Ruffinati, F. A. & Distasi, C., 2018. Nanoparticles and potential neurotoxicity: Focus on molecular mechanisms. *AIMS Molecular Science,* 5(1), pp. 1-13.

Luo, N. et al., 2017. PEGylated Graphene Oxide Elicits Strong Immunological Responses despite Surface Passivation. *Nature comunucation,* Volume 8, p. 14537.

Ma, J. et al., 2015. Crucial Role of Lateral Size for Graphene Oxide in Activating Macrophages and Stimulating Pro-Inflammatory Responses in Cells and Animals.. *ACS Nano,* Volume 9, pp. 10498-10515.

Malesevic, A. et al., 2008. A versatile plasma tool for the synthesis of carbon nanotubes and few-layer graphene sheets. *Journal of Optoelectronics and Advanced Materials ,* Volume 10, pp. 2052-2055.

Maliyekkal, S. M. et al., 2013. Graphene: A Reusable Substrate for Unprecedented Adsorption of Pesticides. *Nano Micro Small,* 28 1, 9(2), pp. 273-283.

Manna, S. et al., 2005. Single-Walled Carbon Nanotube Induces Oxidative Stress and Activates Nuclear Transcription Factor-κB in Human Keratinocytes. *Nano Letters,* 13 8, 5(9), pp. 1676-1684.

Maojo, V. et al., 2012. Nanoinformatics: a new area of research in nanomedicine. *International journal of Nanomedicine,* Volume 7, p. 3867.

Marquez-Ramirez, S. G. et al., 2012. Titanium dioxide nanoparticles inhibit proliferation and induce morphological changes and apoptosis in glial cells. *Toxicology,* 302(2-3), pp. 146-156.

Matesanz, M. C. et al., 2013. TheEffectsof Graphene Oxide Nanosheets Localized on F-Actin Filaments on Cell- Cycle Alterations. *Biomaterials,* Volume 34, pp. 1562-1569.

Mcconnell, E. E. et al., 1999. Studies on the inhalation toxicology of two fiberglasses and amosite asbestos in the Syrian golden hamster. Part II. Results of chronic exposurev. *Inhalation Toxicology,* 9, 11(9), pp. 785-835.

Michael, J. S., Lee, B., Zhang, M. & Yu, D. J., 2018. Nanotechnology for Treatment of Glioblastoma Multiforme. *Journal of Translational Internal Medicine,* 6(3), pp. 128-133.

Michalkova, H. et al., 2020. Complex cytotoxicity mechanism of bundles formed from self-organised 1-D anodic TiO2 nanotubes layers. *Journal of Hazardous Materials,* 15 4, Volume 388, p. 122054.

Miclaus, T. et al., 2016. Dynamic protein coronas revealed as a modula- tor of silver nanoparticle sulphidation in vitro.. *Nature Communications,* Volume 7, p. 11770.

Monteiro-Riviere, N. A. & Inman, A. O., 2005. Challenges for assessing carbon nanomaterial toxicity to the skin. *Carbon,* 23 9, Volume 44, pp. 1070-1078.

Moratin, H. et al., 2017. Toxicological characterization of ZnO nanoparticles in malignant and non-malignant cells. *Environmental and Molecular Mutagenesis,* 18 11, 59(3), pp. 247-259.

Muller, J. et al., 2005. Respiratory toxicity of multi-wall carbon nanotubes. *Toxicology and Applied PharmacologyToxicology and Applied Pharmacology,* 15 9, 207(3), pp. 221-231.

Muller, J. et al., 2008. Clastogenic and aneugenic effects of multi-wall carbon nanotubes in epithelial cells.. *Casrcinogenesis,* 29(2), pp. 427-433.

Muller, J. et al., 2008. Clastogenic and aneugenic effects of multi-wall carbon nanotubes in epithelial cells. *Carcinogenesis ,* 29(2), pp. 427-433.

Muller, J. et al., 2008. Structural defects play a major role in the acute lung toxicity of multiwall carbon nanotubes: toxicological aspects. *Chem Res Toxicol .,* 21(9), pp. 1698-1705.

Murphy, F. A. et al., 2011. Length-Dependent Retention of Carbon Nanotubes in the Pleural Space of Mice Initiates Sustained Inflammation and Progressive Fibrosis on the Parietal Pleura. *The American Journal of Pathology,* 6, 178(6), pp. 2587-2600.

Nam, S. et al., 2015. Adsorption characteristics of diclofenac and sulfamethoxazole to graphene oxide in aqueous solution Author links open overlay panel. *Chemosphere,* 10, Volume 136, pp. 20-26.

Neuwel, E. A. et al., 2011. Engaging neuroscience to advance translational research in brain barrier biology. *Nature Reviews Neuroscience volume,* Volume 12, pp. 169-182.

Novoselov, K. S. et al., 2004. Graphene:carbon in two dimensions. *Materials Today,* Volume 306, p. 666.

Nupearachchi, C. N., Mahatantila, K. & Vithanage, M., 2017. Application of graphene for decontamination of water; Implications for

sorptive removal. *Groundwater for Sustainable Developmen,* 30 6, Volume 5, pp. 206-215.

Oberdorster, G., Oberdorster, E. & Oberdorster, J., 2005. Nano-toxicology: An Emerging Discipline Evolving from Studies of Ultrafine Particles. *Environmental Health Perspectives,* Volume 113, pp. 823-839.

Obraztsov, A. N. et al., 2003. DC discharge plasma studies for nanostructured carbon CVD. *Diamond and Related Materials,* 12(3-7), pp. 917-920.

Pacurari, M. et al., 2008. Raw Single-Wall Carbon Nanotubes Induce Oxidative Stress and Activate MAPKs, AP-1, NF-κB, and Akt in Normal and Malignant Human Mesothelial CellsRaw Single-Wall Carbon Nanotubes Induce Oxidative Stress and Activate MAPKs, AP-1, NF-κB, and Akt in Normal an. *Environmental Health Perspectives,* 16 5, Volume 116, pp. 1211-1217.

Pacurari, M. et al., 2008. Raw single-wall carbon nanotubes induce oxidative stress and activate MAPKs, AP-1, NF-kappaB, and Akt in normal and malignant human mesothelial cells. *Environmental Health Prospectives,* 116(1-2), pp. 70-77.

Paino, I. M., Gonçalves, F. J., Souza, F. L. & Zucolotto, V., 2016. Zinc Oxide Flower-Like Nanostructures That Exhibit Enhanced Toxicology

Effects in Cancer Cells. *ACS Applied Materials & Interfaces,* 23 11, 8(48), pp. 32699-32705.

Pantarotto, D., Briand, J., Prato, M. & Bianco, A., 2003. Pantarotto D, Briand JP, Prato M, et al. (2004) Translocation of bioactive peptides across cell membranes by carbon nanotubes.. *Chemical Communications,* 3 11, 7(1), p. 16–17.

Paramasivam, V., Yee, T. S., Dhillon, S. K. & Sidhu, A. S., 2014. A methodological review of data mining techniques in predictive medicine: An application in hemodynamic prediction for abdominal aortic aneurysm disease. *Biocybernetics and Biomedical Engineering,* Volume 34, pp. 139-145.

Park, E. et al., 2011. A single intratracheal instillation of single-walled carbon nanotubes induced early lung fibrosis and subchronic tissue damage in mice. *Archives of Toxicology ,* 7 4, Volume 85, pp. 1121-1131.

Poland, C. A. et al., 2008. Carbon nanotubes introduced into the abdominal cavity of mice show asbestos- like pathogenicity in a pilot study. *nature nanotechnology,* 20 5, Volume 3, pp. 423-428.

Presolski, S. & Pumera, M., 2016. Covalent functionalization of MoS2. *Materials today,* 19(3), pp. 140-145.

Pulskamp, K., Diabate, S. & Krug, H. F., 2007. Carbon nanotubes show no sign of acute toxicity but induce intracellular reactive oxygen species in dependence on contaminants. *Toxicology Letters,* 10 1, 168(1), pp. 58-74.

Pulskamp, K., Diabate, S. & Krug, H. F., 2007. Carbon nanotubes show no sign of acute toxicity but induce intracellular reactive oxygen species in dependence on contami- nants.. *Toxicology Letters,* 168(1), pp. 58-74.

Rauti, R. et al., 2016. Graphene Oxide Nanosheets Reshape Synaptic Function in Cultured Brain Networks. *ACS Nano,* Volume 10, pp. 4459-4471.

Roca, C. P., Rallo, R., Fernandez, A. & Girald, F., 2012. Towards Efficient Designing of Safe Nanomaterials: Innovative Merge of Computa- tional Approaches and Experimental Techniques. *Royal Society of Chemistry,* p. 89.

Roshini, A. et al., 2017. Synthesis and evaluation of the cytotoxic and anti-proliferative properties of ZnO quantum dots against MCF-7 and MDA-MB-231 human breast cancer cells. *Materials Science and Engineering: C,* 1 12, Volume 81, pp. 551-560.

Russier , J. et al., 2013. Evidencing the Mask Effect of Graphene Oxide: A Comparative Study on Primary Human and Murine Phagocytic Cells.. *Nanoscale,* Volume 5, pp. 11234-11247.

Salazar-Garcia, S. et al., 2015. Comparative effects on rat primary astrocytes and C6 rat glioma cells cultures after 24-h exposure to silver nanoparticles (AgNPs). *Journal of Nanoparticle Research volume,* 17(11), pp. 1-13.

Sambale, F. et al., 2015. Three dimensional spheroid cell cul- ture for nanoparticle safety testing.. *Journal of Biothecnology,* Volume 205, pp. 120-129.

Saraiva, C. et al., 2016. Nanoparticle-mediated brain drug delivery: Overcoming blood–brain barrier to treat neurodegenerative diseases. *Journal of Controlled Release,* Volume 235, pp. 34-47.

Sargent, L. M., Reynolds, S. H. & Castranova, V., 2010. Potential pulmonary effects of engineered carbon nanotubes: In vitro genotoxic effects.. *Nanotoxicology,* Volume 4, pp. 398-408.

Schedin, F. et al., 2007. Detection of individual gas molecules adsorbed on graphene. *Nature Materials,* 29 7, Volume 6, pp. 652-655.
Shan, C. et al., 2009. Direct Electrochemistry of Glucose Oxidase and Biosensing for Glucose Based on Graphene. *Analytical Chemistry,* 19 2, 18(6), pp. 2378-2382.

Sharma, et al., 2021. Porous nanomaterials: Main vein of agricultural nanotechnology. *Progress in Materials Science,* 3 05, Volume 121, pp. 1-51.

Shedin, F. et al., 2007. Detection of individual gas molecules adsorbed on graphene. *Nature Materials,* Volume 6, p. 652.

Shi Kam, N. W., Jessop, T. C., Wender, P. A. & Dai, H., 2004. Nanotube Molecular Transporters: Internalization of Carbon Nanotube−Protein Conjugates into Mammalian Cells. *Journal of the American Chemical Society,* 13 5, 126(22), pp. 6850-6851.

Shin, J. H. et al., 2015. 5-Day Repeated Inhalation and 28-Day Post-Exposure Study of Graphene.. *Nanotoxicology,* Volume 9, pp. 1023-1031.

Shukla, A. et al., 1999. Inhaled Particulate Matter Causes Expression of Nuclear Factor (NF)- κ B–Related Genes and Oxidant-Dependent NF- κ B Activation In Vitro. *American Journal of Respiratory Cell and Molecular Biology,* 22 11, 23(2), pp. 182-187.

Shvedova, A. A. et al., 2005. Unusual inflammatory and fibrogenic pulmonary responses to single-walled carbon nanotubes in mice. *Am J Physiol Lung Cell Mol Physiolv,* 10 6, Volume 289, pp. 698-708.

Shvedova, A. A. et al., 2008. Inhalation vs. Aspiration of single-walled carbon nanotubes in c57bl/6 mice: Inflammation, fibrosis, oxidative stress, and mutagenesis.. *Am J Physiol Lung Cell Mol Physiol ,* Volume 295, pp. L552-565.

Shvedova, A. A. et al., 2014. Long-term effects of carbon containing engineered nanomaterials and asbestos in the lung: one year postexposure comparisons. *American Journal of Physiology,* 306(2), pp. L170-L182.

Simon-Deckers, A. et al., 2008. In vitro investigation of oxide nanoparticle and carbon nanotube toxicity and intracellular accumulation in A549 human pneumocytes. *Toxicology,* 20 11, 253(1-3), pp. 137-146.

Sophia, A. C., Lima, E. C., Allaudeen, N. & Rajan, S., 2016. Application of graphene based materials for adsorption of pharmaceutical traces from water and wastewater- a review. *Desalination and Water Treatment,* 28 3, Volume 57, pp. 27573-27586.

Srivastava, G. et al., 2014. Functionalized Graphene Sheets As Immobilization Matrix for Fenugreek b-Amylase: Enzyme Kinetics and Stability Studies. *Plos one,* 20 11, 9(11), p. e113408.

Srivastava, R. K. et al., 2011. Multi-walled carbon nanotubes induce oxidative stress and apoptosis in human lung cancer cell line-A549. *Nanotoxicology,* Volume 5, pp. 195-207.

Stankovich, S. et al., 2005. Stable aqueous dispersions of graphitic nanoplatelets via the reduction of exfoliated graphite oxide in the

presence of poly(sodium 4-styrenesulfonate). *J. Mater. Chem.,* 21 11, Volume 16, pp. 155-158.

Stone, V. et al., 2017. Nanomaterials Versus Ambient Ultrafine Particles: An Opportunity to Exchange Toxicology Knowledge. *Environmental Health Prespectives,* Volume 125, p. 106002.

Sun, S. & Chang, C. P., 2008. Ballistic transport in bilayer nano-graphite ribbons under gate and magnetic fields. *The European Physical Journal B volume,* Volume 64, pp. 249-255.

Sureshbabu, A. R. et al., 2015. Degradation-by-design: Surface modification with functional substrates that enhance the enzymatic degradation of carbon nanotubes. *Biomaterials,* Volume 72, pp. 20-28.

Tabet, L. et al., 2008. Adverse Effects of Industrial Multiwalled Carbon Nanotubes on Human Pulmonary Cells. *Journal of Toxicology and Environmental Health,* 16 5, 72(2), pp. 60-73.

Thakur, S. A., Hamilton, R., Pikkarainen, T. & Holian, A., 2009. Differential Binding of Inorganic Particles to MARCO. *Toxicological Science,* 1, 107(1), pp. 238-246.

Thurnherr, T. et al., 2011. A comparison of acute and long-term effects of industrial multiwalled carbon nanotubes on human lung and immune cells in vitro. *Toxicology Letters,* 200(3), pp. 176-186.

Ursini, C. L. et al., 2014. Evaluation of cytotoxic, genotoxic and inflammatory response in human alveolar and bronchial epithelial cells exposed to titanium dioxide nanoparticles. *Journal of Applied Toxicology,* 16 9, 34(11), pp. 1209-1219.

Varsou, D. et al., 2019. A safe-by-design tool for functionalised nanomaterials through the Enalos Nanoinformatics Cloud platform. *Nanoscale Adv.,* Volume 1, pp. 706-718.

Wagner, J. C., Sleggs, C. A. & Marchand, P., 1960. Diffuse pleural mesothelioma and asbestos exposure in the north western cape province. *Brit. J. industr. Med.,* 24 4, Issue 17, pp. 260-271.

Wang, J. et al., 2004b. Synthesis of carbon nanosheets by inductively coupled radio-frequency plasma enhanced chemical vapor deposition. *Carbon,* 14 8, 42(14), pp. 2867-2872.

Wang, J. et al., 2014. ZnO nanoparticle-induced oxidative stress triggers apoptosis by activating JNK signaling pathway in cultured primary astrocytes.. *Nanoscale Research Letters,* 9(1), pp. 1-12.

Wang, J. J. et al., 2004. Free-standing subnanometer graphite sheets. *Applied Physics Letters,* 10 8, 85(7), p. 1265.

Wang, L. et al., 2010. Dispersion of single-walled carbon nanotubes by a natural lung surfactant for pulmonary in vitro and in vivo toxicity studies.. *Particle and Fibre Toxicology,* Volume 7, p. 31.

Wang, S., Sun, H., Ang, H. M. & Tadé, 2013. Adsorptive remediation of environmental pollutants using novel graphene-based nanomaterials,. *Chemical Engineering Journal,* Volume 226, pp. 336-347.

Wick, P. et al., 2007. The degree and kind of agglomeration affect carbon nanotube cytotoxicity. *Toxicology Letters,* 30 1, 168(2), pp. 121-123.

Wick, P. et al., 2007. The degree and kind of agglomeration affect carbon nanotube cytotoxicity. *Toxicology Letters,* 30 1, 168(2), pp. 121-123.

Winzen, S. et al., 2015. Complementary analysis of the hard and soft protein corona: sample preparation critically effects corona composition. *Nanoscale,* 7(7), pp. 2992-3001.

Wong, H. L., Wu, X. Y. & Bendayan, R., 2012. Nanotechnological advances for the delivery of CNS therapeutics. *Advanced Drug Delivery Reviews,* Volume 64, pp. 686-700.

Xie, J. et al., 2019. Nanomaterial-based blood-brain-barrier (BBB) crossing strategies. *Biomaterials,* Volume 224, p. 119491.

Yan, L. et al., 2019. A Safe-by-Design Strategy towards Safer Nanomaterials in Nanomedicines. *Advanced Material,* Volume 31, p. 1805391.

Yang, H. et al., 2008. Comparative study of cytotoxicity, oxidative stress and genotoxicity induced by four typical nanomaterials: the role of particle size, shape and composition. *Applied Toxicology,* 29 8, 29(1), pp. 69-78.

Yang, S., Luo, J., Zhou, Q. & Wang, H., 2012. Pharmacokinetics, Metabolism and Toxicity of Carbon Nanotubes for Biomedical Purposes. *Theranostics,* 2(3), pp. 271-282.

You, Y. et al., 2019. Designing dual-functionalized carbon nanotubes with high blood–brain-barrier permeability for precise orthotopic glioma therapy. *Dalton Transaction,* 48(5), pp. 1569-1573.

Yu, J. C. et al., 2002. Effects of F- Doping on the Photocatalytic Activity and Microstructures of Nanocrystalline TiO2 Powders. *Chemistry of Materials,* 14(9), pp. 3808-3816.

Yuan, X. et al., 2013. Calcined graphene/MgAl-layered double hydroxides for enhanced Cr(VI) removal. *Chemical Engineering Journal,* Volume 221, pp. 204-213.

Yung, S. & Chan, T. M., 2007. Mesothelial cells. *Peritoneal Dialysis International,* 27(2), pp. S110-S115.

Zanella, C. L., Posada, J., Tritton, T. R. & Mossoman, B. T., 1996. Asbestos causes stimulation of the extracellular signal-regulated kinase 1 mitogen-activated protein kinase cascade after phosphorylation of the epidermal growth factor receptorv. *Cancer Research,* 56(23), pp. 5334-5338.

Zhang, H. et al., 2021. Development of curcumin-loaded zein nanoparticles for transport across the blood–brain barrier and inhibition of glioblastoma cell growth. *Biomaterials Science,* Volume 9, pp. 7092-7103.

Zhang, M. et al., 2012. Synthesis, characterization, and environmental implications of graphene-coated biochar. *Science of The Total Environment,* 1 10, Volume 435-436, pp. 567-572.

Zhang, T. et al., 2019. MWCNT interactions with protein: surface-induced changes in protein adsorption and the impact of protein corona on cellular uptake and cytotoxicity. *International Journal ofv Nanomedicine,* Volume 14, pp. 993-1009.

Chapter 2

Outline of the thesis

As just described in the introductory chapter, the world of nanotechnology has been in great expansion in recent decades for many different reasons. First of all, it was the unique physical and chemical properties of these materials that enabled some applications, for example in medicine (CNTs are used for bone scaffolds, vascular stents, neuron growth and regeneration (Donaldson, et al., 2012); graphene showed good sensing properties for biological molecules, such as glucose, catecholamine neurotransmitter (Alwarappan et al. 2009), which were initially impossible. Moreover, as has just been pointed out, the global market for nanotechnology was expected to exceed a value of $125 billion by 2024, not including the case of graphene, whose market was estimated at 1.3 billion by 2023, with an annual growth rate of almost 47% compared to 2018 (De Marchi et al. 2018). The innovative power emanating from these new technologies and their predictable and incisive presence in many health and economic sectors, as well as the paucity of data on their toxicity, have led us to design an efficient approach to assess the toxicity of nanoparticles. Based on our own application project in biotechnology, we considered it fundamental to approach this application with a safe-by-design approach and evaluate the toxicity of the materials used in

our application. The toxicity of different types of carbon nanomaterials was evaluated using two different cell models (MeT-5A and/or C6 cells). The selection was made considering the possible target of toxicity of the materials and the possible mode of exposure. The nanomaterials tested were: CNTs (different types with different dimensions - short and long; nanomaterial in fibrous form), N-doped graphene (2D carbon nanomaterial), carbon black (non-fibrous form). Cells were also exposed to a non-nanofibrous positive control (asbestos fibers). We used a multistage approach based on four levels of toxicity testing. The first tier was based on toxicity tests (Alamar blue, crystal violet, and LDH assay). The protocols had to be modified somewhat to adapt them to the use of nanoparticles. At this level, it is possible to define the range of action of nanomaterials and to study the effects of exposure on cell viability and metabolism. At the second level, it's toxicogenomic analysis. This type of test allows a more comprehensive and complete view of what type of response the cells show to exposure to the materials. Moreover, toxicogenomics being a no-hypothesis driven approach, allows an unbiased investigation on the functional effecst of a given materials. As a third and fourth level, we looked at genotoxicity and ROS formation, which can be highly interconnected. Overall, this multi-level approach is the basis to build up an Integrated Approach to Testing and Assessment (IATA) of carbon nanomaterial.

Bibliography

Alwarappan, S., Erdem, A., Liu, C. & Li, C., 2009. Probing the Electrochemical Properties of Graphene Nanosheets for Biosensing Applications. *The Journal of Physical Chemistry*, Volume 113, pp. 8853-8857.

Donaldson, K., Poland, C. A., Duffin, R. & Bonner, J., 2012. *The toxicology of carbon nanotubes.* New York: Cambridge University Press.

De Marchi, L., Pretti, C., Gabriel, B., Marques, P. A., Freitas, R., & Neto, V., 2018. An overview of graphene materials: Properties, applications and toxicity on aquatic environments. *Science of the Total Environment*, Volume 631-632, pp. 1440-1456.

Chapter 3

Unraveling the potential toxicity of carbon nanotubes by RNA-seq transcriptomics

(manuscript intended for submission in Nanotoxicology)

Abstract

Toxicity of carbon nanomaterials (NMs) such as CNTs is linked to bio-nano interface with the environment. Nanostructures with rigid surface, like some CNTs, can interact with biological systems giving rise to membrane damage, frustrated phagocytosis, DNA insults. CNTs may activate immune cells generating cytokines, like interleukins and Tumor Necrosis Factor (TNF)-a, and/or activate signalling cascade such as mitogenic activated phosphorylation kinase (MAPK). Despite the aforementioned effects have been fairly described in literature, often CNT preparations may be barely cytotoxic and have been put in the market into different products. Due to the uncertainty of long-term NM effects on human health a safe-by-design approach for developing new NM-applications has been recently proposed. Here we propose the use of a multi-tier approach encompassing quantitative transcriptomics to predict long-term toxicity of multi-walled carbon nanotubes (MWCNTs) in a human mesothelial cellular model. MET5A cells were challenged with carbon fibers (CNTs) and non-fibrous carbons(carbon blacks) at 4-256 μg/mL (1.25-80 μg/squared cm). Cytotoxicity assays showed no loss of cell viability, almost always increased cell growth

and in a few cases marginal effects at the membrane level as judged by the external LDH activity. By contrast quantitative RNA-sequencing highlighted hundreds of differentially expressed genes in all treatments suggesting significant biological interactions. Our results showed that some CNTs shared a consistent number of differentially expressed genes with tumorigenic crocidolite asbestos and those genes are involved in cellular processes related to cell cycle control, DNA metabolism and repair, chromosome stability and cancer. CNT elicited genotoxicity and high rate of ROS formation suggests the two responses are linked A multi tier approach including quantitative transcriptomics may represent a significant advance over classical cytotoxicity assay to predict long-term effects/risks of CNTs before they enter market applications or for the development of safe-by-design approaches.

Keywords: Asbestos, Cancer, Nanomaterial, Next Generation Sequencing (NGS)

1. Introduction

In the last decades nanomaterials (NMs) have seen great increase in their production and use in many products. Global nanotechnology market is expected to exceed 125 billion $ by 2024 (O' Coileain , 2021).

Carbon nanotubes (CNTs) represent a very interesting group of NMs for a large number of applications due to their unique qualities. In addition, they are the most important component of the current large-scale production of NMs due to industrial synthesis at the price of $200/kg (Mulvaney & Weiss 2016, Kane et al. 2018). They are

formed from a sheet of hexagonal-shaped carbon atoms rolled up to create a cylinder. There are two forms of CNTs depending on the numbers of their layers. They are referred to as single walled carbon nanotubes (SWCNTs) when they are formed from a single layer of graphene sheets and multi-walled carbon nanotubes (MWCNTs) when they are formed from more than one concentric layer of graphene.

CNTs have unique mechanical (flexibility and resilience), electronic (metallic or semiconducting) properties, and their high aspect ratio makes them capable of bridging a lot of molecules. These unique properties makes them useful in many application areas, from electronic devices (such as atomic force microscopy or scanning tunneling microscopy), to field- emission devices (such as flat-panel display, X-ray sources, electron guns for electron microscopy, microwave amplifiers), to transistor and optoelectronic devices (CNT field-effect transistor are at the base of photoswitches, photodetectors, solar cells), electrodes (touch-screen displays, photovoltaic, display bus bar, supercapacitors, lithium batteries, fuel cells, sensors), hydrogen storage, biomedical applications (CNTs are used for drug delivery, in imaging techniques, functionalized CNTs are used for bone scaffolds, vascular stents, neuron growth and regeneration) (Donaldson et al. 2012). Taking into account the widespread use of CNTs it has become important to assess their possible impact on human health. Indeed, in 2004, the Royal Society and the Royal Academy of Engineering admitted the physical similarity to asbestos fibers and thus the potential risk for human health (Kane et al. 2018).

CNTs can enter into the human body through various ways of exposure such as dermal explosion and ingestion, but the most interesting way

is the respiratory system. The importance of assessing possible accumulation in lungs is also linked to the structure of CNTs, which resembles fibers. Several *in vivo* experiments have demonstrated the pulmonary effect of CNTs. In mice, CNTs showed peri-bronchial inflammation, necrosis, granulomas and fibrosis, oxidative stress, collagen deposition (Lam et al. 2004, Shvedova et al. 2005, Li et al. 2007, Poland et al. 2008). Similar type of responses were founded in rat exposed to CNTs, with inflammation, granulomas, lung fibrosis and collagen deposition (Warheit et al. 2004, Muller et al. 2005, Morimoto et al. 2012, Francis et al. 2015, Francis & Davasena, 2018). The time-consuming and unsuitability for high-throughput screening of *in vivo* models determined the need for good *in vitro* models to study CNTs. Following the inhalation model, the most suitable cell types for *in vitro* studies were alveolar and bronchial epithelial cells (they represent the site of fiber deposition), macrophages, which have the role of clearing the respiratory system of foreign particles, and mesothelial cells, which represent the main target where mesothelioma develops. The largest number of experiments were conducted on epithelial cells, demonstrating a dose-dependent decrease in cell viability for (Srivastava et al. 2011). Cytotoxicity was also observed in A549 and BEAS-2B exposed to SWCNTs (Herzog et al. 2007). Dispersion of CNTs was shown to increase cytotoxicity in epithelial models; lung surfactant, sonication or different types of solvent were used for dispersion (Wang et al. 2010, Asakura et al. 2010). In epithelial cells (A549 cells) exposed to MWCNTs or SWCNTs, a dose-dependent increase in ROS generation was observed, production of which was completely stopped after CNTs purification from metal (Pulskamp et

al. 2007). Herzog et al. (2009) exposed epithelial cells to various materials and observed that their effects changed depending on the culture medium and the presence of dispersant, in fact, serum reduced ROS production, whereas lung surfactant increased ROS production.
Data seems to emphasize a low ability of CNTs in epithelial cells to induce the activation of pro-inflammatory responses (Herzog et al. 2009, Muller, et al., 2010). Baktur et al. (2011) in contrast, observed a time-dependent IL-8 secretion by A549 exposed to HiPCO™-derived SWCNTs, with an increased effect in presence of serum. Epithelial cells exposed on CNTs also showed genotoxic effects by micronucleus and Comet assay (Muller et al. 2008, Thurnherr et al. 2011). Fewer data are available on mesothelial cells. Pacurari et al. (2008) showed that SWCNTs stimulate ROS and DNA damage in mesothelial cells with partial reduction in damage by ROS scavengers. Maruyama et al. (2015) showed a reduction in cell viability in a dose-dependent way in human mesothelial cells, but still higher than in human bronchial epithelial cells. Haniu et al. (2014) showed consistently lower toxicity in mesothelial cells than in epithelial cells, in fact, epithelial cells had most CNTs in lysosomes whereas mesothelial cells had CNTs dispersed in cytoplasm. Lohcharoenkal et al. (2013) observed that human lung mesothelial cells exposed to SWCNTs, MWCNTs and asbestos showed a significantly higher growth rate than controls, and cells exposed to CNTs also showed a significant increase in cell invasion and migration.
These cells also showed a high regulation of MMP-2 expression along with other genes such as SERPINE1, CAV1 and AKT1, that are also up regulated in asbestos-transformed cells. To confirm MMP-1

centrality in the invasion mechanism, they generated knockdown of MMP-1 and obtained a substantial reduction in cell invasion compared with control cells. Lindberg et al. (2013) showed EC50 in the cytotoxicity of human lung mesothelial cells exposed to SWCNTs and MWCNTs after 24-48-72 h exposure between 40-60-100 μg/cm^3 exposure dose. Cells showed the ability to uptake CNTs into the cytoplasm. SWCNTs induced DNA damages after both 24 and 48 h exposition tests. MWCNTs induced a significant increase in DNA damage in 48 h of exposure only in the highest doses treatments.

The International Agency for Research on Cancer had mandated experts in occupational health, epidemiology and toxicology to identify the potential carcinogenesis of CNTs. Human carcinogenesis is classified into four group of exposure agents: group 1- carcinogenic to humans, group 2A- probably carcinogenic to humans, group 2B- possibly carcinogenic to humans, group 3- not carcinogenic to humans and group 4- probably not carcinogenic to humans. The great variability of CNTs data *in vivo* and *in vitro* studies and the absence of epidemiological data for humans have made CNTs classification very difficult, so that only one type of CNTs (MWCNT-7) has been classified in group 2B as possibly carcinogenic to humans, i.e. long, large-diameter and rigid (Grosse et al. 2014, Kane et al. 2018, Moller et al. 2021). However, in genotoxicity assay short MWCNTs (<1 μm in length) can induce DNA damage (Kuempel et al. 2017, Kane et al. 2018).

In this study, a broad transcriptome analysis was performed to investigate the mechanistic effects of carbon nanotubes, incorporating this assessment into a multi-tier approach of cytotoxicity and

genotoxicity. The approach was validated using a library of CNTs of varying composition, size, purity, and diameter in a human pleural mesothelial model, MeT5A cells. Reference materials such as carbon black nanoparticles were used as a form of amorphous carbon.

2. Materials and Methods

2.1. Materials

Multi walled-carbon nanotubes (MWCNTs) were produced and supplied by Nanothinx S.A. (Rio Patras, Greece) as part of the H2020 MSCA-RISE Nanogentools project. Three different types were provided with two sizes, long and short (suffix s) (NTX1; NTX1s; NTX3; NTX3s; NTX4; NTX4s). Preparation of the MWCNTs was performed by the chemical vapor deposition (CVD) method from hydrocarbon sources on metal oxide (aluminum) substrates permeated with different metal catalysts (trade secret belonging to the manufacturer). Characterisation of the MWCNTs was performed using scanning electron microscopy (SEM), Raman spectroscopy, energy dispersive X-ray spectroscopy (EDX) and X-ray crystallography (XRD) as described in (Manfredi et al. 2016; Sweeney et al., 2015). The purity of the materials was estimated by thermo-gravimetric analysis (TGA), following post-deposition treatment (Bardi et al. 2009). A few other materials were used as reference controls. Carbon Black nanoparticles used in this work are commercially available under the Vulcan XC-72R™ (Fuel Cell, College Station, TX, USA). N-

graphene was manufactured by means of exfoliation of graphite rods via pulses of current methods as previously described in Baldea et al., (2020). Crocidolite asbestos was used at 5 μg/mL in the ROS assay (kind gift of Dr. Alessandro Croce, DISIT, University of Piemonte Orientale).

2.2. Cellular cultures

MeT-5A cells were cultured in Dulbecco's Modified Eagle's Medium (DMEM) with 10% foetal bovine serum and 1% penicillin-streptomycin, at 37 °C under controlled humidity and 5% CO_2 (Han et al. 2012). Cells were grown on multi-well plates and seeded 24 h before treatment to allow them to reach 40-50% confluence level. CNTs were prepared as 100x concentrated stable suspension in PBS/2% fetal bovine serum and autoclaved for 20 minutes at 121°C. Dilutions for each concentration tested were prepared in complete cell culture medium immediately prior to the start of the experiment. Four concentration levels were used: 4 μg/mL, 16 μg/mL, 64 μg/mL, 256 μg/mL corresponding to 1.25; 5; 20; 80 μg /cm^2. Cells were incubated for 72 hours in a controlled environment incubator.

2.3. Cytotoxicity testing

For the Alamar Blue assay, resazurin (Calbiochem Research Biochemicals, Merck, Darmstadt, Germany) was prepared at a concentration of 10 mg/mL in sterile PBS and used as a 10X concentrated stock solution. Cells were prepared and processed as described in Section 2.2. After addition of resazurin, cells were incubated for 2 h at 37 °C, 5% CO_2 and fluorescence was read in a final volume of 150 µl using an Infinite® 200 Pro plate reader (Tecan Sales AG, Mannedorf, Switzerland) with a 540- 570 nm excitation / 580-610 nm emission filter set. Data are presented as arbitrary units of fluorescence. Extracellular LDH enzyme levels were determined semi-quantitatively with the CyQUANT LDH Cytotoxicity Assay (Thermofisher Scientific, Waltham, MA, USA) using 50 µl of cell culture supernatant. Intrinsic N-graphene activity was subtracted to calculate net extracellular LDH values. Data are presented as absorbance units at 490 nm.

2.4. RNA sequencing

Cell samples were lysed in a microplate using a lysis buffer. The cell medium was removed and the cells were washed twice with sterile PBS. Cell lysis was performed with the lysis buffer directly in the microplate. Immediately, RNA extraction was performed with the RNA kit based on serial centrifugation on silica membrane, with DNase added (NucleoSpin®-RNA II- Macherey-Nagel, Duren,

Germany). Elution was performed with RNase-free water. Samples were stored in a freezer at -80 °C. The quality of each RNA preparation was verified by both UV/vis spectroscopy (230/260 nm) and high-resolution TBE 1.3% agarose gel electrophoresis in the presence of ethidium bromide loading buffer (Banni, et al., 2011). The RNA samples were analyzed by massive parallel sequencing on an NextSeq 500 system™ (Illumina Inc, San Diego, CA, USA). The cRNA libraries were prepared from 100 ng of total RNA using the TruSeq Stranded (reverse) mRNA kit® (Illumina, Inc, San Diego, CA, USA). Sample preparation, including controls, and sequencing were outsourced to Genomix4Life (Salerno, Italy). Sequences in compressed Fastaq (Gunzip) format were analysed using MiARma-seq (Andrès-Leon et al, 2016) .

2.5 RNA sequencing (RNA-seq)

The 18 RNA samples, as previously described, were subjected to massively parallel sequencing on an Illumina NexSeq500 platform, using a MID flowcell with a capacity of 280 million short reads (2x75 bp, Paired-end). The cRNA libraries were prepared from 100 ng of total RNA using the TruSeq Stranded (reverse) mRNA kit (Illumina, Inc.). Sample preparation, including controls, and sequencing were outsourced to Genomix4Life (Salerno, Italy) affiliated with the Laboratory of Molecular Medicine and Genomics, Campus of Medicine, University of Salerno.

Sequences in compressed Fastaq format (Gunzip) were subjected to a bioinformatics procedure using miARma software (Andrès-Leon et al., 2016) in a Unix/Posix mainframe system equipped with AMD EPYC 7351P Naples 16C/32T 2.4GHz 64Bit processor (Advanced Micro Devices, Inc, USA); 32GB DDR4-2400MHz Ecc-Registered RAM memory (Kingston Technology Company, USA); SuperMicro h11ssl-i-b motherboard (Super Micro Computer, Inc, USA); Ubuntu Server 16.04.4 LTS operating system (GNU/Linux 4.15.0-24-generic x86_64).

MiARma is a software that allocates other specific software including dependencies for their operation. The procedure set up in miARma consists of: 1) Mapping of reads to the Homo sapiens GRCh37 reference genome (Ensembl); 2) ReadCount, which consists of annotation of mapped reads and the frequency obtained in individual samples; 3) DE Analysis, analysis of differentially expressed genes. Each cRNA library obtained from each of the 18 samples was sequenced in paired mode from both ends of the library, generating high-quality aligned sequence data. For each sample, therefore, 2 files, called R1 and R2, were obtained, each of approximately 8 million reads of 75 bp. Bowtie2 software was used for paired-mode reads mapping through the following options:

[Aligner]

aligner=tophat

tophat_aligner=bowtie2
bowtie2index=/Homo_sapiens/Ensembl/GRCh37/Sequence/Bowtie2Index/genome
gtf=/Homo_sapiens/Ensembl/GRCh37/Annotation/Genes/genes.gtf

The ReadCount command, implemented in miARma, was used in meta-feature mode (through the -g Gene_id option) to create a contingency table between each mapped Homo sapiens gene and its respective relative frequency (per million reads) in each of the 18 samples. MiARma requires an annotation file in Gtf2.2 format (http://mblab.wustl.edu/GTF22.html). The parameters used for ReadCount were as follows:

[ReadCount]

database=/Homo_sapiens/Ensembl/GRCh37/Annotation/Genes/genes.gtf

seqid=gene_id

featuretype=exon

parameters=-O -M --fraction

Finally, EdgeR software (Robinson et al., 2010) was used to evaluate differentially expressed genes. The following parameters were used for DE analysis:

[DEAnalysis] desoft=EdgeR

filter=yes

cpmvalue=2 edger_normethod=TMM replicates=yes Translated with

2.6. ROS formation Assay

ROS formation was semiquantitatively evaluated using the cell-permeant 2',7'-dichlorodihydrofluorescein diacetate (H2DCFDA) dye (Thermofisher Scientific, Waltham, MA, USA). After cell exposure, cells were washed three times in sterile PBS and H2DCFDA dissolved in DMSO was added at a final concentration of 2.5 µM from a 100-fold concentrated stock solution. After incubation at 37 °C for 30 min to allow dye penetration, cells were washed twice in PBS. Finally, 100 µl of PBS was added to each well and fluorescence was recorded for 30 min using a 485 nm excitation and 535 nm emission filter in a plate-reading fluorimeter (Tecan). ROS are expressed as arbitrary units representing the slope of the linear curve obtained from the kinetic measurement.

2.7. Micronucleus Assay

The micronucleus assay was performed with cells grown on glass coverslips. The assay procedure and micronucleus frequency counting were performed according to Fenech (2007). After exposure, the cell medium was removed, the cells were washed three times in sterile PBS

and left in air for 10 minutes. One (1) ml of methanol was added and incubated for 15 minutes for fixation. The methanol was discarded and the samples were allowed to air dry completely. The samples were rehydrated in Hank's balanced salt solution, and the coverslips were cleared of excess liquid and embedded in Floromount-G™ with DAPI (Invitrogen, Thermofisher Scientific, Waltham, MA, USA). Slides were evaluated under a fluorescence microscope at 400x magnification and analysed for micronucleus frequency using digital image analysis.

2.8. Statistical analysis

Statistical analysis was performed using ANOVA after square root or logarithmic transformation of the data, tests of homogeneity (Levene's test) and normality (Lilliefors K-S test and Shapiro-Wilk test). The data analysed resulted from at least four independent experiments. Non-parametric statistics (Kruskal-Wallis two-sample test and Kolmogorov-Smirnov test) were used at $p \leq 0.05$, when it was not possible to meet the criteria of the ANOVA. Systat 12 statistical software (Systat Software, Inc, San Jose, CA, USA) was used for the calculations. The EdgeR software (Robinson et al., 2010) was used to evaluate differentially expressed genes at $p < 0.05$ with false discovery rate.

3. Results

3.1. Cytotoxicity of CNTs

An overview of the CNT used is presented in Table 1.

Table 1. CNTs features

	NTX1			NTX3			NTX4		
	% Purity	External diameter	Length	% Purity	External diameter	Length	% Purity	External diameter	Length
Long	97	15-35 nm	>10 µm	< 98.5	20-40 nm	>10 µm	<94	6-15 nm	>10 µm
Short (tip sonication)	97	15-35 nm	< 1 µm	< 98.5	20-40 nm	< 1 µm	<94	6-15 nm	< 1 µm

The cytotoxic effect of CNTs was evaluated by three different assays: crystal violet, Alamar blue, and extracellular LDH activity in three different types of CNTs with different length, diameter, and purity. A total of 27 experiments were performed and their results were classified into a matrix of 29 variables that were either continuous or categorical, including some physicochemical descriptors of CNTs, e.g., concentration, size, fiber structure (yes or not), carbon material (yes or not) (Appendix 1, available at https://docs.google.com/spreadsheets/d/1hYWMVgHg_Vqjp2ZVc2HAtJlbp5EMxnC4/edit?usp=sharing&ouid=103966756390968203242&rtpof=true&sd=true). Figure 1 shows the relative effects of CNTs on the viability (Crystal Violet Assay) of MeT5A cells exposed for 72 hours compared to control cells exposed to vehicle. In general, the data showed a statistically significant increase in cell density for the effects of exposure to carbon nanomaterials (Kruskal-Wallis, $p < 0.01$). This difference appears to be due to NTX1 (both long and short) having the

highest mitogenic effect compared to NTX3, NTX4, and CB (Kolmogorov-Smirnov Two Sample Test, $p < 0.01$). The effects of the grouping variables *type* and *concentration* of carbon nanomaterial (either long or short) were statistically significant (Kruskal-Wallis, $p < 0.001$), the effect of *size* was marginally significant ($p=0.065$), while the effect of fiber was not.

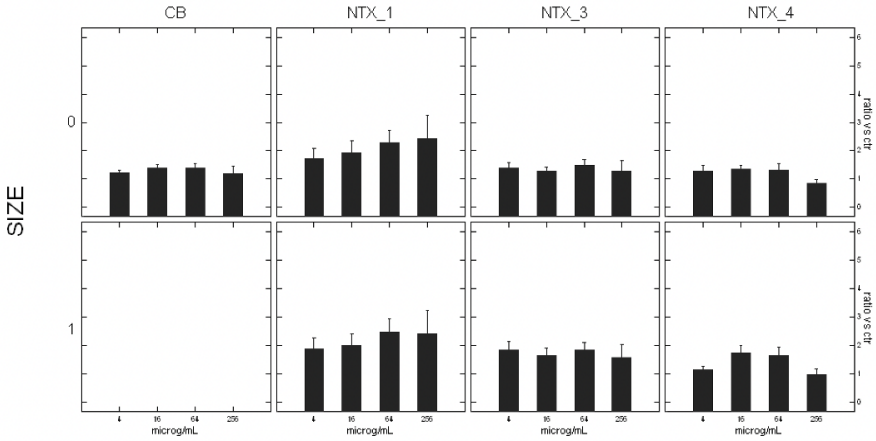

Figure 1. Crystal Violet viability assay. Data (average ± standard error from four independent experiments) are expressed as relative level respect to control vehicle-exposed cells. Legend, NTX_1, NTX_3, NTX_4, Nanothinx CNTs; 0, short CNT; 1 long CNT; CB, carbon black (see text for statistical details).

The results of Alamar Blue were not dissimilar to those of crystal violet (Figure 2). Indeed, the fluorescence level of all treated samples exceeded that of the reference control (Kruskal-Wallis, $p < 0.05$), except for the highest concentration tested (256 µg/mL), which showed a statistically significant decrease in all cases. In fact, statistical analysis showed a significant effect at $p < 0.05$ on cellular metabolism

for the grouping variable *concentration* (either long or short), but not for *type* or *size* or *fiber* (long or short CNT) (Kruskal-Wallis, $p < 0.05$).

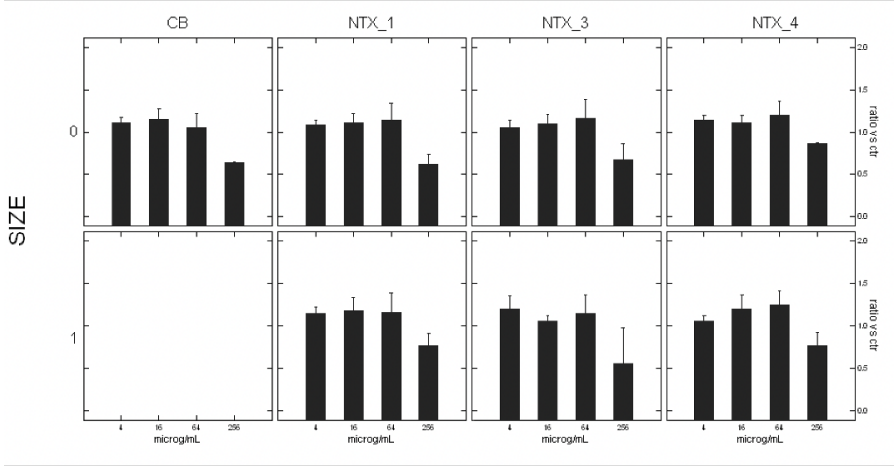

Figure. 2 Alamar Blue assay. Caption as for Figure 1 except results of the Alamar Blue assay are shown.

Figure 3 shows the results of the extracellular LDH assay, which allowed us to investigate possible damage to the plasma membrane caused by fiber puncture. Statistically significant results were obtained only for NTX4, which is the thinner CNT (Kruskal-Wallis, $p < 0.05$). Indeed, NTX4 differs from both the vehicle-exposed control and the other carbon nanomaterials. Other statistically significant associations exist for the grouping variables *fiber*, *types*, *concentration* (short only), but not for *size* itself (Kruskal-Wallis, $p < 0.05$)

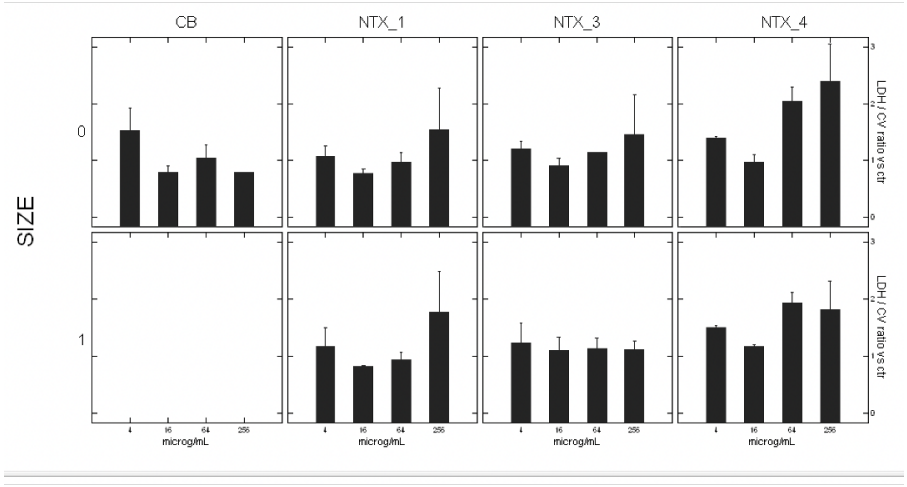

Fig 3. LDH assay. Caption as for Figure 1 except results from the Alamar Blue assay are shown.

3.2. RNA-sequencing

Toxicogenomics by RNA-seq short reads transcriptomics yielded 259,750,112 total reads for 9 different conditions (long or short NTX1, NTX3, NTX4; CB, crocidolite asbestos (CR), and the reference control) and two replicates, of which 223,906,126 (89.17%) mapped to the reference genome GRCh37 (Ensembl). The annotated and counted reads were annotated using the ReadCount tool to determine the relative abundances of expressed genes. Differentially expressed genes (DEGs) were finally identified using EdgeR compared to MeT5A (vehicle) control samples. Figure 4 shows the number of differentially expressed genes for each treatment.

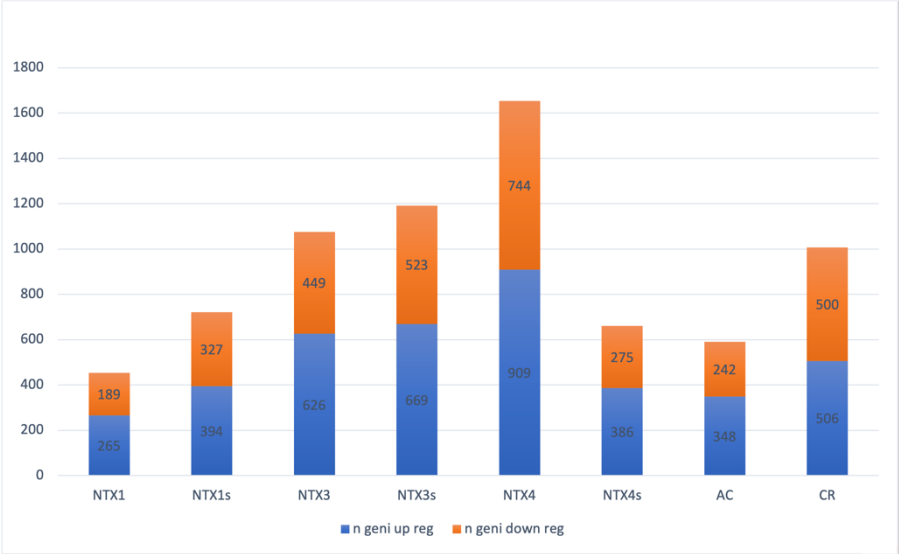

Figure 4. Differentially expressed genes in MeT5a. Legend, NTX1, NTX3, NTX4, Nanothinx long CNTs; NTX1s-3s, Nanothinx short CNTs; AC, carbon black; CR, crocidolite asbestos.

The DEGs were grouped using the Venn diagram to look for patterns between the different treatments. It was found that most DEGs match between fibrous (CNTs) and amorphous carbon (carbon black) (Figure 5; Table 2), suggesting that there is a core response to carbon nanomaterials that is not necessarily fiber-dependent. At the same time, there is a consistent overlap between long and short fibers and with crocidolite asbestos. In addition, NTX4 showed the greatest overlap with CR, NTX3 occupied an intermediate position, while NTX1 showed the least overlap (Figure 5). Surprisingly, NTX1s behaved differently from the other CNTs in the sense that the short fiber elicited

a stronger response in terms of the number of DeG and similarities with carcinogenic long asbestos fibers.

Table 2. Results of pairwise comparisons obtained by Venn diagram.

DEG		454	721	1075	1192	1653	661	1006	590
		NTX1	NTX1s	NTX3	NTX3s	NTX4	NTX4s	CR	CB
454	NTX1		33%	29%	24%	20%	30%	25%	36%
721	NTX1s	52%		49%	40%	35%	69%	49%	63%
1075	NTX3	69%	73%		59%	49%	73%	56%	73%
1192	NTX3s	63%	66%	65%		48%	68%	52%	76%
1653	NTX4	74%	80%	78%	67%		80%	58%	80%
661	NTX4s	44%	64%	45%	38%	32%		32%	60%
1006	CR	56%	69%	52%	44%	36%	49%		70%
590	CB	47%	52%	40%	38%	29%	54%	41%	

The table shows the number of total DE genes and the percentages of overlap between the conditions analyzed. The results can be interpreted bi-directionally, e.g. AC vs NTX4 or NTX4 vs AC. Legend as in Figure 4.

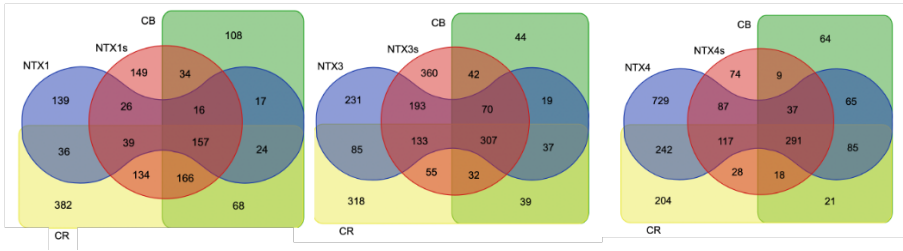

Figure 5. Venn diagram classification. Figure shows Venn diagrams with 4 conditions obtained from DEG of long and short CNTs and crocidolite asbestos. The figure shows the number of DE genes found under the different experimental conditions. Legend as in Figure 4.

Pathway analysis was used for functional analysis of differentially expressed genes in CNTs, carbon black, and crocidolite asbestos using various open source tools such as gProfile software (Raudvere, et al., 2019). Through an additional Venn diagram considering common genes related to the comparison in Figure 5, we extrapolated 128 genes representing the core of the molecular response observed in MeT-5A cells in response to carbon nanomaterials and crocidolite asbestos. These genes are listed in Table 3.

Table 3. The core response of MeT-5A to carbon materials and crocidolite asbestos

pathway	*description*	*count in gene set*	*false discovery rate*
hsa03030	DNA replication	12 of 36	1.23E-14
hsa04110	Cell cycle	11 of 123	4.36E-08
hsa05206	MicroRNAs in cancer	7 of 149	0.002
hsa01522	Endocrine resistance	6 of 95	0.002
hsa03410	Base excision repair	4 of 33	0.0026
hsa03420	Nucleotide excision repair	4 of 46	0.0071
hsa03430	Mismatch repair	3 of 23	0.0133
hsa05418	Fluid shear stress and atherosclerosis	5 of 133	0.034
hsa05224	Breast cancer	5 of 147	0.0462
hsa05222	Small cell lung cancer	4 of 92	0.0462
hsa05215	Prostate cancer	4 of 97	0.0462
hsa05200	Pathways in cancer	9 of 515	0.0462
hsa05166	HTLV-I infection	6 of 250	0.0462
hsa05165	Human papillomavirus infection	7 of 317	0.0462
hsa04750	Inflammatory mediator regulation of TRP channels	4 of 92	0.0462
hsa04658	Th1 and Th2 cell differentiation	4 of 88	0.0462
hsa04330	Notch signaling pathway	3 of 48	0.0462
hsa04218	Cellular senescence	5 of 156	0.0462
hsa00533	Glycosaminoglycan biosynthesis - keratan sulfate	2 of 13	0.0462
hsa00240	Pyrimidine metabolism	4 of 100	0.0462

Shown are Kegg Pathway ID, description, count and p value (false discovery rate)

DNA replication and cell cycle are strikingly significant, then the list is dominated by several cancer-related pathways, immune related disease and DNA repair systems.

In Supplementary Information of this chapter, the whole set of pathway analysis is presented. Clearly long NTX3, long NTX4 and short NTX1 present several enriched pathways linked to DNA insult, DNA repair, p53, tumor, etc.

3.3. Micronucleus assay

Micronucleus frequency assay measures unrepairable double-stranded DNA breaks in replicating cells. For these experiments, cells were

exposed to the lowest contaminant concentration of 4 μg/mL for 72 hours. The results are shown in Figure 6. All treatments showed a statistically significant increase in micronucleus formation (Kolmogorov-Smirnov Two Sample Test, $p < 0.001$), except for cells exposed to CB and NTX4 short. The highest increase in micronucleus formation was observed in cells exposed to NTX3 long. There were no significant differences in the effect of NTX1 regardless of fiberand size, whereas for NTX3 and NTX4 size was significant (Figure 6, left panel). The data were also pooled and analyzed by group, resulting in the finding that treatment with non-fibrous materials (CB, N graphene) was not different from the reference control, while there was a significant difference between fibers and non-fibers (Kruskal Wallis < 0.01).

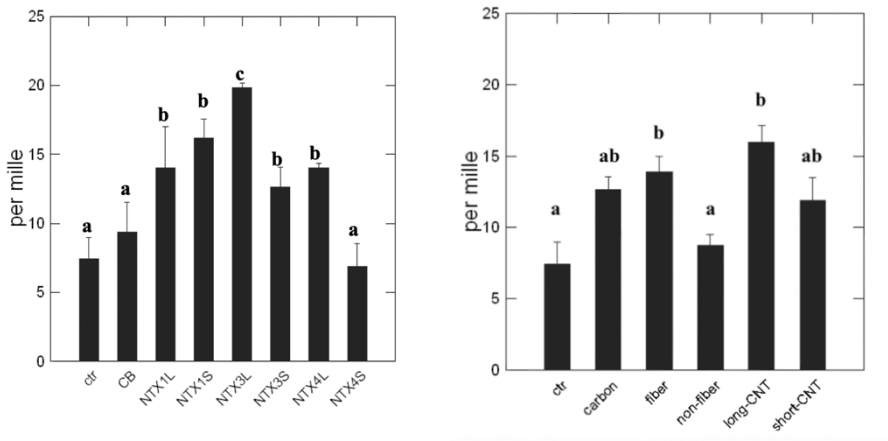

Figure 6 CNT genotoxicity. Micronucleus frequency (per mille) ± standard error from four independent experiments was evaluated in MeT5a cells exposed to each material at 4 µg/mL for 72 h (Left Panel) or group of material (right Panel). Bars that do not share a common letter are significantly different from each other (two side probabilities from Kolmogorov-Smirnov Two Sample Test, $p < 0.001$). Legend: ctr, vehicle exposed reference control; CB, Carbon Black; NTX1L,NTX1s, NTX3L, NTX3s, NTX4L,NTX4s, Nanothinx CNTs, S- short and L- long.

3.4. ROS formation

ROS represent a triggering event for genotoxicity, therefore the formation of ROS in MeT5a cells at low CNT exposure was assessed as described for micronuclei. Figure 7 shows the significant increase of ROS in NTX3 effects and to a lesser extent in NTX1 and NTX4. NTX3 scored the highest and no size effects were observed. Crocidolite asbestos was used as a positive marker.

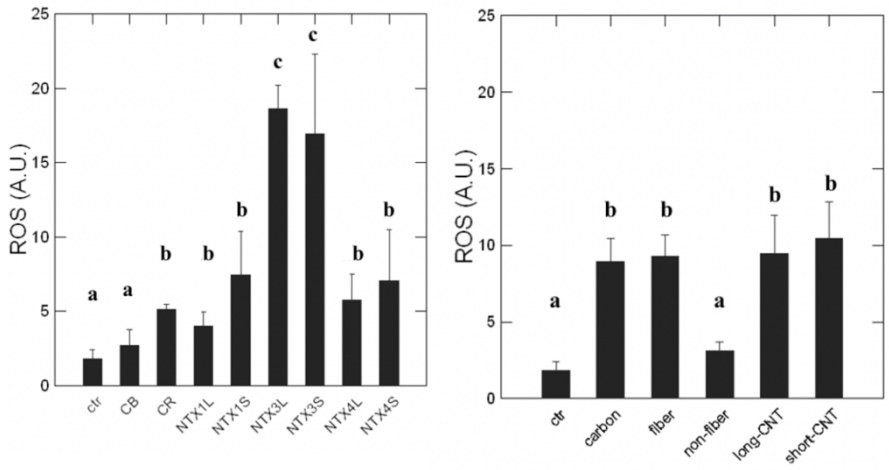

Figure 7. ROS formation. As for Figure 6 except ROS arbitrary units ± standard error from four independent experiments. Bars that do not share a common letter are significantly different from each other (two-way ANOVA, $p < 0.05$, Tukey's post hoc test for pairwise comparison).

Regarding micronuclei, after regrouping materials into treatment classes, a significant increase in ROS values is observed for carbon, fiber, long-CNT, and short-CNT. While fiber and non-fiber are different, non-fiber and control showed no statistically different effects at $p < 0.05$ (Tukey's post hoc pairwise comparison)

4. Discussion

In this study, we aimed to investigate the potential toxicity of CNTs in a human pleural mesothelial cell model (MeT-5A). MeT-5A is a good model for the toxicology of CNTs (Lindberg, et al., 2013), but there are limited data on the toxicology of CNTs in mesothelial cells, the target of mesothelioma tumor. Three different types of MWCNTs (NTX1, NTX3 and NTX4) in two sizes (short and long), a non-fibrous form of carbon nanomaterial (CB - Carbon Black) were used as model carbon nanomaterials. The method for testing the toxicity of the CNTs was based on a multi-tier approach including cytotoxicity assays (Alamar Blue, Crystal Violet and LDH assay), genotoxicity (micronucleus assay), mechanistic assays (ROS level assay) and toxicogenomic analysis. The cytotoxicity assay showed us a general increase in cell numbers and cell activity, which always highlights a significance for the concentration of contaminants. As with the LDH assay, both the type and concentration of exposure showed a significant increase in membrane damage, with the thinner CNTs in particular being the most effective. When we compare our results with data from the literature, we find that most of them indicate inhibition of cell viability. (Rozhina, et al., 2021) showed that A549 cells exposed to MWCNTs exhibited a dose-dependent inhibition of viability, which was due to a decrease in proliferation and metabolic activity of the cells. In the same cell type, other authors confirmed the same results, namely a decrease in cell viability (Azari & Mohammadian, 2020) (Requardt, et al., 2019). It is important to emphasize that mesothelial cells do not have high endocytosis rates and therefore the uptake of

nanomaterials is definitely lower than other cell types. In fact, Lohcharoenkal, et al. (2013) found a significant increase in proliferation of mesothelial cells exposed to SWCNTs and MWCNTs upon chronic exposure. Requardt, et al. (2019) showed an increase in LDH release in two cell types (A549 and HepG2) exposed to CNTs, indicating membrane damage. However, cytotoxicity is not fully informative and, in particular, does not take into account the mode of action of the toxic agent. Therefore, we used toxicogenomics by RNA sequencing as the second step of toxicological evaluation. The results obtained showed a large number of genes differentially expressed in cells exposed to CNTs, particularly in NTX3 (long and short) and NTX4. Thanks to the classification of differentially expressed genes, we found that 359 genes overlap in the molecular response signature of NTX4 and crocidolite and 218 genes overlap between NTX3 and crocidolite, a tumorigenic fiber, but at the same time these features are not differentially expressed in amorphous carbon (CB). NTX1 has only 75 genes in common, and NTX1 short 173. Pathway analysis related to DNA damage and cancer: p53, TP53, activation of ATR in response to replication stress, defective DNA repair, telomere C-strand process, chromosome maintenance. These results, which we found mainly in NTX3 and NTX4, suggest genomic instability and could be fully confirmed by the genotoxicity and ROS formation data. We cannot say that NTX1 (both long or short) lacks terms related to tumor, cell cycle, and/or DNA repair, but it clearly lacks some more specific terms found in NTX3 and 4 repertoire. This evidence seems to suggest that NTX1 may be less reactive and represent lower risk compared to the other two CNTs. This part of the work was performed immediately after the

cytotoxicity tests, so we could focus our interest on genotoxicity. The third stage of toxicity assessment was indeed genotoxicity based on micronucleus frequency. We chose to measure double-strand breaks because they are non- repairable, inheritable, and predictive of the risk of exposure to carbon nanomaterials in this and future generations. MeT-5A exposed to the lower concentration of carbon nanotubes showed significant production of micronucleus in all treatments except NTX4 short. Other researchers have tested possible DNA damage in cells exposed to CNTs. For example, (Moller, et al., 2021) described different experiments performed on BEAS-2A and A549 cells that yielded different results. Louro, et al, (2016) showed that the results of exposing BEAS-2A and A549 cells to four different types of MWCNTs could be very different in the formation of micronuclei, with production increasing in A549 cells exposed to NM -401 and NM -402 CNTs, while this was not the case for the same cell type exposed to NM -403 and NM -400 CNTs. At the same time, BEAS-2A cells exposed to all four MWCNT types showed no effect on micronuclei formation. It is important to emphasize that these MWCNTs may differ in diameter, length, purity, and stiffness. In other literature data, an increase in micronucleus formation was observed in BEAS-2A cells exposed to MWCNTs-7 (Fraser, et al., 2020). ROS may be responsible for DNA damage and cancer-related processes. Often, the formation of ROS is the initiating event of a complex pathological condition. Our results showed a significant increase in ROS concentration in cells exposed to all CNT types, regardless of size. It is worth mentioning that CNT may be more effective than crocidolite asbestos in the formation of ROS. This kind of result highlights how fibrous

components lead to ROS formation, and at the same time, we have shown that size does not matter for the production of ROS because there is no difference between the effects of long and short CNTs. In the micronuclei assay, we did not detect a significant size effect due to the high effects found for NTX1 short. However, these data may indicate that ROS alone is not sufficient to induce genotoxicity. Regarding the production of ROS, our hypothesis is that they are generated by metals, especially iron and nickel, used in vapor deposition to produce CNTs. Despite it's trade secret, Sweeney et al,. 2015 demonstrated the presence of such metals in several CNT preparations of this type. We frequently observed micronuclei in cells surrounded by tangled CNT clusters (see supplemental information). Another fundamental area in the toxicological evaluation of NMs is omics techniques. Considering all the points of this investigation through an "expert judgment", it is possible to confirm the existence of a risk for these CNTs. In defining the risk, it is important to consider the actual possibility of human exposure to the contaminant. It has been calculated that the major source of CNTs is the work environment and that the exposure dose for workers throughout their working lives ranges from 12.4-46.5 $\mu g/cm^2$ the (alveolar dose) (Gangwal, et al., 2011; Moller, et al., 2021). This value correspond to 7.5 10^{-3} $\mu g/cm^2$/day during the entire working life, considering we provided 1.25 $\mu g/cm^2$ the risk quotient is very low (1/6000), but this is a rough extrapolation that does not make any sense regardless to stimulate us to identify more sensitive Point of Departure and/or early warning markers of lung fibrosis to prevent mesothelioma tumors.

5. Conclusion

The results of this experimental work allowed the validation of a multilevel approach for assessing the hazard and risk of NMs. This approach also allowed for a simpler, faster, and more reliable assessment of the toxicity of carbon nanomaterials. Using an "expert judgment," we were able to define a potential long-term risk for the CNTs tested. In the future, these data could be incorporated into an integrated testing and assessment approach (IATA) for a structured safe-by-design approach for NM (bio)technological applications.

Bibliography

1. Andrés-León, E., Núñez-Torres, R. and Rojas, A.M., 2016. miARma-Seq: a comprehensive tool for miRNA, mRNA and circRNA analysis. Scientific reports, 6(1), pp.1-8.

2. Asakura, M., Sasaki, T., Sugiyama, T., Takaya, M., Koda, S., Nagano, K., Arito, H., Fukushima, S., 2010. Genotoxicity and Cytotoxicity of Multi-wall Carbon Nanotubes in Cultured Chinese Hamster Lung Cells in Comparison with Chrysotile A Fibers. Journal of Occupational Health. 52, 155-166.

3. Azari, M.R., Mohammadian, Y., 2020. Comparing in vitro cytotoxicity of graphite, short multi-walled carbon nanotubes, and long multi-walled carbon nanotubes. Environmental Science and Pollution Research. 27, 15401-15406.

4. Baktur, R., Patel, H., Kwon, S., 2011. Effect of exposure conditions on SWCNT- induced inflammatory response in human alveolar epithelial cells.. Toxicology In Vitro. 25, 1153-1160.

5. Banni, M., Negri, A., Mignone, F., Bousetta, H., Viarengo, A., Dondero, F. , 2011. Gene Expression Rhythms in the Mussel *Mytilus galloprovincialis* (Lam.) across an Annual Cycle. Plos One. 6(5), e18904.

6. Bardi, G., Vittorio, O., Maffei, M., Pizzorusso, T., Costa, M., 2009. Adipocytes differentiation in the presence of Pluronic F127-coated carbon nanotubes. Nanomedicine: Nanotechnology, Biology, and Medicine. 5, 378-381.

7. Donaldson, K., Poland, C. A., Duffin, R. & Bonner, J., 2012. The toxicology of carbon nanotubes. 1st Edition ed. Cambridge University Press, New York.

8. Fenech, M., 2007. Cytokinesis-block micronucleus cytome assay. Nature Protocols. 2(5), 1084-1104.

9. Francis, A.P., Davasena, T., 2018. Toxicity of carbon nanotubes: A review. Toxicology and Industrial Health. 1-2, 1-11.

10. Francis, A.P., Ganapathy, S., Palla, V.R., Murthy, P.B., Ramaprabhu, S., Devasena, T., 2015. One time nose-only inhalation of MWCNTs: Exploring the mechanism of toxicity by intermittent sacrifice in Wistar rats. Toxicology Reports. 2, 111-120.

11. Fraser, K., Kodali, V., Yanamala, N., Birch, M.E., Cena, L., Casuccio, G., Bunker, K., Lersch, T.L., Evans, D.E., Stefaniak, A., Hammer, M.A., Kashon, M.L., Boots, T., Eye, T. , Hubaczak, J., Friend, S.A., Dahm, M., Schubauer-Berigan, M.K., Siegrist., 2020. Physicochemical characterization and genotoxicity of the broad class of carbon nanotubes and nanofibers used or produced in U.S. facilities. Particle and Fibre Toxicology. 17, 62.

12. Gangwal, S., Brown, J.S., Wang, A., Houck, K.A., Dix, D.J., Kavlock, R.J., Hubal, E.A., 2011. Informing Selection of Nanomaterial Concentrations for ToxCast *in Vitro* Testing Based on Occupational Exposure Potential. Environmental Health Perspectives. 119, 1539-1546.

13. Grosse, Y., Loomis, D., Guyton, K.Z., Lauby-Secretan, B., El Ghissassi, F., Bouvard, V., Benbbrahim-Tallaa, L., Guha, N., Scoccianti,C., Mattock, H., Straif, K., 2014. Carcinogenicity of fluoro-edenite, silicon carbide fibres and whiskers, and carbon nanotubes. Lancet Oncology. 15, 1427–1428.

14. Haniu, H., Saito, N., Matsuda, Y., Tsukahara, T., Usui, Y., Maruyama, Takanashi,K.S., Aoki, K., Kobayashi, S., Nomura, H., Tanaka, M., Okamoto, M., Kato, H., 2014. Biological responses according to the shape and size of carbon nanotubes in Beas-2B and MesO-1 cells. International Journal of Nanomedicine. 9, 1979-1990.

15. Herzog, E., Casey, A., Lyng, F.M., Chambers, G., Byrne, H. J., Davoren, M., 2007. A new approach to the toxicity testing of

carbon-based nanomaterials—The clonogenic assay. Toxicology Letters. 174, 49-60.

16. Herzog, E., Byrne, H.J., Davoren, M., Casey, A., Duschl, A., Oostingh, G.J., 2009. Dispersion medium modulates oxidative stress response of human lung epithelial cells upon exposure to carbon nanomaterial samples. Toxicology and Applied Pharmacology. 236, 276-281.

17. Kane, A.B., Hurt, R.H., Gao, H., 2018. The asbestos-carbon nanotube analogy: An update. Toxicology and Applied Pharmacology. 361, 68-80.

18. Kuempel, E.D., Juarand, M.C., Moller, P., Morimoto, Y., Kobayashi, N., Pinkerton, K.E., Sargent, L.M., Vermeulen, R.C.H. , Fubini, B., Kane, A.B., 2017. Evaluating the me- chanistic evidence and key data gaps in assessing the potential carcinogenicity of carbon nanotubes and nanofibers in humans. Critical Reviews in Toxicology. 47, 1–58.

19. Lam, C.W., James, J.T., McCluskey, R., Hunter, R.L., 2004. Pulmonary toxicity of single-wall carbon nanotubes in mice 7 and 90 days after intratracheal instillation. Toxicological Sciences. 77(1), 126-134.

20. Li, Z., Hulderman, T., Salmen, R., Chapman, R., Leonard, S.S., Young, S., Shvedova, A., Luster, M.I., Simeonova, P.P., 2007. Cardiovascular Effects of Pulmonary Exposure to Single-Wall Carbon Nanotubes. Environmental Health Perspectives. 115, 377.

21. Lindberg, H.K., Falck, G.C., Singh, R., Suhonen, S., Jarventaus, H., Vanhala, E., Catalan, J., Farmer, P.B., Savolainen, K.M., Norppa, H., 2013. Genotoxicity of short single-wall and multi-wall carbon nanotubes in human bronchial epithelial and mesothelial cells *in vitro*. Toxicology. 313, 24-37.

22. Lohcharoenkal, W., Wang, L., Stueckle, T.A., Dinu, C.Z., Castranova, V., Liu, Y., Rojanasakul, Y. , 2013. Chronic Exposure to Carbon Nanotubes Induces Invasion of Human Mesothelial Cells through Matrix Metalloproteinase-2. ACS Nano. 7, 7711-7723.

23. Louro, H., Pinhao, M., Santos, J., Tavares, A., Vital, N., Silva, M.J., 2016. Evaluation of the cytotoxic and genotoxic effects of benchmark multi-walled carbon nanotubes in relation to their physicochemical properties. Toxicology Letters. 262, 123-134.

24. Manfredi, M., Martinotti, S., Gosetti, F., Ranzato, E., Marengo, E., 2016. The secretome signature of malignant mesothelioma cell lines. Journal of Proteomics. 145, 3-10

25. Maruyama, K., Haniu, H., Saito, N., Matsuda, Y., Tsukahara, T., Kobayashi, S., Tanaka, M., Aoki, K., Takanashi, S., Okamoto, M., Kato, H., 2015. Endocytosis of Multiwalled Carbon Nanotubes in Bronchial Epithelial and Mesothelial Cells. Biomed Research International. 2015, 9.

26. Moller, P., Wils, R.S., Di Ianni, E., Gutierrez, C.A., Roursgaard, M., Jacobsen, R., 2021. Genotoxicity of multi-walled carbon

nanotube reference materials in mammalian cells and animals. Mutation Research-Reviews in Mutation Research. 788, 108393.

27. Morimoto, Y., Hirohashi, M., Ogami, A., Oyabu, T., Myojo, T., Todoroki, M., Yamamoto, M., Hashiba, M., Mizuguchi, Y. , Lee, B. W., Kuroda, E., Shimada, M., Wang, W., Yamamoto, K., Fujita, K., Endoh, S., Uchida, K., Kobayashi, N., Mizuno, K., Inada, M., 2012. Pulmonary toxicity of well-dispersed multi-wall carbon nanotubes following inhalation and intratracheal instillation. Nanotoxicology. 6, 587-599.

28. Muller, J., Huaux, F., Moreau, N., Misson, P., Heilier, J., Delos, M., Arras,M., Fonseca, A., Nagy, J.B., Lison, D., 2005. Respiratory toxicity of multi-wall carbon nanotubes Author links open overlay panel. Toxicology and Applied Pharmacology. 207, 221-231.

29. Muller, J., Decordier, I., Hoet, P.H., Lombaert, N., Thomassen, L., Huaux, F., Lison, D., Kirsch-Volders, M., 2008. Clastogenic and aneugenic effects of multi-wall carbon nanotubes in epithelial cells. Carcinogenesis. 29, 427-433.

30. Muller, L., Riediker, M., Wick, P., Mohr, M., Gehr, P., Rothen-Rutishauser, B., 2010. Oxidative stress and inflammation response after nanoparticle exposure: differences between human lung cell monocultures and an advanced three-dimensional model of the human epithelial airways. Journal of the Royal Society Interface. 7, S27-S40.

31. Mulvaney, P., Weiss, P. S., 2016. Have nanoscience and nanotechnology delivered?. ACS Nano. 10, 7225–7226.

32. O' Coileain, C., 2021. Nanotechnology The influence, risks and opportunities of a rising technology. Library & Research Service. 5, 3-30.

33. Pacurari, M., Yin, X.J., Zhao, J., Ding, M., Leonard, S.S., Schwegler-Berry, D., Ducatman, B. S., Sbarra, D., Hoover, M. D., Castranova, M., Vallyathan, V., 2008. Raw Single-Wall Carbon Nanotubes Induce Oxidative Stress and Activate MAPKs, AP-1, NF-κB, and Akt in Normal and Malignant Human Mesothelial Cells. Environmental Health Perspectives. 116, 1211-1217.

34. Poland, C. A., Duffin, R., Kinloch, I., Maynard, A., Wallace, W.A., Seaton, A., Stone, V., Brown, S, MacNee, W., Stone, V., S. Brown, MacNee, W., Donaldson, K., 2008. Carbon nano- tubes introduced into the abdominal cavity of mice show asbestos-like pathogenicity in a pilot study. Nature Nanotechnology. 3, 423-428.

35. Pulskamp, K., Diabate, S., Krung, H.F., 2007. Carbon nanotubes show no sign of acute toxicity but induce intracellular reactive oxygen species in dependence on contami- nants.. Toxicology Letters. 168, 58-74.

36. Raudvere, U., Kolberg, L., Kuzmin, I., Arak, T., Adler, P., Peterson, H., Vilo, J., 2019. g:Profiler: a web server for functional enrichment analysis and conversions of gene lists (2019 update). Nucleic Acids Research. 47, W191-W198.

37. Requardt, H., Braun, A., Steinberg, P., Hampel, S., Hansen, T., 2019. Surface defects reduce carbon nanotube toxicity *in vitro*. Toxicology in Vitro. 60, 12-18.

38. Rozhina, E., Batasheva, S., Miftakova, R., Yan, X., Vikulina, A., Volodkin, D., Fakhrullin, R., 2021. Comparative cytotoxicity of kaolinite, halloysite, multiwalled carbon nanotubes and graphene oxide. Applied Clay Science. 205, 106041.

39. Shvedova, A.A., Kisin, E.R., Mercer, R., Murray, A. R., Johnson, V. J., Potapovich, A. I., Tyurina,Y.Y., Gorelik, O., Arepalli, S., Schwegeler-Berry, D., Hubbs, A.F., Antonini, J., Evans, D.E., Ku, B., Ramsey, D., Maynard, A., Kagan,V.E., Castrano, 2005. Unusual inflammatory and fibrogenic pulmonary responses to single-walled carbon nanotubes in mice. American Journal of Physiology-Lung Cellular and Molecular Physiology. 289, L698-L708.

40. Srivastava, R., Pant, A.B., Kashyap, M.P., Kumar, V., Lohani, M., Jonas, L., Rahman, Q., 2011. Multi-walled carbon nanotubes induce oxidative stress and apoptosis in human lung cancer cell line-A549. Nanotoxicology. 5, 195-207.

41. Thurnherr, T., Brandenberger, C., Fischer, K., Diener, L., Manser, P., Maeder-Althaus, X., Kaiser, J., Krug, H.F., Rothen-Rutishauser, B., Wick, P., 2011. A comparison of acute and long-term effects of industrial multiwalled carbon nanotubes on human lung and immune cells *in vitro*. Toxicology Letters. 200, 176-186.

42. Wang, L., Castranova, V., Mishra, A., Chen, B., Mercer, R. R., Schwegler-Berry, D., Rojanasakul, Y., 2010. Dispersion of single-walled carbon nanotubes by a natural lung surfactant for pulmonary *in vitro* and *in vivo* toxicity studies. Particle and Fiber Toxicology. 7, 31.

43. Warheit, D.B., Laurence, B.R., Reed, K.L., Roach, D.H., Reynolds, G.A., Webb, T.R., 2004. Comparative Pulmonary Toxicity Assessment of Single-wall Carbon Nanotubes in Rats. Toxicological Sciences. 77, 117-125.

Supplementary information: Unravelling the potential toxicity of carbon nanotubes by RNA-seq transcriptomics

1. **Supplementary Information Figure S1:Micronucleus images from fluorescence microscopy**

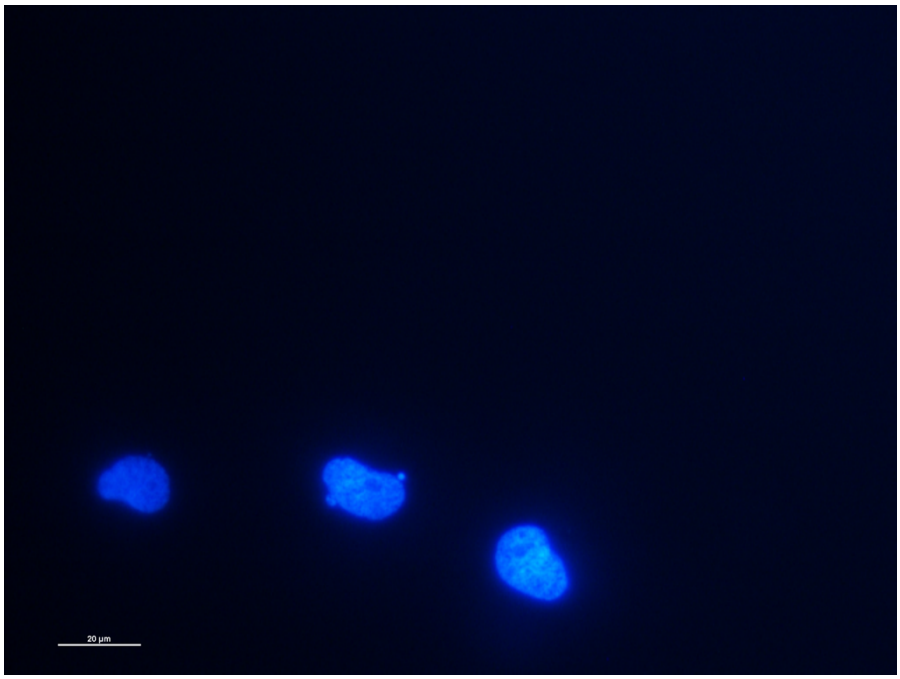

Fig.1 NTX3 long

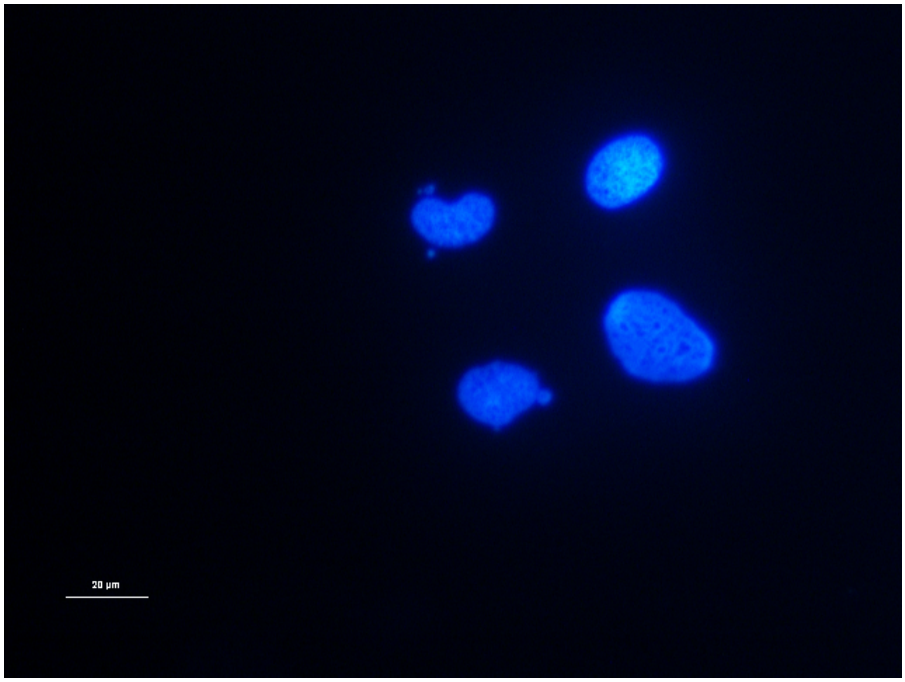

Fig.2 NTX3 long

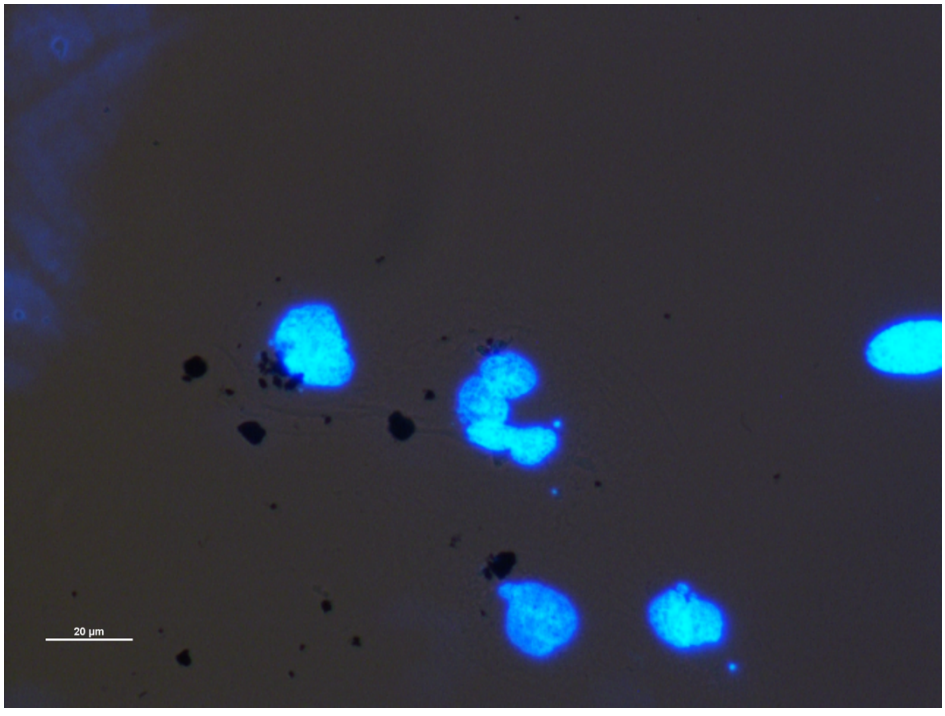

Fig.3 NTX3 long: visible CNTs aggregates.

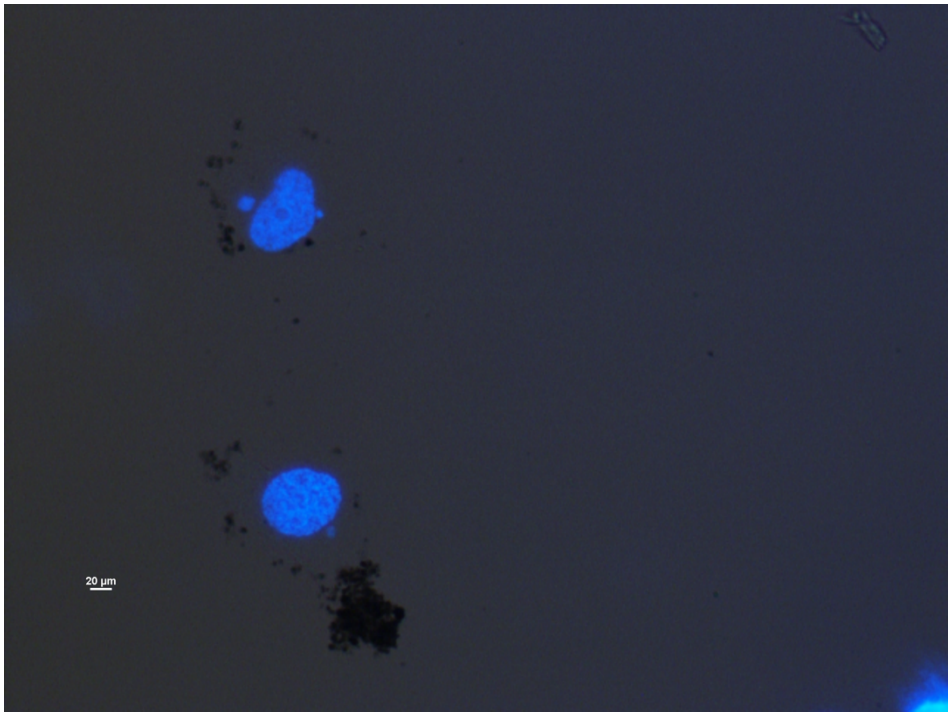

Fig.4 NTX4 long: visible CNTs aggregates.

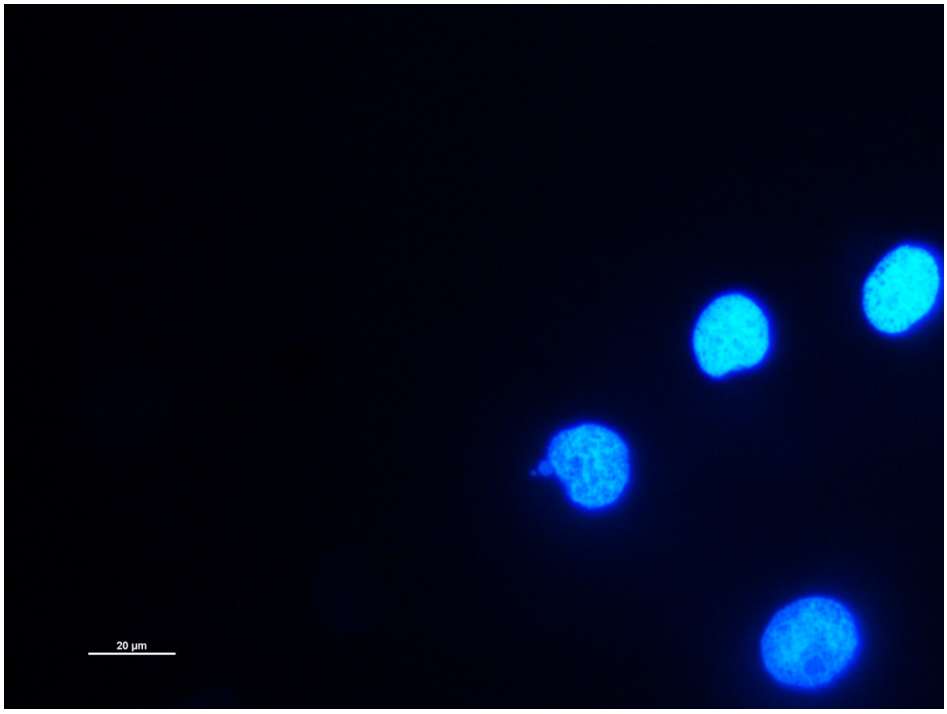

Fig.5 NTX4 long

2. Supplementary Information Table S2: Transcriptomic pathway

Table 1: NTX1

source	term_name	term_id	adjusted_p_value
REAC	DNA strand elongation	REAC:R-HSA-69190	2.27E-19
REAC	DNA Replication	REAC:R-HSA-69306	1.75E-17
REAC	Cell Cycle	REAC:R-HSA-1640170	3.15E-17
REAC	Cell Cycle, Mitotic	REAC:R-HSA-69278	2.61E-14
REAC	Activation of the pre-replicative complex	REAC:R-HSA-68962	4.76E-14
REAC	Unwinding of DNA	REAC:R-HSA-176974	8.76E-13
REAC	Synthesis of DNA	REAC:R-HSA-69239	9.93E-13
REAC	S Phase	REAC:R-HSA-69242	1.07E-12
REAC	Mitotic G1 phase and G1/S transition	REAC:R-HSA-453279	1.08E-12
REAC	G1/S Transition	REAC:R-HSA-69206	6.16E-12
REAC	DNA Replication Pre-Initiation	REAC:R-HSA-69002	1.99E-10
REAC	Activation of ATR in response to replication stress	REAC:R-HSA-176187	1.53E-07
REAC	Processive synthesis on the lagging strand	REAC:R-HSA-69183	1.60E-07
REAC	Lagging Strand Synthesis	REAC:R-HSA-69186	2.83755E-06
REAC	Removal of the Flap Intermediate	REAC:R-HSA-69166	3.86183E-06
REAC	Cell Cycle Checkpoints	REAC:R-HSA-69620	4.37286E-06
REAC	Telomere C-strand (Lagging Strand) Synthesis	REAC:R-HSA-174417	2.00631E-05
REAC	G2/M Checkpoints	REAC:R-HSA-69481	2.11763E-05
REAC	Homology Directed Repair	REAC:R-HSA-5693538	3.9953E-05
REAC	Extension of Telomeres	REAC:R-HSA-180786	7.76447E-05
REAC	Leading Strand Synthesis	REAC:R-HSA-69109	0.000149499
REAC	Polymerase switching	REAC:R-HSA-69091	0.000149499
REAC	DNA Repair	REAC:R-HSA-73894	0.000204144
REAC	Resolution of AP sites via the multiple-nucleotide patch replacement pathway	REAC:R-HSA-110373	0.000436478
REAC	DNA Double-Strand Break Repair	REAC:R-HSA-5693532	0.000552122
REAC	Polymerase switching on the C-strand of the telomere	REAC:R-HSA-174411	0.000585769
REAC	HDR through Homologous Recombination (HRR) or Single Strand Annealing (SSA)	REAC:R-HSA-5693567	0.000772456
REAC	G1/S-Specific Transcription	REAC:R-HSA-69205	0.000775543
REAC	HDR through Homologous Recombination (HRR)	REAC:R-HSA-5685942	0.001094673
REAC	Assembly of the pre-replicative complex	REAC:R-HSA-68867	0.00125805
REAC	Chromosome Maintenance	REAC:R-HSA-73886	0.001434654
REAC	PCNA-Dependent Long Patch Base Excision Repair	REAC:R-HSA-5651801	0.002362332
REAC	Resolution of Abasic Sites (AP sites)	REAC:R-HSA-73933	0.006120095
REAC	DNA replication initiation	REAC:R-HSA-68952	0.007560869
REAC	G0 and Early G1	REAC:R-HSA-1538133	0.009108945
REAC	Orc1 removal from chromatin	REAC:R-HSA-68949	0.01367393
REAC	Switching of origins to a post-replicative state	REAC:R-HSA-69052	0.017584207
REAC	Telomere Maintenance	REAC:R-HSA-157579	0.020850756
REAC	Processive synthesis on the C-strand of the telomere	REAC:R-HSA-174414	0.023278542
REAC	Resolution of D-loop Structures through Holliday Junction Intermediates	REAC:R-HSA-5693568	0.038341641
REAC	Resolution of D-Loop Structures	REAC:R-HSA-5693537	0.045679074
REAC	TP53 Regulates Transcription of Cell Cycle Genes	REAC:R-HSA-6791312	0.048950778
REAC	E2F mediated regulation of DNA replication	REAC:R-HSA-113510	0.049852631

source	term_name	term_id	adjusted_p_value
KEGG	DNA replication	KEGG:03030	2.00E-15
KEGG	Cell cycle	KEGG:04110	5.83E-08
KEGG	Base excision repair	KEGG:03410	0.000870786
KEGG	Homologous recombination	KEGG:03440	0.003913381
KEGG	Cellular senescence	KEGG:04218	0.006834291
KEGG	Fanconi anemia pathway	KEGG:03460	0.023869121
KEGG	Small cell lung cancer	KEGG:05222	0.028046096

Table 2: NTX1s

source	term_name	term_id	adjusted_p_value
REAC	DNA strand elongation	REAC:R-HSA-69190	1.08E-07
REAC	Unwinding of DNA	REAC:R-HSA-176974	3.35E-07
REAC	S Phase	REAC:R-HSA-69242	1.0101E-05
REAC	DNA Replication	REAC:R-HSA-69306	2.4622E-05
REAC	G1/S Transition	REAC:R-HSA-69206	3.17978E-05
REAC	Mitotic G1 phase and G1/S transition	REAC:R-HSA-453279	4.84437E-05
REAC	Synthesis of DNA	REAC:R-HSA-69239	0.000250223
REAC	Activation of the pre-replicative complex	REAC:R-HSA-68962	0.00047139
REAC	Neutrophil degranulation	REAC:R-HSA-6798695	0.005402172
REAC	Cell Cycle, Mitotic	REAC:R-HSA-69278	0.008530578
REAC	Cell Cycle	REAC:R-HSA-1640170	0.009398075
REAC	DNA Replication Pre-Initiation	REAC:R-HSA-69002	0.01259187
REAC	TP53 Regulates Transcription of Cell Cycle Genes	REAC:R-HSA-6791312	0.015598403
REAC	TP53 Regulates Transcription of Genes Involved in G1 Cell Cycle Arrest	REAC:R-HSA-6804116	0.032655826
REAC	Assembly of the pre-replicative complex	REAC:R-HSA-68867	0.041869069

source	term_name	term_id	adjusted_p_value
KEGG	DNA replication	KEGG:03030	3.39E-07
KEGG	Cell cycle	KEGG:04110	1.77565E-05
KEGG	Human papillomavirus infection	KEGG:05165	0.000514907
KEGG	Melanoma	KEGG:05218	0.001254762
KEGG	Cellular senescence	KEGG:04218	0.001904136
KEGG	Chronic myeloid leukemia	KEGG:05220	0.002218749
KEGG	Lysosome	KEGG:04142	0.003044252
KEGG	Breast cancer	KEGG:05224	0.003175269
KEGG	Small cell lung cancer	KEGG:05222	0.003424926
KEGG	Endocrine resistance	KEGG:01522	0.004844667
KEGG	Epstein-Barr virus infection	KEGG:05169	0.014479849
KEGG	Glioma	KEGG:05214	0.045896436

Table 3: NTX3

source	term_name	term_id	adjusted_p_value
REAC	DNA strand elongation	REACR-HSA-69190	1.84E-18
REAC	Cell Cycle	REACR-HSA-1640170	9.55E-16
REAC	Cell Cycle, Mitotic	REACR-HSA-69278	5.49E-15
REAC	S Phase	REACR-HSA-69242	7.55E-14
REAC	Mitotic G1 phase and G1/S transition	REACR-HSA-453279	1.06E-13
REAC	DNA Replication	REACR-HSA-69306	2.52E-13
REAC	G1/S Transition	REACR-HSA-69206	2.88E-12
REAC	Activation of the pre-replicative complex	REACR-HSA-68962	6.17E-11
REAC	Synthesis of DNA	REACR-HSA-69239	4.27E-10
REAC	Processive synthesis on the lagging strand	REACR-HSA-69183	6.04E-09
REAC	Unwinding of DNA	REACR-HSA-176974	6.05E-09
REAC	Lagging Strand Synthesis	REACR-HSA-69186	2.42E-08
REAC	Removal of the Flap Intermediate	REACR-HSA-69166	8.31E-08
REAC	DNA Replication Pre-Initiation	REACR-HSA-69002	2.39E-07
REAC	Telomere C-strand (Lagging Strand) Synthesis	REACR-HSA-174417	4.91544E-06
REAC	Activation of ATR in response to replication stress	REACR-HSA-176187	1.62281E-05
REAC	Cell Cycle Checkpoints	REACR-HSA-69620	2.04349E-05
REAC	G1/S-Specific Transcription	REACR-HSA-69205	3.16853E-05
REAC	Polymerase switching	REACR-HSA-69091	7.95841E-05
REAC	Leading Strand Synthesis	REACR-HSA-69109	7.95841E-05
REAC	TP53 Regulates Transcription of Cell Cycle Genes	REACR-HSA-6791312	9.323E-05
REAC	Resolution of AP sites via the multiple-nucleotide patch replacement pathway	REACR-HSA-110373	0.000157499
REAC	Extension of Telomeres	REACR-HSA-180786	0.000161378
REAC	PCNA-Dependent Long Patch Base Excision Repair	REACR-HSA-5651801	0.000309331
REAC	Aberrant regulation of mitotic G1/S transition in cancer due to RB1 defects	REACR-HSA-9659787	0.000556999
REAC	Defective binding of RB1 mutants to E2F1,(E2F2, E2F3)	REACR-HSA-9661069	0.000556999
REAC	Signaling by Rho GTPases	REACR-HSA-194315	0.001233708
REAC	DNA Repair	REACR-HSA-73894	0.001555956
REAC	Processive synthesis on the C-strand of the telomere	REACR-HSA-174414	0.00157187
REAC	Mismatch repair (MMR) directed by MSH2:MSH6 (MutSalpha)	REACR-HSA-5358565	0.001625692
REAC	Mismatch repair (MMR) directed by MSH2:MSH3 (MutSbeta)	REACR-HSA-5358606	0.001625692
REAC	G2/M Checkpoints	REACR-HSA-69481	0.001878755
REAC	Signaling by Rho GTPases, Miro GTPases and RHOBTB3	REACR-HSA-9716542	0.00256522
REAC	Polymerase switching on the C-strand of the telomere	REACR-HSA-174411	0.002574718
REAC	Chromosome Maintenance	REACR-HSA-73886	0.002583472
REAC	Transcriptional Regulation by TP53	REACR-HSA-3700989	0.002747222
REAC	Mismatch Repair	REACR-HSA-5358508	0.002906023
REAC	Resolution of Abasic Sites (AP sites)	REACR-HSA-73933	0.007121504
REAC	Homology Directed Repair	REACR-HSA-5693538	0.007865958
REAC	RHO GTPase cycle	REACR-HSA-9012999	0.007929437
REAC	Removal of the Flap Intermediate from the C-strand	REACR-HSA-174437	0.00798348
REAC	Recognition of DNA damage by PCNA-containing replication complex	REACR-HSA-110314	0.009698399
REAC	G1 Phase	REACR-HSA-69236	0.012630626
REAC	Cyclin D associated events in G1	REACR-HSA-69231	0.012630626
REAC	DNA Double-Strand Break Repair	REACR-HSA-5693532	0.016463305
REAC	Gap-filling DNA repair synthesis and ligation in GG-NER	REACR-HSA-5696397	0.016832731
REAC	G0 and Early G1	REACR-HSA-1538133	0.023169626
REAC	TP53 Regulates Transcription of Genes Involved in G1 Cell Cycle Arrest	REACR-HSA-6804116	0.025470461
REAC	HDR through Homologous Recombination (HRR)	REACR-HSA-5685942	0.025732799
REAC	Assembly of the pre-replicative complex	REACR-HSA-68867	0.030267767
REAC	HDR through Homologous Recombination (HRR) or Single Strand Annealing (SSA)	REACR-HSA-5693567	0.04310137
REAC	Neutrophil degranulation	REACR-HSA-6798695	0.044549692
REAC	Aberrant regulation of mitotic cell cycle due to RB1 defects	REACR-HSA-9687139	0.047652202

source	term_name	term_id	adjusted_p_value
KEGG	DNA replication	KEGG:03030	1.54E-14
KEGG	Cell cycle	KEGG:04110	7.35E-08
KEGG	p53 signaling pathway	KEGG:04115	1.35E-07
KEGG	Cellular senescence	KEGG:04218	0.000127842
KEGG	Small cell lung cancer	KEGG:05222	0.000228607
KEGG	Human papillomavirus infection	KEGG:05165	0.00050096
KEGG	Epstein-Barr virus infection	KEGG:05169	0.001143295
KEGG	Chronic myeloid leukemia	KEGG:05220	0.001469313
KEGG	Endocrine resistance	KEGG:01522	0.001549088
KEGG	Mismatch repair	KEGG:03430	0.00213597
KEGG	Protein processing in endoplasmic reticulum	KEGG:04141	0.005392318
KEGG	Breast cancer	KEGG:05224	0.005592986
KEGG	Base excision repair	KEGG:03410	0.005771462
KEGG	Pancreatic cancer	KEGG:05212	0.0064131
KEGG	Colorectal cancer	KEGG:05210	0.006791249
KEGG	Hepatocellular carcinoma	KEGG:05225	0.011770498
KEGG	Melanoma	KEGG:05218	0.014605972
KEGG	Gastric cancer	KEGG:05226	0.018493681
KEGG	Glioma	KEGG:05214	0.022434555
KEGG	Lysosome	KEGG:04142	0.034849398
KEGG	Homologous recombination	KEGG:03440	0.035418872

Table 4: NTX3s

source	term_name	term_id	adjusted_p_value
REAC	DNA strand elongation	REAC:R-HSA-69190	1.10E-11
REAC	Cell Cycle	REAC:R-HSA-1640170	5.34E-09
REAC	Cell Cycle, Mitotic	REAC:R-HSA-69278	7.61E-09
REAC	DNA Replication	REAC:R-HSA-69306	4.63E-08
REAC	Activation of the pre-replicative complex	REAC:R-HSA-68962	9.25E-08
REAC	S Phase	REAC:R-HSA-69242	9.76E-07
REAC	Unwinding of DNA	REAC:R-HSA-176974	1.02145E-06
REAC	Mitotic G1 phase and G1/S transition	REAC:R-HSA-453279	1.63512E-06
REAC	G1/S Transition	REAC:R-HSA-69206	6.78417E-06
REAC	Processive synthesis on the lagging strand	REAC:R-HSA-69183	1.96801E-05
REAC	Synthesis of DNA	REAC:R-HSA-69239	2.19735E-05
REAC	Removal of the Flap Intermediate	REAC:R-HSA-69166	0.000197289
REAC	DNA Replication Pre-Initiation	REAC:R-HSA-69002	0.000293797
REAC	Cell Cycle Checkpoints	REAC:R-HSA-69620	0.000438236
REAC	Lagging Strand Synthesis	REAC:R-HSA-69186	0.00050096
REAC	TP53 Regulates Transcription of Cell Cycle Genes	REAC:R-HSA-6791312	0.002399111
REAC	Activation of ATR in response to replication stress	REAC:R-HSA-176187	0.003914495
REAC	Telomere C-strand (Lagging Strand) Synthesis	REAC:R-HSA-174417	0.011327479
REAC	Defective binding of RB1 mutants to E2F1,(E2F2, E2F3)	REAC:R-HSA-9661069	0.01721239
REAC	Aberrant regulation of mitotic G1/S transition in cancer due to RB1 defects	REAC:R-HSA-9659787	0.01721239
REAC	Neutrophil degranulation	REAC:R-HSA-6798695	0.025165193
REAC	Signaling by Rho GTPases, Miro GTPases and RHOBTB3	REAC:R-HSA-9716542	0.03220996
REAC	Processive synthesis on the C-strand of the telomere	REAC:R-HSA-174414	0.040062965
REAC	TP53 Regulates Transcription of Genes Involved in G1 Cell Cycle Arrest	REAC:R-HSA-6804116	0.049542388
REAC	Mismatch repair (MMR) directed by MSH2:MSH3 (MutSbeta)	REAC:R-HSA-5358606	0.049542388
REAC	Mismatch repair (MMR) directed by MSH2:MSH6 (MutSalpha)	REAC:R-HSA-5358565	0.049542388

source	term_name	term_id	adjusted_p_value
KEGG	DNA replication	KEGG:03030	3.49E-10
KEGG	Cell cycle	KEGG:04110	3.03563E-05
KEGG	p53 signaling pathway	KEGG:04115	9.28141E-05
KEGG	Melanoma	KEGG:05218	0.001774721
KEGG	Chronic myeloid leukemia	KEGG:05220	0.003504525
KEGG	Prostate cancer	KEGG:05215	0.005288244
KEGG	Fanconi anemia pathway	KEGG:03460	0.006455946
KEGG	Endocrine resistance	KEGG:01522	0.0144081
KEGG	Human papillomavirus infection	KEGG:05165	0.030177335
KEGG	Platinum drug resistance	KEGG:01524	0.030240412
KEGG	Small cell lung cancer	KEGG:05222	0.033711244
KEGG	Non-alcoholic fatty liver disease	KEGG:04932	0.034047427
KEGG	Breast cancer	KEGG:05224	0.044609741

Table 5: NTX4

source	term_name	term_id	adjusted_p_value
REAC	DNA strand elongation	REAC:R-HSA-69190	2.08E-14
REAC	Cell Cycle	REAC:R-HSA-1640170	1.12E-12
REAC	Cell Cycle, Mitotic	REAC:R-HSA-69278	1.23E-12
REAC	DNA Replication	REAC:R-HSA-69306	7.81E-10
REAC	S Phase	REAC:R-HSA-69242	1.43E-09
REAC	Mitotic G1 phase and G1/S transition	REAC:R-HSA-453279	1.87E-08
REAC	Activation of the pre-replicative complex	REAC:R-HSA-68962	6.44E-08
REAC	G1/S Transition	REAC:R-HSA-69206	1.23E-07
REAC	Synthesis of DNA	REAC:R-HSA-69239	2.19E-07
REAC	Unwinding of DNA	REAC:R-HSA-176974	4.46E-07
REAC	Processive synthesis on the lagging strand	REAC:R-HSA-69183	6.49E-07
REAC	Lagging Strand Synthesis	REAC:R-HSA-69186	3.58952E-06
REAC	Removal of the Flap Intermediate	REAC:R-HSA-69166	5.78561E-06
REAC	Telomere C-strand (Lagging Strand) Synthesis	REAC:R-HSA-174417	1.21027E-05
REAC	Extension of Telomeres	REAC:R-HSA-180786	0.000193049
REAC	Cell Cycle Checkpoints	REAC:R-HSA-69620	0.000262036
REAC	G1/S-Specific Transcription	REAC:R-HSA-69205	0.0002858
REAC	DNA Replication Pre-Initiation	REAC:R-HSA-69002	0.0005632
REAC	Polymerase switching on the C-strand of the telomere	REAC:R-HSA-174411	0.001555195
REAC	Leading Strand Synthesis	REAC:R-HSA-69109	0.002203106
REAC	Polymerase switching	REAC:R-HSA-69091	0.002203106
REAC	Signaling by Rho GTPases	REAC:R-HSA-194315	0.002241871
REAC	Activation of ATR in response to replication stress	REAC:R-HSA-176187	0.002355252
REAC	TP53 Regulates Transcription of Cell Cycle Genes	REAC:R-HSA-6791312	0.00312381
REAC	Processive synthesis on the C-strand of the telomere	REAC:R-HSA-174414	0.004095231
REAC	Signaling by Rho GTPases, Miro GTPases and RHOBTB3	REAC:R-HSA-9716542	0.005405802
REAC	Unfolded Protein Response (UPR)	REAC:R-HSA-381119	0.006948125
REAC	Metabolism of proteins	REAC:R-HSA-392499	0.007498978
REAC	Recognition of DNA damage by PCNA-containing replication complex	REAC:R-HSA-110314	0.008056914
REAC	Resolution of AP sites via the multiple-nucleotide patch replacement pathway	REAC:R-HSA-110373	0.008061645
REAC	Mitotic Prometaphase	REAC:R-HSA-68877	0.008646551
REAC	Resolution of Abasic Sites (AP sites)	REAC:R-HSA-73933	0.010175551
REAC	DNA Repair	REAC:R-HSA-73894	0.010562453
REAC	PCNA-Dependent Long Patch Base Excision Repair	REAC:R-HSA-5651801	0.011181627
REAC	Resolution of Sister Chromatid Cohesion	REAC:R-HSA-2500257	0.011587141
REAC	G0 and Early G1	REAC:R-HSA-1538133	0.012128175
REAC	Removal of the Flap Intermediate from the C-strand	REAC:R-HSA-174437	0.014210472
REAC	Mismatch repair (MMR) directed by MSH2:MSH3 (MutSbeta)	REAC:R-HSA-5358606	0.028472343
REAC	Mismatch repair (MMR) directed by MSH2:MSH6 (MutSalpha)	REAC:R-HSA-5358565	0.028472343
REAC	Chromosome Maintenance	REAC:R-HSA-73886	0.035804171
REAC	Mismatch Repair	REAC:R-HSA-5358508	0.049556364

source	term_name	term_id	adjusted_p_value
KEGG	DNA replication	KEGG:03030	5.22E-11
KEGG	Protein processing in endoplasmic reticulum	KEGG:04141	4.12078E-05
KEGG	Lysosome	KEGG:04142	0.000118535
KEGG	Cell cycle	KEGG:04110	0.00014302
KEGG	Base excision repair	KEGG:03410	0.005526313
KEGG	Small cell lung cancer	KEGG:05222	0.006742084
KEGG	Human papillomavirus infection	KEGG:05165	0.023525156
KEGG	Mismatch repair	KEGG:03430	0.044568645

Table 6: NTX4s

source	term_name	term_id	adjusted_p_value
REAC	DNA strand elongation	REAC:R-HSA-69190	5.96E-08
REAC	Unwinding of DNA	REAC:R-HSA-176974	1.06051E-05
REAC	S Phase	REAC:R-HSA-69242	2.11571E-05
REAC	DNA Replication	REAC:R-HSA-69306	6.17976E-05
REAC	Synthesis of DNA	REAC:R-HSA-69239	0.000124061
REAC	Neutrophil degranulation	REAC:R-HSA-6798695	0.001906462
REAC	Activation of the pre-replicative complex	REAC:R-HSA-68962	0.003331178
REAC	G1/S Transition	REAC:R-HSA-69206	0.008247324
REAC	Glycosphingolipid metabolism	REAC:R-HSA-1660662	0.026250836
REAC	Mitotic G1 phase and G1/S transition	REAC:R-HSA-453279	0.035088648
REAC	Processive synthesis on the lagging strand	REAC:R-HSA-69183	0.035104483

source	term_name	term_id	adjusted_p_value
KEGG	DNA replication	KEGG:03030	6.75E-09
KEGG	Lysosome	KEGG:04142	0.000200708
KEGG	Cell cycle	KEGG:04110	0.000487636
KEGG	Other glycan degradation	KEGG:00511	0.026204153
KEGG	Human papillomavirus infection	KEGG:05165	0.03408796
KEGG	Breast cancer	KEGG:05224	0.044610398

Table 7: CB

source	term_name	term_id	adjusted_p_value
REAC	DNA strand elongation	REAC:R-HSA-69190	5.15E-14
REAC	Cell Cycle, Mitotic	REAC:R-HSA-69278	7.28E-12
REAC	DNA Replication	REAC:R-HSA-69306	2.21E-11
REAC	Cell Cycle	REAC:R-HSA-1640170	7.76E-11
REAC	Activation of the pre-replicative complex	REAC:R-HSA-68962	7.96E-11
REAC	S Phase	REAC:R-HSA-69242	1.02E-10
REAC	Unwinding of DNA	REAC:R-HSA-176974	1.65E-09
REAC	G1/S Transition	REAC:R-HSA-69206	2.08E-09
REAC	Synthesis of DNA	REAC:R-HSA-69239	2.94E-09
REAC	Mitotic G1 phase and G1/S transition	REAC:R-HSA-453279	4.22E-09
REAC	DNA Replication Pre-Initiation	REAC:R-HSA-69002	1.25763E-05
REAC	Activation of ATR in response to replication stress	REAC:R-HSA-176187	4.01294E-05
REAC	Processive synthesis on the lagging strand	REAC:R-HSA-69183	5.01134E-05
REAC	Lagging Strand Synthesis	REAC:R-HSA-69186	0.000530652
REAC	PCNA-Dependent Long Patch Base Excision Repair	REAC:R-HSA-5651801	0.000775732
REAC	TP53 Regulates Transcription of Genes Involved in G1 Cell Cycle Arrest	REAC:R-HSA-6804116	0.000801382
REAC	Removal of the Flap Intermediate	REAC:R-HSA-69166	0.000801382
REAC	Cell Cycle Checkpoints	REAC:R-HSA-69620	0.000884343
REAC	Telomere C-strand (Lagging Strand) Synthesis	REAC:R-HSA-174417	0.002573923
REAC	Resolution of AP sites via the multiple-nucleotide patch replacement pathway	REAC:R-HSA-110373	0.0028931
REAC	G1/S-Specific Transcription	REAC:R-HSA-69205	0.005076723
REAC	Processive synthesis on the C-strand of the telomere	REAC:R-HSA-174414	0.006379883
REAC	Extension of Telomeres	REAC:R-HSA-180786	0.008187997
REAC	Recognition of DNA damage by PCNA-containing replication complex	REAC:R-HSA-110314	0.01077514
REAC	Assembly of the pre-replicative complex	REAC:R-HSA-68867	0.014744817
REAC	Mismatch repair (MMR) directed by MSH2:MSH6 (MutSalpha)	REAC:R-HSA-5358565	0.0178333
REAC	Mismatch repair (MMR) directed by MSH2:MSH3 (MutSbeta)	REAC:R-HSA-5358606	0.0178333
REAC	Orc1 removal from chromatin	REAC:R-HSA-68949	0.02163413
REAC	Signaling by Rho GTPases	REAC:R-HSA-194315	0.022991828
REAC	DNA Repair	REAC:R-HSA-73894	0.023442968
REAC	Mismatch Repair	REAC:R-HSA-5358508	0.026098836
REAC	Gap-filling DNA repair synthesis and ligation in GG-NER	REAC:R-HSA-5696397	0.035792064
REAC	Signaling by Rho GTPases, Miro GTPases and RHOBTB3	REAC:R-HSA-9716542	0.036805327
REAC	DNA Damage Bypass	REAC:R-HSA-73893	0.03718366
REAC	Resolution of Abasic Sites (AP sites)	REAC:R-HSA-73933	0.037882209
REAC	Switching of origins to a post-replicative state	REAC:R-HSA-69052	0.038339588

source	term_name	term_id	adjusted_p_value
KEGG	DNA replication	KEGG:03030	2.52E-12
KEGG	Cell cycle	KEGG:04110	4.33E-07
KEGG	Chronic myeloid leukemia	KEGG:05220	0.001328693
KEGG	Endocrine resistance	KEGG:01522	0.011047678
KEGG	Proteoglycans in cancer	KEGG:05205	0.012028129
KEGG	Human papillomavirus infection	KEGG:05165	0.012066507
KEGG	Cellular senescence	KEGG:04218	0.021388864
KEGG	Nucleotide excision repair	KEGG:03420	0.033196985
KEGG	Base excision repair	KEGG:03410	0.037515186
KEGG	Small cell lung cancer	KEGG:05222	0.038360929
KEGG	Mismatch repair	KEGG:03430	0.049746125

Table 8: CR

source	term_name	term_id	adjusted_p_value
REAC	DNA strand elongation	REAC:R-HSA-69190	6.39E-11
REAC	DNA Replication	REAC:R-HSA-69306	2.49E-09
REAC	S Phase	REAC:R-HSA-69242	6.18E-09
REAC	Unwinding of DNA	REAC:R-HSA-176974	9.70E-08
REAC	Synthesis of DNA	REAC:R-HSA-69239	5.95E-07
REAC	Mitotic G1 phase and G1/S transition	REAC:R-HSA-453279	1.93279E-06
REAC	G1/S Transition	REAC:R-HSA-69206	3.20413E-06
REAC	Cell Cycle, Mitotic	REAC:R-HSA-69278	1.17331E-05
REAC	Cell Cycle	REAC:R-HSA-1640170	5.32782E-05
REAC	Activation of the pre-replicative complex	REAC:R-HSA-68962	8.00863E-05
REAC	DNA Replication Pre-Initiation	REAC:R-HSA-69002	0.000828378
REAC	Processive synthesis on the lagging strand	REAC:R-HSA-69183	0.001082248
REAC	Apoptotic execution phase	REAC:R-HSA-75153	0.001445815
REAC	Programmed Cell Death	REAC:R-HSA-5357801	0.001721232
REAC	Processive synthesis on the C-strand of the telomere	REAC:R-HSA-174414	0.007188998
REAC	Extension of Telomeres	REAC:R-HSA-180786	0.009137462
REAC	Telomere C-strand (Lagging Strand) Synthesis	REAC:R-HSA-174417	0.00914546
REAC	Lagging Strand Synthesis	REAC:R-HSA-69186	0.010615126
REAC	Removal of the Flap Intermediate	REAC:R-HSA-69166	0.01095507
REAC	Apoptosis	REAC:R-HSA-109581	0.0121525
REAC	Signaling by VEGF	REAC:R-HSA-194138	0.012243308
REAC	PCNA-Dependent Long Patch Base Excision Repair	REAC:R-HSA-5651801	0.015282643
REAC	Apoptotic cleavage of cellular proteins	REAC:R-HSA-111465	0.019125218
REAC	Activation of ATR in response to replication stress	REAC:R-HSA-176187	0.019125218
REAC	Cyclin D associated events in G1	REAC:R-HSA-69231	0.020378827
REAC	G1 Phase	REAC:R-HSA-69236	0.020378827
REAC	Assembly of the pre-replicative complex	REAC:R-HSA-68867	0.032030048
REAC	TP53 Regulates Transcription of Cell Cycle Genes	REAC:R-HSA-6791312	0.036193961
REAC	Removal of the Flap Intermediate from the C-strand	REAC:R-HSA-174437	0.040008849
REAC	Aberrant regulation of mitotic G1/S transition in cancer due to RB1 defects	REAC:R-HSA-9659787	0.040008849
REAC	Defective binding of RB1 mutants to E2F1,(E2F2, E2F3)	REAC:R-HSA-9661069	0.040008849
REAC	Signal Transduction	REAC:R-HSA-162582	0.047744351
REAC	Orc1 removal from chromatin	REAC:R-HSA-68949	0.049543172

source	term_name	term_id	adjusted_p_value
KEGG	DNA replication	KEGG:03030	4.07E-09
KEGG	Cell cycle	KEGG:04110	7.32693E-05
KEGG	Cellular senescence	KEGG:04218	0.000200293
KEGG	Small cell lung cancer	KEGG:05222	0.00090838
KEGG	Chronic myeloid leukemia	KEGG:05220	0.001693613
KEGG	Base excision repair	KEGG:03410	0.002202171
KEGG	Neurotrophin signaling pathway	KEGG:04722	0.006803977
KEGG	Human papillomavirus infection	KEGG:05165	0.007713761
KEGG	Epstein-Barr virus infection	KEGG:05169	0.010475075
KEGG	Human cytomegalovirus infection	KEGG:05163	0.024437749
KEGG	MAPK signaling pathway	KEGG:04010	0.025659128
KEGG	Prostate cancer	KEGG:05215	0.026987622
KEGG	Pancreatic cancer	KEGG:05212	0.031867064
KEGG	Pathways in cancer	KEGG:05200	0.035953304

Chapter 4

Carbon nanomaterial functionalization with pesticide-detoxifying carboxylesterase enzyme

(published on Chemosphere)

Keywords: biochar, carbon black, carbon nanotubes, ciliates, N-graphene, water remediation

Abstract

Four carbon materials, spent coffee ground biochar, carbon black, short CNTs and N-doped few-layer graphene were tested for functionalization with a commercial carboxylesterase. Their robustness to variations in time and key physicochemical parameters (temperature and pH) was analysed. In general, carbon nanomaterials showed better performance than biochar, both in terms of binding capacity and resilience in harsh conditions, at statistically significant levels. Among the tested materials, functionalized N-graphene also showed the highest level of inhibition of carboxylesterase by pesticide exposure. Therefore, N-graphene was selected for biotechnological application of pesticide scavenging toxicity in *T. thermophila*, a ciliate bioindicator of water quality. While immobilisation of the enzyme was not effective for carbaryl, a methyl carbamate, in the case of the organophosphorus dichlorvos, a 1- or 30-min contact time with a water solution containing 5 times the LC100 -0.5 mM- allowed 50% and

100% rescue of ciliate survival, respectively. These results indicate that functionalization with carboxylesterase may be of additional benefit compared to bare carbon in water clean-up procedures, especially for highly hydrophilic pesticides such as dichlorvos.

1.Introduction

In the last few decades Nanotechnologies (NTs) has offered ground-breaking innovation in several industrial and technological fields such as coating and painting, automotive, electronics and medicine. Since 1980 a lot of new nanomaterials have been discovered and characterised, among these, carbon-based nanomaterials (NMs), like carbon nanotubes (CNTs), fullerenes and more recently graphene have been the most promising candidates for their unique structural, chemical and physical characteristics (Hirsch et al., 2010; Oliveira et al., 2015; Yan et al., 2019). Particularly, CNTs were discovered in 1991 by Iijima (1991), and are composed by one (single-walled) or more cylinders (MWNTs) formed of graphene sheets with diameters of 1-3 nm or 5-40 nm, respectively. Their structure gives them unique characteristics of rigidity, strength and elasticity compared with other non-nano materials. One major feature is the High Aspect Ratio (HAR) and high thermal and electrical conductivity. Unique optical and electrochemical characteristics of carbon-based NMs make them suitable also for imaging and tracking of (macro)molecules, optical biosensors, drug scaffolding and delivery, or to create catalytically active systems (Oliveira et al., 2015). Carbon-based NMs also have multiple environmental applications, such as fertilisers, plant growth

stimulators, soil conditioners, and nano-encapsulated biocides. CNTs have been shown to gain adsorption capacity of microcystins (cyanobacterial toxins), heavy metals (e.g. lead and copper) outperforming standard activated carbons. Likewise, MWCNTs have been used also for immobilising different environmental contaminants like antibiotics, herbicides, pesticides, nitrogen or phosphorus, dyes, pharmaceuticals/drugs, organic pollutants like phenol and derivatives (Zaytsev and Neumann, 2016; Saxena et al., 2020). For these properties one of the most interesting and promising applications for CNTs is their use in wastewater treatment.

Among the various NMs, graphene seems to be the new top material that has attracted the attention of scientists in recent years. Interest in this material has grown thanks to physicochemical properties such as high electrical conductivity or high specific surface area, mechanical strength, among other desirable properties (Carmalin et al., 2016). It was discovered that it is also an remarkable adsorption material, so this ability has been studied for various applications. The structure of graphene itself seems to give it optimal adsorption ability, and the negative surface charge of graphene oxide (GO) or reduced graphene oxide (rGO) helps in the efficient removal of cationic pollutants such as heavy metals. In addition, graphene has been successfully used in the adsorption of organic pollutants in various forms of polycyclic aromatic hydrocarbons, gasoline, and dyes (Nupearachchi et al., 2017; Lu and Astruc, 2020). Graphene is used to remove pharmaceutical traces from water and wastewater; it is able to remove aspirin, acetaminophen and caffeine, GO is used to remove dorzolamide, tetracycline, ciprofloxacin, norfloxacin, diclofenac, sulfamethoxazole,

beta blockers. Graphene nanosheets and GO are used to remove naphthalene, 2-naphthol, 1-naphthylamine and tylosin; rGO can adsorb organic compounds such as ketoprofen, carbamazepine and bisphenol (Ji et al., 2010; Yuan et al, 2012; Tang et al, 2013; Ghadim et al, 2013; Liu et al, 2014; Al-Khateeb et al, 2014; Kyzas et al, 2014; George et al, 2015; Nam et al, 2015; Carmalin et al, 2016; Lu and Astruc, 2020). Thanks to the properties of graphene, research is focused on developing and improving new methods and techniques for engineering and biological remediations. Furthermore, graphene has been used successfully as a matrix for enzyme immobilisation in different technological applications (Soozanipour and Taheri-Kafrani, 2018; Zhang et al 2010).

Bioremediation enables the removal of toxic compounds in an environmental compartment, and consists in the chemical decomposition by organisms minimising the formation of intermediates of complicated degradation (Matula et al., 2020). The potential of bioremediation was recognized decades ago by Raymond et al. (1975), who reported the degradation of petroleum-derived hydrocarbons by microbial populations. Nowadays, bioremediation is mainly performed with native or indigenous microorganisms because of restrictive regulations in the USA and Europe that limit or prohibit the use and release of genetically modified organisms into the environment. To overcome this restriction, many researchers have explored the potential use of cell-free enzymes to decontaminate the environment (Thakur et al., 2019). Pollutants that are susceptible for enzymatic bioremediation include organophosphorus compounds (OP) (Oakeshott et al. 2004).

Pesticides remain an integral part of agricultural practice, with tens of thousands of tons used worldwide each year. OP compounds account for over 38% of total pesticides used, and the World Health Organisation confirms that there are three million pesticide poisonings each year. In addition, these compounds are often mobile and can contaminate aquifers and other environmental compartments. All these characteristics make OPs priority targets for bioremediation studies. An ideal candidate for OP enzymatic remediation must be able to rapidly detoxify the contaminant and be environmentally friendly without causing lasting harm to the environment. Several enzymes capable of degrading OPs occur in nature, and much research is being done to improve their efficiency and stability. The efficiency and stability of enzymes have been explored in a variety of ways, from direct modification of the amino acid sequence to immobilisation on solid supports or in membrane vesicles. One example is the use of phosphotriesterase-immobilised on semiconductor quantum dot nanomaterials, creating a highly active enzyme structure with a 2-fold increase in efficiency over the free enzyme (Thakur et al., 2019). From this perspective, the aim of this work was to develop a safe, stable, and efficient application of carbonaceous nano- and non-nano-materials with an OP-inactivating enzyme.

In this study, we compared four carbon (nano)-materials for a biotechnological application to remediate freshwater from OP and methylcarbamate pesticides. We considered three nanomaterials (1D, 2D, and 3D), respectively carbon nanotubes, N-graphene, a commercial carbon black nanoparticle, and biochar derived from spent coffee grounds. After determining the optimal functionalization

protocol and the robustness of enzyme immobilisation, we investigated the ability to reduce/abolish pesticide toxicity in the bioindicator ciliate *T. thermophila*.

2. Materials and methods

2.1 Carbon materials.

Biochar from spent coffee grounds used in this study has been previously described in Sanchez-Hernandez (2018). Carbon nanotube NTX1S was manufactured by Nanothinx S.A. (Rio Patras, Greece) into the framework of the H2020 MSCA-RISE project Nanogentools. According to the manufacturer, short NTX1 (sensu MWCNT-6 μm Sweeney et al., 2015), had 97% purity (as carbon content by thermogravimetric analysis), 30.6 mm external diameter and median length 1.1 μm as by scanning electron microscopy image analysis. The Carbon Black nanoparticles used in this work are commercially available under the Vulcan XC-72R™ (Fuel Cell, College Station, TX, USA).

The nitrogen-doped graphene (N-graphene) was manufactured by means of exfoliation of graphite rods via pulses of current methods as previously described in Baldea et al., (2020). According to the manufacturer, in this batch the content of graphene-oxide, few layer graphene and monolayer graphene accounted for 6%, 75% and 19%, respectively. Elemental analysis of the sample indicated that the sample contains hetero atoms, nitrogen (2.41 % wt) and sulfur (0.93 % wt).

2.2 Functionalization of carbon materials

Biochar, carbon black, carbon nanotubes, and N-graphene were used for enzymatic functionalization using carboxylesterase as the model enzyme (porcine liver carboxylesterase, Sigma-Aldrich®, Merck, Darmstadt, Germany), following the method described by Sanchez-Hernandez (2018) with minor modifications. Essentially, the carbon materials were incubated for 1 h (continuous agitation) in sodium acetate buffer 0.05 M pH 5.2 at a ratio of 1 mg/mL (W/V) with serial concentrations of the enzyme (20-400 µg/ml) prepared in the same medium. Afterward, the carbon particles were centrifuged at 21460 g for 10 min at 10° C and washed twice in sodium acetate buffer. The supernatants were used to measure the residual enzyme not bound onto the particle surface. The bicinchoninic acid (BCA) method (Thermofisher-Scientifics, Waltham, MA, USA) was used to such a purpose using known concentrations of carboxylesterase as reference standards.

In a typical functionalization trial, 1 mg of each carbon material was incubated with 400 µg carboxylesterase in sodium acetate buffer, as described. After the BCA assay, samples were diluted in acetate buffer at a fixed enzyme concentration of 200 µg carbon-bound enzyme mL^{-1} and then stored at 4°C for 1-5 days until needed. When needed, each preparation was diluted 1:10 to 20 µg carbon-bound enzyme mL^{-1} and used for subsequent analyses.

2.3 Enzyme activity assay

Aliquots of each functionalized (20 µg of carbon-bound enzyme) or not-functionalized carbon material were centrifuged for 10 min at

21460 g at 10°C. Pellets and supernatants were tested for carboxylesterase activity in 0.1 M Tris-HCl pH 8.4 in the presence of 2 mM 4-nitrophenyl butyrate (NPB) as substrate. Four independent reactions were continued for 5, 9, 12 and 15 minutes at RT. Samples were centrifuged and the absorbance of the supernatant recorded in a volume of 150 µl using a Infinite® 200 Pro (Tecan Sales AG, Mannedorf, Switzerland) plate reader photometer at 405 nm. For the calculation of the enzyme activity (Vmax) a path length of 0.42 cm was considered along with a molar extinction coefficient for nitrophenol of 18,330 M^{-1} cm^{-1} (Biggs 1954). True enzyme activity was calculated in the linear regime after subtraction of the intrinsic activity of non-functionalized carbon material. Definition of the carboxylesterase enzymatic activity, 1 Unit of enzyme catalyses the hydrolysis of 1 µmol min^{-1} of NPB to 4-nitrophenolate.

2.4 Stability of carboxylesterase activity

Stability of enzymatically functionalized carbons was tested in accordance with Petersen et al., (2011). To test the effect of time, functionalized carbon materials (20 µg of carbon-bound enzyme) prepared in sodium acetate buffer pH 5.2 were left at 25°C in the dark for 24h, 96h and 168h. Subsequently, the residual enzyme activity was evaluated in both pellet and supernatant. For temperature effects, functionalized carbon materials were incubated at 37 °C or 47 °C for 1 h in vertical agitation and residual carboxylesterase activity evaluated in pellet and supernatant. For pH, carbon materials were centrifuged to allow for buffer exchange using either 0.1 M Tris-HCl pH 8.4 or 9.5.

After 1 h in vertical agitation at 25°C the residual enzymatic activity was evaluated in the pellet and supernatant.

2.5 Response of carboxylesterase functionalized carbons to pesticides

To test the response of functionalized carbons to selected pesticides, functionalized material (20 µg of carbon-bound enzyme) were incubated in sodium acetate buffer in the presence of 0.5 µM 2,2-dichloroethenyl dimethyl phosphate (dichlorvos) (Sigma-Aldrich®, Merck, Darmstadt, Germany) or 30 µM naphthalen-1-yl N-methylcarbamate (carbaryl) (Sigma-Aldrich®, Merck, Darmstadt, Germany) prepared from concentrated stock solution (10 mM dichlorvos in ethanol; 6 mM carbaryl in DMSO). Samples were set in vertical agitation for 1 h at 25°C. After centrifugation at 21460 g, 10 min at 10°C, carboxylesterase activity was determined in the pellet and supernatant as previously described.

2.6 Protective effect of carboxylesterase bound graphene against pesticide toxicity in the ciliate T. thermophila

T. thermophila CU427 was grown axenically in PPY medium to late log phase -10^6 cells / ml density- at 30° C with agitation as previously described (Smith and Doerder 1992).

To determine the range of pesticide toxicity, approximately 10^4 ciliates were exposed to increasing concentrations of carbaryl or dichlorvos (1, 5, 10, 30, 50, 100, 500 µM) in physiological saline, 5 mM Tris-HCl pH 7.5, for 48 h. For survival assessment, organisms were counted after serial dilution in concave wells at 50X magnification. Cells were considered alive if swimming. The least full effective concentration for

immobilisation (as an indicator of mortality) was 30 µM and 100 µM, respectively. This concentration is known as LC100.

Carboxylesterase-bound graphene was prepared in larger functionalization batches of 10 or 25 mg at a standard ratio of 400 µg carboxylesterase / mg carbon material, essentially as previously described. Carbaryl or dichlorvos were dissolved in 5 mM Tris-HCl, pH 7.5 at 100 or 500 µM, respectively (higher carbaryl preparations showed precipitation). Ten (10) or 25 mL of pesticide solution were incubated respectively with 10 or 25 mg of carboxylesterase functionalized or non-functionalized N-graphene for 1 or 30 min under vertical agitation. The contacted pesticide solutions were recovered by centrifugation at 4500 g for 20 min at 10°C in conical tubes and used for toxicity assessment. Residual toxicity in *T. thermophila* was determined as previously described.

2.7 Statistics

Data from at least four independent experiments were analysed by means of ANOVA after square root transformation and checking for homogeneity (Levene's test) and normality (Lilliefors K-S and Shapiro-Wilk tests). When ANOVA criteria could not be fulfilled, data were analysed using non parametric statistics (Kruskal-Wallis and Kolmogorov-Smirnov two sample tests) at $p \leq 0.05$. Other statistical details may be found in text. The Systat 12 (Systat Software, Inc, San Jose, CA, USA) statistical software package was used for computation. Stabilisation of carboxylesterase activity onto carbonaceous material was evaluated by measuring periodically the enzyme activity in the

carbonaceous particles for a week. The enzyme activity was fitted to the first-decay kinetic mode:

EA = EA0 x e^(-kt)

Where EA is the initial enzyme activity a time *t* (hours) after incubation the materials with a carboxylesterase solution, EA0 is the initial enzyme activity and k is the lost rate of enzyme activity. The model allowed us to calculate the half-time (t1/2) of activity lost.

3. Results

3.1 Functionalization of carbon materials with the carboxylesterase enzyme

Using a range between 20-400 μg/mL carboxylesterase enzyme, we tested the binding capacity of the different carbon materials for their surface functionalization capability. Statistically significant differences were observed for both the type of material and concentration (Kruskal-Wallis Test, p-value < 0.01). In general, results showed that the enzyme saturated the biochar surface at a much lower level than nanomaterials (Figure 1). Pairwise comparisons confirmed these effects, particularly for CB and NTX1, which had higher overall binding capacity (KS Kolmogorov-Smirnov Two Sample Test, p-value < 0.05).

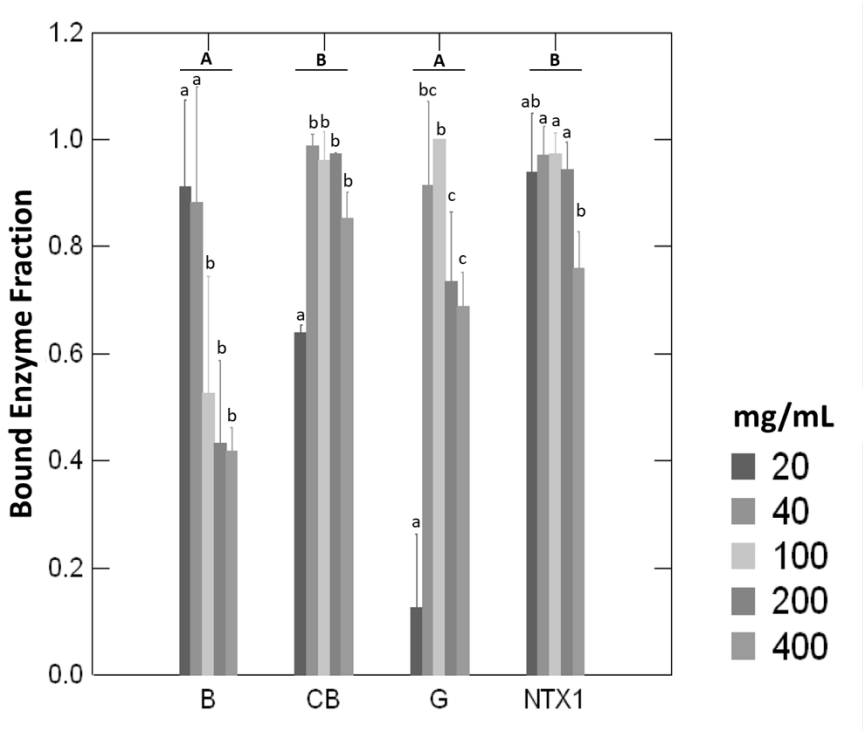

Figure 1. Binding capacity of functionalized carbon nanomaterial.

Shown are **bound-enzyme fraction**s (average +/- standard errors). Increasing amounts of carboxylesterase (20, 40, 100, 400 µg) were used to functionalize 1 mg of each of the four different carbon materials. The quantity of carbon-bound enzyme was determined indirectly by the unbound residual amount in the functionalization buffer. Groups / bars that do not share a common letter are significantly different from each other. Capital letters refer to differences among groups of carbon materials. Lowercase letters refer to differences within the same group (two side probabilities from Kolmogorov-Smirnov Two Sample Test, $p < 0.05$). Legend: B (biochar); CB (carbon black); G (N-graphene); NTX1 (carbon nanotubes).

The average basic activity of the bound-carboxylesterase enzyme was 770 U / mg protein and showed no significant differences between the different carbon materials (see Figures 2-4). After examining the basic

activity of the bound carboxylesterase enzyme, we evaluated its robustness as a function of time, pH, and temperature.

3.2 Chemical-physical robustness of functionalized materials

In the first step of the assay, the residual activity of carboxylesterase was determined periodically over a period of 7 days post-functionalization under standard conditions (25°C and pH 5.2). There was a significant effect of time on enzymatic activity (Kruskal-Wallis test statistic, p-value < 0.0001) with some marginally significant differences between materials driven by N-graphene showing the most performing functionalization half-life (Figure 2). In general, most of the activity was lost within the first 96 hours, after which it tends to stabilis, varying between 150 and 200 U.

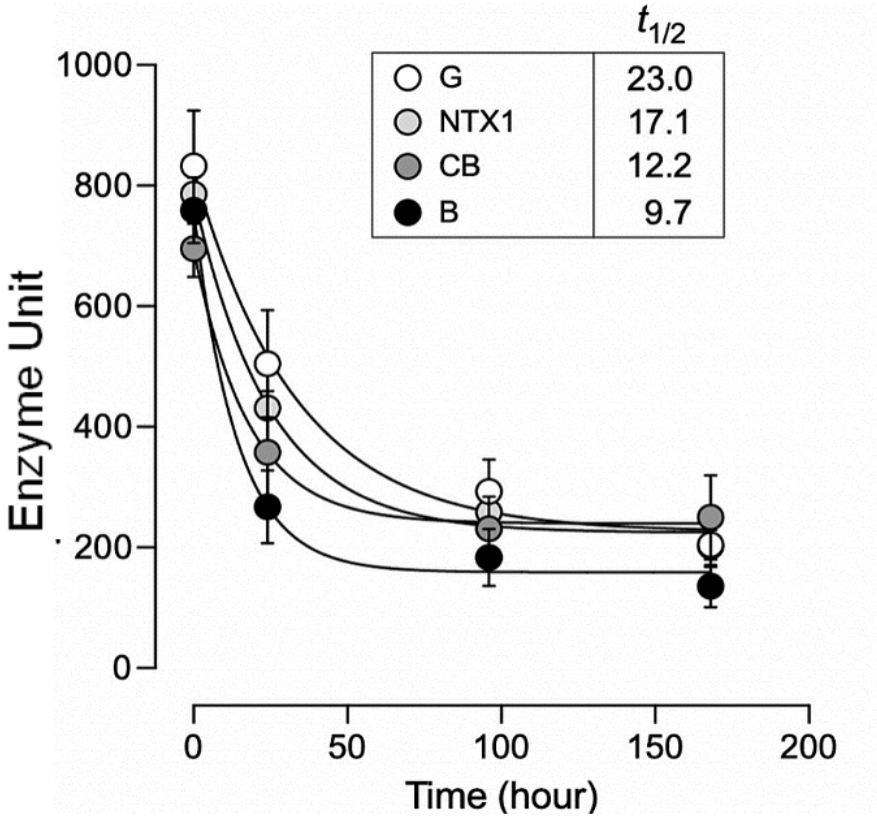

Figure 2. Stability of enzyme activity over time. Carbon materials were incubated in the presence of carboxylesterase (20 μg/mL), and the hydrolytic activity was measured at different times using the substrate 4-nitro-phenylbutyrate. Symbols represent the mean value (+/- SEM) of four independent trials. Legend: NTX1 (CNT), CB (Carbon black), B (Biochar), G (N-graphene). Other statistical details can be found in text.

We tested the enzymatic activity on functionalized carbons at two temperatures, i.e., 37°C and 47°C (Figure 3). The temperature had a significant inhibitory effect on the enzyme activity (Kruskal-Wallis test statistic, $p< 0.0001$). The enzyme activity drops (>60% of the

initial activity) between the standard value (25°C) and the two contrasting temperature ranges. These changes were statistically significant as well as the effect between 37°C and 47°C (two side probability from Kolmogorov-Smirnov Two Sample test, p <0.0001 or 0.002, respectively). Conversely, there were no statistically significant differences between the material types.

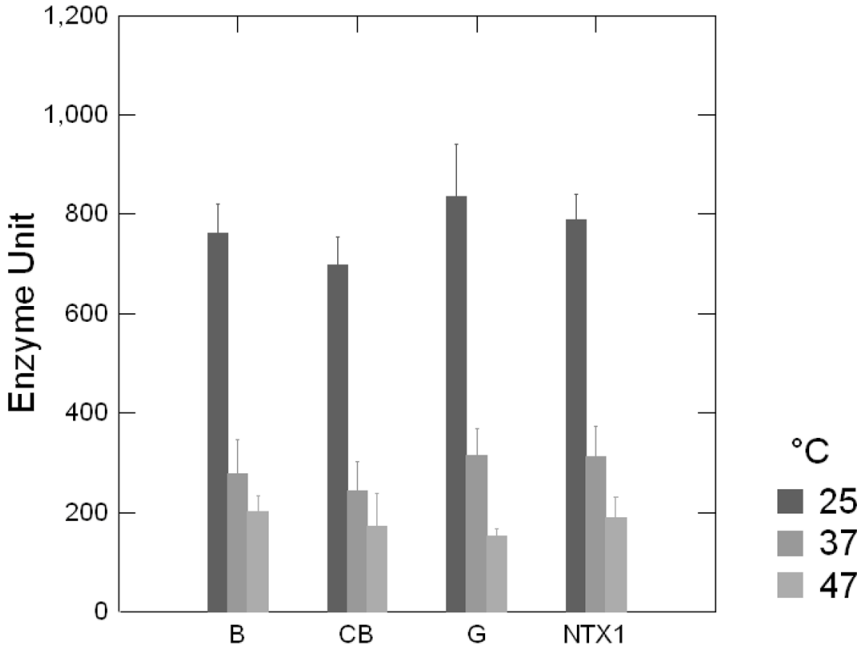

Figure 3. **Effects of temperature on carboxylesterase activity.** Explanation and legend as for Figure 2 except temperature was considered. No statistically significant differences were found among groups (carbon types). Other statistical details can be found in text.

Likewise, pH was another variable with a significant impact on enzyme activity (Kruskal-Wallis test, p < 0.0001Similarly, pH was another variable with a significant effect on enzyme activity (Kruskal-Wallis

test, $p < 0.0001$). Although an enhanced inhibitory effect was observed with increasing pH, the difference between pH 8.4 and 9.6 was significant only for biochar and NTX1 (Kolmogorov-Smirnov Two Sample Test p values 0.009 and 0.003, respectively). Biochar lost a significant amount of enzyme activity at extremely alkaline pH than carbon nanotubes, which displayed the greatest robustness against strong variation of pH (Figure 4).

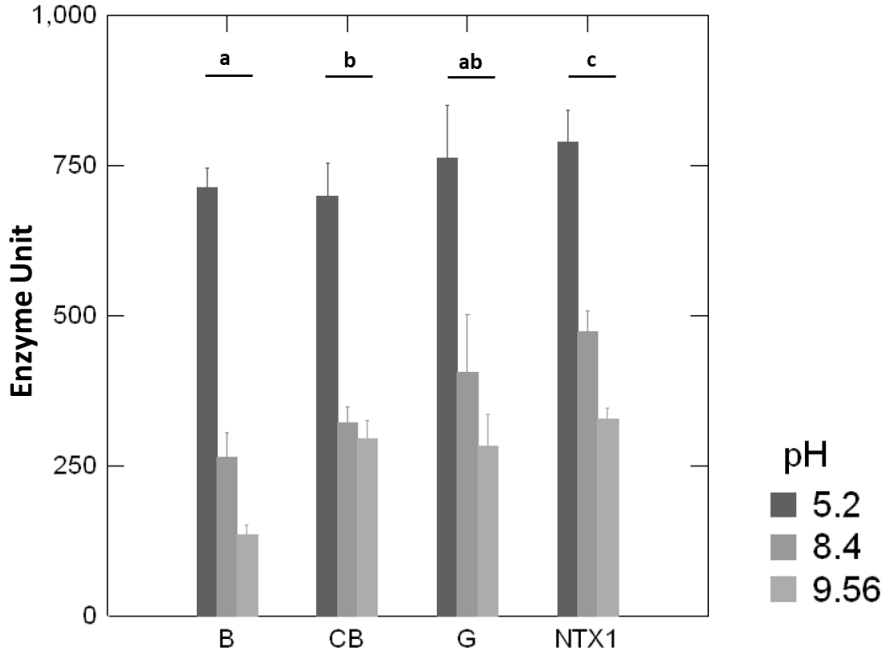

Figure 4. Effects of pH on carboxylesterase activity. Explanation, legend and statistics as for Figure 2 except pH was considered. Two side probabilities (p-values) from Kolmogorov-Smirnov Two Sample Test for NTX1 were 0.004, 0.079, and 0.050 respectively for B, CB and G; CB vs B, 0.065. Other statistical details can be found in text.

In general, it is important to highlight that no enzymatic activity was detected in the supernatant in the trials examining the effects of time,

temperature or pH (data not shown). This finding suggests that the lack of activity was due to the inhibition of the particle-bound enzyme, not by desorption from the particle surface.

3.3. Pesticide inhibition of carboxylesterase bound enzyme activity.

Functionalized carbons were exposed to two different pesticides, carbaryl and dichlorvos, at concentrations of 30 μM and 0.5 μM, respectively, which correspond to the average EC50 value for the acute test with water flea obtained from the EPA Toxicity Database (https://cfpub.epa.gov/ecotox/).

The effect of carbaryl on carboxylesterase activity was highly statistically significant (Two way ANOVA, $p < 0.0001$), but not that of carbon type and their interaction. After exposure to carbaryl, all functionalized carbons showed a significant decrease in enzymatic activity compared to the control, with the exception of biochar. The greatest inhibition was observed for the enzyme bound to N-graphene, which had a residual activity of 30%. For NTX1, CB and B, the residual activity was 44%, 53% and 60%, respectively (Figure 5). N-graphene activity was also statistically different from that of Biochar according to Two Way ANOVA ($p < 0.05$).

The effects of dichlorvos were also statistically significant ($p = 0.001$), but they were clearly driven by N-graphene (Figure 5). The enzyme bound to 2D nanomaterial, in fact, showed the greatest inhibition (44% residual activity) and was the only one that was statistically significant. For the other materials, residual activity was determined to be 61%, 72%, and 65% for B, CB, and NTX1, respectively.

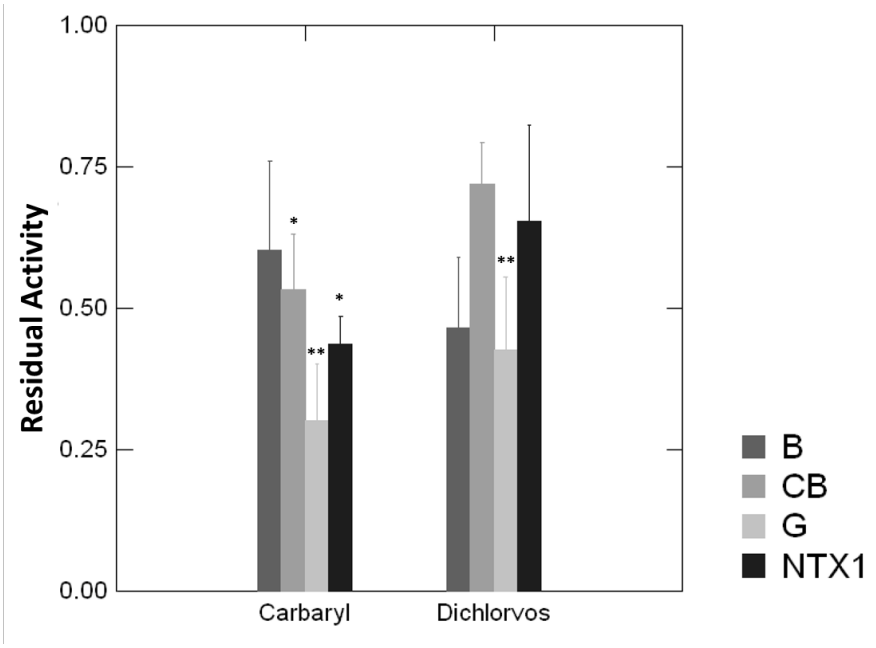

Figure 5. Effects of pesticide on bound carboxylesterase activity. Residual activity of bound carboxylesterase for the effects of pesticide treatment (average +/- standard errors from four independent experiments). Statistical differences from control , *p < 0.05; ** p < 0.01, (Two Way ANOVA, Fisher post hoc test for pairwise comparison). Legend: NTX1 (CNT), CB (Carbon black), B (Biochar), G (N-graphene).

3.4 Protective effect of carboxylesterase bound graphene

We tested carboxylesterase-functionalized N-graphene for its ability to protect the bioindicator *Tetrahymena thermophila* from pesticide toxicity (Figure 6). Our data showed that functionalization (yes or no), type of pesticide (carbaryl or dichlorvos), and contact time of N-graphene with pesticide (1 or 30 min) were highly significant factors for survival (two-way ANOVA, $p < 0.0001$; $p = 0.004$ for

functionalization). Moreover, the enzymatic functionalization of N-graphene was beneficial only in the case of exposure to dichlorvos, while in the case of carbaryl the protective effect appeared independent of enzyme functionalization (Figure 6). This interaction was also evident in the two-way ANOVA analysis ($p < 0.0001$).

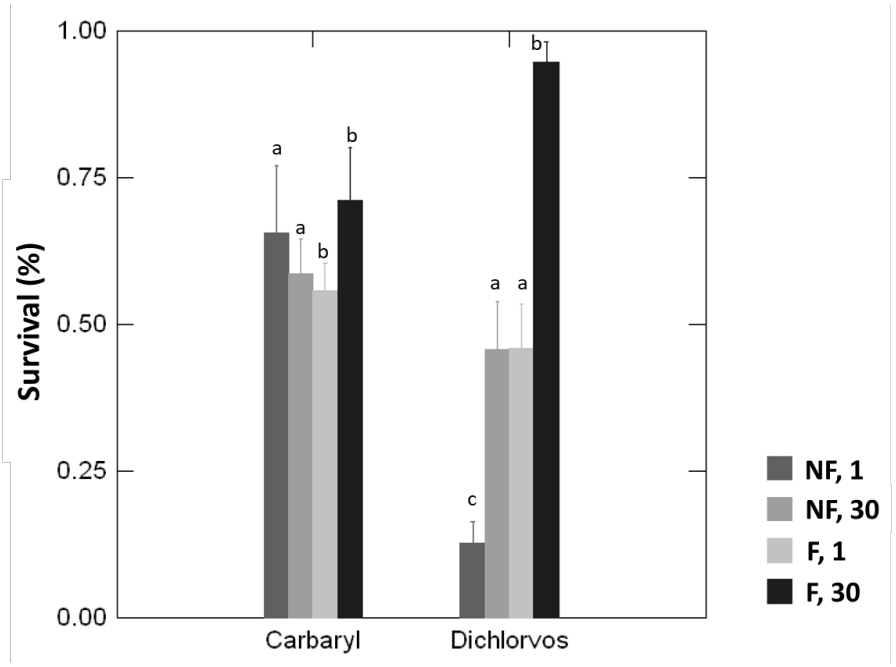

Figure 6. Protective effect of carboxylesterase functionalized N-graphene in *T. thermophila*. Shown are fractions +/- standard errors (four independent experiments) of living cells after exposure of ciliates to a full lethal concentration of carbaryl or dichlorvos, respectively 100 or 500 microM, that has been previously conditioned with carboxylesterase functionalized N-graphene for 1 or 30 minutes (see methods for experimental details). Bars that do not share a common letter are significantly different from each other (two-way ANOVA, $p < 0.05$, Tukey's post hoc test for pairwise comparison) Legend: (NF, 1), 1 min contact time, not functionalized N-graphene; (NF, 30), 30 min contact time, not functionalized N-graphene; (F, 1), 1

min contact time, functionalized N-graphene; (F, 30), 30 min contact time, functionalized N-graphene. CA, carbaryl; DI, dichlorvos.

4. Discussion

In this study, we compared the performance of four different carbon materials with respect to their use in the biotechnological application of water clean up from pesticides. The materials selected for testing were high-purity (97%) short (average length 1.1 micron) carbon nanotubes (NTX1), nitrogen-doped graphene (2.41 % N), a commercial carbon black (CB) and biochar (B). With the exception of biochar, these substances represent 1, 2 and 3 D nanomaterials. Charcoal has been used since ancient times to bind harmful chemicals in water purification technologies (Bandosz, 2006) and more recently, carbon nanomaterials have demonstrated higher performance, at least at low technology readiness level lab-scale applications. In fact, carbon nanomaterials such as CNTs (either single- or multi-walled) showed exceptional ability to adsorb antibiotics such as tetracycline with 1-2 orders of magnitude higher than bulky activated carbons. Similarly, CNTs showed high efficiency in removing heavy metals, pharmaceutical dyes, organic contaminants, and pesticides from wastewater (Ji et al., 2009; Youssef et al., 2018; Saxena et al., 2020). Graphene also showed a great ability to adsorb a large number of pharmaceuticals, as well as inorganic pollutants (i.e., metal ions and other ions), organic pollutants such as dyes, aromatic compounds, and gasoline (Sophia et al., 2016; Nupearachchi et al., 2017; Lu and Astruc, 2020). Biochar is charcoal obtained by pyrolysis from solid organic

residues as diverse as agri-waste, biosolids, pine needles, coffee grounds, fruit pits, and so on (Lehmann and Joseph, 2009). Biochar has demonstrated to be an efficient heavy metal adsorbent from water (Park et al., 2016) as well as polycyclic aromatic hydrocarbons from pore water (Oleszczuk et al., 2012). In all the aforementioned studies, carbon materials were used for their remarkable feature of non-specific adsorption. The novelty of our study was to examine this remediation capacity of biochar and other nanocarbon materials using upgrading materials. Such an upgrading consisted in the enzymatic activation with a pesticide-detoxifying esterase for clean up of two pesticides with markedly different physicochemical properties. For this low TRL application, a low-cost enzyme such as porcine carboxylesterase was selected, which is capable of forming stable ligands with organophosphorus (dichlorvos) and methyl carbamate (carbaryl) pesticides (Sanchez-Hernandez, 2018). The first step of the process was to compare the carboxylesterase enzyme immobilization capacity. As expected, all nanocarbons showed higher performance than biochar, which was more easily saturated with the enzyme. In this regard, CNT and carbon black also outperformed N-graphene (Figure 1). The best performance of carbon nanomaterials could be explained by their unique property of high surface area to volume ratio (Asuri et al., 2006; Zhang et al. 2012). In evaluating enzymatic activity, not only the ability to link enzymes became important, but also whether the linkage created a condition for their activation. Starting from the same functionalization level (20 μg), the basal enzymatic activity showed no significant differences between the different materials including

biochar, suggesting an equal level of interaction between the carbon materials and the enzyme.

The effect of temperature rise was marked for all functionalized materials both at 37°C and 47 °C (Figure 3), with residual activity ranging from about 40 % to 20 %. This behaviour is in line with previous reports (Srivastava et al., 2014). pH effects were tested at values higher than the optimal one for functionalization, 8.4 and 9.4, the latter being the upper law-limit for wastewaters according to the Italian decree-law 152/2006. pH increase above 5.2 significantly impacted carboxylesterase activity, with carbon nanotubes showing the best robustness and biochar the worst one (Figure 4). Literature data are consistent with our observations (Antón-Millán et al., 2018; Sanchez- Hernandez, 2018; Srivastava et al., 2014;). Non-covalent enzyme immobilization, in fact, is usually favoured at acidic pH for the formation of electrostatic interactions among positivized protein residues and negative charges onto carbon materials. As shown in Lu and Astruc (2020), the adsorption of organic compounds on carbon-based nanomaterials is based on the π-π-electron interaction between the surface of the material and the compound. In this π-π-electron interaction, pH played an important role because a change in pH led to a change in surface charge and thus a different interaction between the two compounds.

The final step of the evaluation was to test the system for the effects of pesticides. Pesticides are still one of the main problems of environmental sustainability. They are, in fact, an integral part of agriculture, and tens of thousands tons are applied worldwide each year. OPs account for over 38% of the total pesticides used, also

causing three million poisonings each year, while carbamates and pyrethroids practically make up the rest of the total insecticides used for parasite control in agriculture and residential areas and public facilities worldwide (Thakur et al., 2019; Matula et al., 2020). Thus, improving the bioremediation of pesticides is a topic of great interest, especially when new materials with particular surface-to-volume ratio performances could be used. Pesticide bioremediation can be performed by means of selected enzymes, some of which have been identified over the year for OPs such as diisopropyl fluorophosphatase, paraoxonase, phosphotriesterase, organophosphate hydrolase, carboxylesterase etc. (Thakur et al., 2019). In a test for the degradation of OPs, it was found that the functionality of phosphotriesterase is increased when it is immobilised on a solid surface. This system, in fact, displayed an improvement in thermal stability, pH effect and Vmax (Breger et al, 2015; Karami et al, 2016; Raynes et al. 2011; Thakur et al, 2019). In our case, we chose to functionalize different carbon nanomaterials with a low cost, commercially available carboxylesterase which is also active towards carbamates (Sterri and Fonnum 2009) as a relatively simple test bed to characterise a hybrid material system and demonstrate its practical efficacy in a pesticide scavenging application. Enzyme functionalized N-doped graphene was finally selected because this system showed overall good performance in terms of enzyme binding, resilience of enzymatic activity and robustness to changes in physicochemical conditions. Moreover, it also showed the highest inhibition after both pesticide exposures, suggesting the formation of larger amounts of stable enzyme-pesticide ligands and thus a higher scavenging potential. Last but not least, it is

worth noting N-graphene is not toxic (Baldea et al., 2020), while there is a growing literature on the hazard of other carbon nanomaterials, in particular CNTs (Sawicka et al., 2021). The exposition of *T. thermophila* to pesticides allowed us to evaluate the scavenging effect of carboxylesterase functionalized N-graphene towards ciliate survival. We found that contact between graphene and pesticides generally leads to a reduction in toxicity, with the greatest reduction obtained with increasing duration of contact. We also could find that functionalized and non-functionalized graphene scavenge pesticide toxicity. However, there was a different response between the two pesticides. While carbaryl toxicity is scavenged either by functionalized or non-functionalized graphene at the same extent suggesting no role for the enzyme, the biotest response revealed an interesting role of functionalization for dichlorvos.

The effect of carboxylesterase in fact, was decisive when survival of *T. thermophila* was challenged by 500 µM dichlorvos, a concentration 5 times higher than that giving a full mortality effect (LC_{100}). Pretreatment for only 1 min improved survival from 10 to 50% and from 50 to 100% after 30 min compared to N-graphene alone. In contrast, in the case of carbaryl, functionalization provided no advantage over the already excellent scavenging ability of bare N-graphene, which was able to prevent 70% and 100% of carbamate mortality in just 1 min or 30 min of contact, at a concentration of 100 µM, three times more than LC_{100} (higher concentrations could not be tested as they were not stable in the aqueous exposure medium). Although various forms of graphene, including pyridine (N)-doped graphene, showed unfavourable endothermic physisorption with

carbaryl (Mandeep et al., 2021), the graphite rod exfoliated N-graphene presented in this study performed well. It is worth noting that this carbon nanomaterial consisted of monolayer graphene (19%), few layer graphene (75%) and graphene oxide (6%) (Baldea et al., 2020) and besides oxygen, other heteroatoms such as nitrogen (2.41%) and sulphur (0.93%) were detected. Such a high level of defects and complexity in the graphene structure would allow for strong exothermic interactions in nature either by physisorption or chemisorption. Indeed, electrostatic interactions, hydrophobic interactions, hydrogen bonds, and/or chemical bonds may occur between adsorbate and adsorbent. Further studies such as the Langmuir-Freundlich isotherm model and density functional theory may help to clarify their nature. The structure of the two molecules allows some speculations. Indeed, these two pesticides have different degrees of lipophilicity, as indicated by their different solubility in water (8 g vs. 0.11 g L^{-1}) and their average computed logP value, 1.3 against 2.94 (calculated by means of the ALOGPS2.1 software, Tetko and Tanchuk, 2002). The OP compound tends to form H-bonds between its electronegative O-atom and the positively charged hydrogen atoms in defects of N-graphene as shown for other carbon materials such as coconut fibre biochar (An Binh and Kajitvichyanukul, 2019). However, there would also be an obvious competition with H-atoms of water molecules. Formation of stable bonds with carboxylesterase can explain the removal of dichlorvos from solution and subsequent survival of the ciliate. Carbaryl has a biplanar conformation, in which the first level contains the naphthalene ring with a pi-electron cloud. With the exception of the carbon atoms

bonded to the more electronegative oxygen atoms of the side chain, all carbon atoms of carbaryl have a small negative charge. In the side chain the oxygen atoms and the nitrogen atom are negatively charged due to their high electronegativity, while the hydrogen atoms are positively charged due to their electropositive nature (Mandeep et al., 2021). It also has a large lipophilic naphthoxy moiety and a weakly hydrophilic carbonyl group (Sandoz et al., 2000). This structure makes it predominantly a lipophilic molecule that tends to escape from water e.g. by means of hydrogen bonding with N-graphene. However more energetic chemical binding cannot be excluded due to the good electrophilic nature of carbaryl (Mandeep et al., 2021) and the richness of nucleophilic heteroatoms in N-graphene (Baldea et al 2020).

5. Conclusions

Results of the current study proved that the use of carbon materials such as graphite rod exfoliated N-doped graphene can be an optimal solution for enzymatic remediation of pesticide-contaminated water. Enzymatically functionalized materials showed a high capacity to remove organophosphate pesticide (dichlorvos) probably via phosphorylation of the active site of the carboxylesterase bound onto the surface of carbonaceous materials. It is well known that such pesticide-enzyme interaction is irreversible, which means that the remediation system may be highly effective but saturated when all enzyme molecules are phosphorylated. Future research should focus on scaling-up the readiness level of this application assessing more pesticides, mixtures, real water effluents, and exploring the advantage

of extremozymes with covalent functionalization for a longer durability. In addition, more studies on the hazard level of N-graphene are due, accomplishing a "safe by design" approach for new nanomaterials and products containing nanomaterials, thus minimising environmental and health risks.

Acknowledgment

This work was financially supported under H2020-EU.1.3.3. by the NANOGENTOOLS Project, contract No. 691095

References

Al-Khateeb, L.A., Almotiry, S., Salam, M.A., 2014. Adsorption of pharmaceutical pollutants onto graphene nanoplatelets. Chemical Engineering Journal. 248, 191–199.

An Binh, Q., Kajitvichyanukul, P., 2019. Adsorption mechanism of dichlorvos onto coconut fibre biochar: the significant dependence of H-bonding and the pore-filling mechanism. Water Science &Technology. 75, 886-876.

Antón-Millán, N., García-Tojal, J., Marty-Roda, M., Garroni, S., Cuesta-López, S., Tamayo-Ramos, J.A., 2018. Influence of Three Commercial Graphene Derivatives on the Catalytic Properties of a *Lactobacillus plantarum* α-l-Rhamnosidase When Used as

Immobilization Matrices. ACS applied materials & interfaces. 10, 18170–18182.

Baldea, I., Olteanu, D., Filip, G. A., Pogacean, F., Coros, M., Sociu, M., Tripon, S. C., Cenarium, M., Megarusan, L., Staden, R. S., Pruneanu,S. , 2020. Cytotoxicity mechanisms of nitrogen-doped graphene obtained by electrochemical exfoliation of graphite rods, on human endothelial and colon cancer cells. Carbon. 158, 267-281.

Bandosz, T.J., 2006. Activated carbon surfaces in environmental remediation. Elsevier, Oxford.

Biggs, A.I., 1954. A spectrophotometric determination of the dissociation constants of p-nitrophenol and papaverine. Transactions of the Faraday Society. 50, 800-802.

Breger, J.C., Ancona, M.G., Walper, S.A., Susumu, E.O.K. , Stewart, M.H., Deschamps, J.R., Medintz, I.L., 2015. Understanding How Nanoparticle Attachment Enhances Phosphotriesterase Kinetic Efficiency. ACS Nano. 9, 8491-8503.

Garcia, J.A., Di Paola R., 2015. Chemohormonal Therapy in Metastatic Hormone-Sensitive Prostate Cancer. The new England Journal of Medicine. 373, 737-746.

George, Z.K., Koltsakidou, A., Stavroula, G.N., Dimitrios, N.B., Dimitra, A.L., 2015. Removal of beta-blockers from aqueous media by adsorption onto graphene oxide. Science of the Total Environment. 537, 411–420.

Ghadim, E., Manouchehri, F., Soleimani, G., Hosseini, H., Kimiagar, S., Nafisi, S., 2013. Adsorption properties of tetracycline onto graphene oxide: Equilibrium, kinetic and thermodynamic studies. PLoS ONE. 8, 1–9.

Hirsch A., 2010. The era of carbon allotropes. Nature Materials. 9 (11), 868–71.

Iijima, S., 1991. Helical microtubules of graphitic carbon. Nature. 54 (6348), 56-58.

Ji, L., Chen, W., Duan, L., Zhu, D., 2009. Mechanisms for strong adsorption of tetracycline to carbon nanotubes: A comparative study using activated carbon and graphite as adsorbents. Environmental Science & Technology. 43, 2322–2327.

Ji, L., Liu, F., Xu, Z., Zheng, S., Zhu, D., 2010. Adsorption of pharmaceutical antibiotics on template-synthesized ordered micro- and mesoporous carbons. Environmental Science & Technology. 44, 3116–3122.

Karami, R., Mohsenifar, A., Mesbah Namini, S. M., Kamelipour, N., Rahmani- Cherati, T., Roodbar Shojaei, T., et al., 2016. A novel nanobiosensor for the detection of paraoxon using chitosan-embedded organophosphorus hydrolase immobilized on Au nanoparticles. Preparative Biochemistry and Biotechnology. 46, 559–566.

Kashefi, S., Borghei, S. M. , Mahmoodi, N.M., 2019. Superparamagnetic enzyme-graphene oxide magnetic nanocomposite as an environmentally friendly biocatalyst: Synthesis and biodegradation of dye using response surface methodology. Microchemical Journal. 145, 547–558.

Kishore, D., Talat, M., Srivastava, O.N., Kayastha, A.M., 2012. Immobilization of b-Galactosidase onto Functionalized Graphene Nano-sheets Using Response Surface Methodology and Its Analytical Applications. PLoS ONE. 7, e40708.

Kyzas, G.Z., Bikiaris, D.N., Seredych, M., Bandosz, T.J., Deliyanni, E.A., 2014. Removal of dorzolamide from biomedical wastewaters with adsorption onto graphite oxide/poly(acrylic acid) grafted chitosan nanocompos- ite. Bioresource technology. 152, 399–406.

Lehmann, J. and Joseph, S., 2009. Biochar systems. In: Lehmann, J. and Joseph, S. (Eds), Biochar for environmental management. Routledge, London. 147-168.

Liu, F.F., Zhao, J., Shuguang, W., Peng, D., Baoshan, X., 2014. Effects of solution chemistry on adsorption of selected pharmaceuticals and personal care products (PPCPs) by graphenes and carbon nanotubes. Environmental Science & Technology. 48, 13197–13206.

Lu, F. and Astruc, D., 2020. Nanocatalysts and other nanomaterials for water remediation from organic pollutants. Coordination Chemistry Reviews. 408, 213180.

Mandeep, G.A., Kakkar, J, Kakkar, R., 2021. DFT study of carbaryl pesticide adsorption on vacancy and nitrogen-doped graphene decorated with platinum clusters. Structural Chemistry. 32, 1541–1551.

Matula, M., Kucera, T., Soukup, O., Pejchal, J., 2020. Enzymatic Degradation of Organophosphorus Pesticides and Nerve Agents by EC: 3.1.8.2. Catalysts. 10, 1365

Mehnati-Najafabadi, V., Taheri-Kafrani, A., Bordbar, A., 2018. Xylanase immobilization on modified superparamagnetic graphene oxide nanocomposite: Effect of PEGylation on activity and stability. International Journal of Biological Macromolecule., 107, 418-425.

Movahedi, M., Shariat, S.Z.A.S., Nazem, H., 2019. Immobilization of Lactoperoxidase on Graphene Oxide Nanosheets and Copper

Oxide Nanoparticles and Evaluation of Their Stability. Catalysis Letters. 149, 562–573.

Nam, S., Jung, C., Hang, L., Miao, Y., Joseph, R.V.F., Linkel, K.B., Namguk, H., Kyung-Duk, Z., Yeomin, Y., 2015. Adsorption characteristics of diclofenac and sul- famethoxazole to graphene oxide in aqueous solution. Chemosphere. 136, 20–26.

Nupearachch, C.N., Mahatantila, K., Vithanage, M., 2017. Application of graphene for decontamination of water; Implications for sorptive removal. Groundwater for Sustainable Development. 5, 206–215.

Oleszczuk, P., Hale, S.E., Lehmann, J. and Cornelissen, G., 2012. Activated carbon and biochar amendments decrease pore-water concentrations of polycyclic aromatic hydrocarbons (PAHs) in sewage sludge. Bioresource Technology. 111, 84-91.

Oliveira, S.F., Bisker,G., Naveed, Bakh, A. , Gibbs, S.L., Landry, M.P., Strano, M.S., 2015. Protein functionalized carbon nanomaterials for biomedical applications. Carbon. 95, 767-779.

Park, J.H., Ok, Y.S., Kim, S.H., Cho, J.S., Heo, J.S., Delaune, R.D., Seo, D.C., 2016. Competitive adsorption of heavy metals onto sesame straw biochar in aqueous solutions. Chemosphere. 142, 77–83.

Petersen, E. J., Zhang, L., Mattison, N. T., O'Carroll, D. M., Whelton, A. J., Uddin, N., Nguyen, T., Huang, Q., Henry, T. B., Holbrook, R. D., Chen K. L., 2011. Potential Release Pathways, Environmental Fate, And Ecological Risks of Carbon Nanotubes. Environmental Science and Technology. 45 (23), 9837-9856.

Raymond, J.L., Jamison, V.W., Hudson, J.O., 1975. Final report on beneficial stimulation of bacterial activity in ground water petroleum products. AlChE Symposium Series. 73, 390.

Raynes, J.K., Pearce, F. G., Meade, S. J., Gerrard, J. A., 2011. Immobilization of organophosphate hydrolase on an amyloid fibril nanoscaffold: towards bioremediation and chemical detoxification. Biotechnology Progress. 27, 360–367.

Sanchez-Hernandez, J.C., 2018. Biochar activation with exoenzymes induced by earthworms: A novel functional strategy for soil quality promotion. Journal of Hazardous Materials. 350, 136-143.

Sandoz, C., Lesca, P., Narbonne, J., Carpy, A., 2000. Molecular Characteristics of Carbaryl, a *CYP1A1* Gene Inducer.Archives of Biochemistry and Biophysics. 373, 275–280.

Singh, N., Srivastava, G., Talat, M., Raghubanshi, H., Srivastava, O. N., Kayastha, A. M., 2014. Cicer a-galactosidase immobilization

onto functionalized graphene nanosheets using response surface method and its applications. Food Chemistry, 142, 430–438.

Smith, D.L., Doerder, F.P., 1992. Multiple effects of mutation on expression of alternative cell surface protein genes in tetrahymena thermophila. Genetics. 130 (1), 97-104.

Soozanipour, A., Taheri-Kafrani, A., 2018. Enzyme immobilization on functionalized graphene oxide nanosheets: efficient and robust biocatalysts. Methods in Enzymology. Academic Press. 608, 371-403.

Sophia, C.A., Lima E.C., Allaudeen N., Rajan S., 2016. Application of graphene based materials for adsorption of pharmaceutical traces from water and wastewater- a review. Desalination and Water Treatment. 57, 27573–27586.

Srivastava, G., Singh, K., Talat, M., Srivastava, O.N. , Kayastha, A.M., 2014. Functionalized Graphene Sheets As Immobilization Matrix for Fenugreek b-Amylase: Enzyme Kinetics and Stability Studies. PLoS ONE. 9, e113408.

Sterri, S.H. and Fonnum, F., 2009. Role of Carboxylesterases in Therapeutic Intervention of Nerve Gas Poisoning. In: Gupta, R.C. (Ed.), Handbook of Toxicology of Chemical Warfare Agents. Academic Press/Elsevier, New York, NY, pp. 1033-1040.

Sweeney, C. J., Chen, Y., Carducci, M., Liu, G., Jarrad, D. F., Eisenberg, M., Wong, Y., Hahn, N., Kohli, M., Cooney, M. M., Dreicer, R., Vogelzang, N. J., Picus, J., Shevrin, D., Hussain, M., Jarcia, J. A., Di Paola, R.S., 2015. Chemohormonal therapy in metastatic hormone-sensitive prostate cancer. New England Journal of Medicine. 373, 737-746.

Tang, Y., Guo, H., Xiao, L., Yu, S., Gao, N., Wang, Y., 2013. Synthesis of reduced graphene oxide/magnetite com- posites and investigation of their adsorption perfor- mance of fluoroquinolone antibiotics. Colloids and Surfaces A: Physicochemical and Engineering Aspects. 424, 74–80.

Tetko, I.V., Tanchuk, V.Y., 2002. Application of associative neural networks for prediction of lipophilicity in ALOGPS 2.1 program, Journal of Chemical Information and Computer Sciences. 42, 1136-45.

Thakur, M., Medintz, I.L., Walper, S.A., 2019. Enzymatic Bioremediation of Organophosphate Compounds—Progress and Remaining Challenges. Enzymes for Organophosphate Bioremediation. 7, 289.

Yan, L., Zhao, F., Wang, J., Zu, Y., Gu, Z., Zhao, Y. ,2019. A Safe-by-Design Strategy towards Safer Nanomaterials in Nanomedicines. Advanced Materials. 31, 1805391.

Youssef, A.M., El-Naggar, M.E., Malhat , F.M., El Sharkawi, H.M., 2019. Efficient removal of pesticides and heavy metals from wastewater and the antimicrobial activity of f-MWCNTs/PVA nanocomposite film. Journal of Cleaner Production. 206, 315-325.

Yuan, G., Yan, L., Liang, Z., Hui, H., Junjie, H., Syed, M.S., Xingguang, S., 2012. Adsorption and removal of tetra- cycline antibiotics from aqueous solution by graphene oxide. Journal of Colloid and Interface Science. 368, 540–546.

Zaytseva, O., Neumann, G., 2016. Carbon nanomaterials: production, impact on plant development, agricultural and environmental applications. Chemical and Biological Technologies in Agriculture. 3, 17.

Zhang, J., Zhang, F., Yang, H., Huang, X., Liu, H., Zhang, J., Guo, S., 2010. Graphene oxide as a matrix for enzyme immobilization. Langmuir. 26 (9), 6083-6085.

Zhang, M., Gao, B., Yao, Y., Xue, Y., Inyang, M., 2012. Synthesis, characterization, and environmental implications of graphene-coated biochar. Science of the Total Environment. 435–436, 567–572.

Chapter 5

N-doped graphene toxicity assessment in human plural mesothelial cell MeT5A and C6 glioma cells

(manuscript intended for submission in Science of the Total Environment)

Abstract

The toxic effects of N-doped graphene were studied in two different cellular model systems, human pleural mesothelial MeT5A and C6 glioma cells using a combination of sublethal cellular assay, the Alamar Blue assay as a general marker of cellular metabolism and LDH retention assay for the assessment of membrane damage. Moreover, reactive oxygen species (ROS) production and the micronucleus frequency were evaluated in low dose N-graphene exposed cells after 72 h. N-graphene caused a dose-dependent effect on the metabolic activity of MeT5A showing significant effects starting from 64 μg/mL, but no effects on LDH. By contrast, in C6 graphene was toxic at 256 μg/mL for metabolic responses, but a threshold effect on the release of LDH was observed starting from the lowest exposure level (4 μg/mL). Finally, N-graphene triggers neither ROS formation nor micronucleus formation in both cellular model systems, indicating the lack of genotoxic effects. These results suggest a moderate risk of the use of graphene in technological applications that pose for a safe-by design approach.

Keywords: 2D carbon nanomaterial; micronucleus, genotoxicity; reactive oxygen species

1. Introduction

In the last years graphene has received a great deal of attention from many research and manufacturing sectors. The value of graphene production was estimated to be around 12 million in 2013 and reached US$ 195 million US$ in 2018, with an expected value of 1.3 billion US$ until 2023 with a 5-year compound annual growth rate of 47.1% from 2018 to 2023 (Zurutuza & Marinelli 2014; BCC Research 2013; Ahmed & Rodrigues 2013; Nazarpour & Waite 2016; De Marchi et al. 2018).

Graphene is a planar sheet structure composed by a two-dimensional hexagonal sheet of carbon atoms. These two-dimensional sheets can compose a single layer graphene or two or multilayer graphene. It has a hybridised sp^2 bond, with three σ-bond on the plane dimension and π orbital perpendicular to the plane. The σ-bond permits the rigidity of hexagonal structure, while π-orbital allows the interaction between the different graphene layers (Choi et al. 2010).

There are numerous forms of graphene and many methods of synthesis. For example, graphene can be synthesised by exfoliation of graphite with chemical or mechanical energy (with the use of ultrasonication). The exfoliation process is carried out in liquid phase (water, phosphate buffer or liquid animal serum recent approaches use liquid nitrogen and several alcohols) (Cai et al. 2012; Hernandez-Sanchez et al. 2016; Pattammattel et al. 2017; Amiri, et al., 2017). Graphene oxide (GO)

was produced using modified Hummers protocol (All-Boucetta et al. 2013). Reduced graphene oxide (rGO) is obtained by reducing GO chemically, thermally, and electro/photochemically. Initially, hydrazine was used for the reduction process, but it was found to be toxic for humans and the environment, so green reducing agents like vitamin C, sugars, and microorganisms were used. In recent works, GO was reduced by ultrasonic irradiation at 50 °C in the absence of reducing agents (De Silva et al. 2017; Fernandez-Merino et al. 2010; Zhu et al. 2010; Akhavan & Ghaderi 2012; Soltani & Lee 2017). For graphene chemical characterisation are used X-ray photoelectron spectroscopy (XPS), Fourier transformation infrared spectroscopy (FTIR), Raman spectroscopy, X-ray diffraction (XRD), thermogravimetric analysis (TGA) and elemental analysis. To define morphology and size of graphene are used transmission electron microscopy (TEM), scanning electron microscopy (SEM) and atomic force microscopy (AFM) (Feedel et al. 2018).

The great popularity of graphene is linked to its many unique properties and application areas, some of them are optical, magnetic, thermal, mechanical, electronic, energy, biomedical, environmental and in personal care (De Marchi et al. 2018). Due to all these unique properties, it has been used in a lot of applications. One of the most interesting are sensors, in fact their electronic ability is based on the variation of its electrical conductivity as result of adsorption of molecules on the graphene surface (Lee et al. 2008). Graphene has shown good qualities as a sensor for gases and biological molecules, such as NO_2, NH_3, H_2O, CO_2, dinitrotoluene, glucose, catecholamine neurotransmitters, or cadmium (Schedin et al. 2007; Fowler et al. 2009;

Alwarappan et al. 2009; Li et al. 2009). Other applications of graphene are field-effect transistors, or transparent electrodes. Due to its peculiar thermal, chemical and mechanical stability, conjugated with its high transparency and atomic layer thickness it could be a good alternative to ITO in liquid crystal display (LCD). Furthermore, its large surface area and inactivity towards oxygen and water make it a promising candidate for photovoltaic applications. Graphene has also shown good ability to be used as anode material in Li-ion batteries, due to its unique electrical conductivity, high surface area and chemical tolerance (Li et al. 2008; Choi et al. 2010). It is important not to forget the use of graphene in environmental decontamination applications. Indeed, it is used to clean up soil from contaminants and pollution, to treat industrial emissions and also for decontamination of water and wastewater (Cohen-Tanugi & Grossman 2014, Nicolai et al. 2014; Konatham, et al. 2013; Sophia et al. 2016). Moreover, it is used in personal care, like inorganic sunscreen and dye protection (Qui et al. 2012; Benitez-Martinez et al. 2016).

Taking in account the increasing use of graphene and the perspective of future production growth, it is easy to assume a consequent discharge into the environment during manufacturing, transportation, use and disposal, with possible toxic impact at ecosystem level (He et al. 2017; De Marchi et al. 2018). Moreover, the production and the use of graphene-based products allows this nanomaterial to enter into the human body through inhalation, dermal absorption and ingestion (Oberdorster et al. 2005; Stone et al. 2017; Feedel et al. 2018).

In the last decades many experiments on the possible toxicity of graphene have been carried out, especially in the context of the

Graphene Flagship Project. This European project started in 2013 aims to assess the impact of graphene-based materials on human health and environment (Ferrari et al. 2015). A lot of study models were used, starting with microorganisms. Gurunathan et al. (2012) exposed *Pseudomonas aeruginosa* to GO and observed a dose-dependent decrease in viability. Ahmed & Rodrigues (2013) exposed a wastewater microbial community to GO and observed dose-dependent toxic effects, with significant impact on metabolic activity, viability and biological removal of nutrients. Other authors have found that cyanobacteria and different green algae species when exposed to graphene family materials exhibited a growth inhibition and ROS generation (Pretti et al. 2014; Wang et al. 2016; Tang et al. 2015; Nogueira et al. 2015). Katsumiti et al. (2017) exposed *Mytilus galloprovincialis* to GO, rGO, rGO with polyvinylpyrrolidone (PVP), GO with polyvinylpyrrolidone (PVP), resulting in a dose-dependent cytotoxicity on haemocytes. In detail, rGO-PVP was found to be more toxic than GO. GO, GO-PVP an rGO-PVP generated membrane damage and ROS-mediated toxicity (De Marchi et al. 2018). In relation to human toxicity have been evaluated all input pathways into the human body and possible areas of translocation, as well as studies on the immune system, lung tissue, cardiovascular and gastrointestinal tissue, effects on the reproductive system and the central nervous system (Feedel et al. 2018).

Effects of GO of different sizes have been evaluated on human and murine macrophages, showing a dose-dependent cytotoxicity and a higher internalisation of the smaller GO with a corresponding significant effect on cell viability and activation (Russier et al. 2013).

Chen et al. (2012) exposed RAW264.7 cells to GO and observed that increasing its concentration resulted in significant cell death, TRL signalling activation and consequent cytokine responses. Using molecular analysis they identified that TLR4 and TLR9 and their down signalling mediator (MyD88, TRAF6 and NF-kB) play an important role in inflammatory response induction by GO. Pulmonary effects of graphene NPs are assessed by inhalation in rats. Animals were evaluated at 1, 28 and 90 days after exposition and graphene was found into macrophages but no signal of inflammation was found. The material was also found in mediastinal lymph nodes, suggesting translocation. The same translocation was observed in animals exposed to various types of pristine and functionalized graphene (Kim et al. 2016; Lee et al. 2017). Graphene has also generated great interest in the area of neuroscience. Its unique properties make it interesting for engineering functional brain implants, in reconstruction of neurons and glial cells networks, but also for neurotherapies (Scaini & Ballerini 2018). The brain cells responses to prolonged GO exposure were evaluated by Rauti et al. (2016). The experiment emphasises cytotoxicity related to the lateral size of GO: large GO generated neuroglial and neuronal cell death. Although small GO did not generate cytotoxicity, it altered synaptic activity, with significant reduction postsynaptic current frequency (Feedel, et al., 2018).

A new interesting form of graphene is Nitrogen-doped graphene, which shown better catalytic properties than noble metal catalysts and better stability, it could be used for biosensing and biomedical applications (Banerjee 2018; Maddi et al. 2018; Agnoli & Favaro 2016). Not to mention its use in prevention and therapy of

atherosclerotic disease due to its electrochemical profile (Rivera et al. 2019; Baldea et al. 2020). However, very little data are available in literature on the toxicity of this specific type of graphene, which is significantly lower than other types.

Despite the great progress made in the last years on graphene toxicity study, there is still much to be done to define a good Safe-by-design approach for assessing quality and possible risks of this material.

To contribute to graphene toxicity assessment, in this work the hazard of N-doped graphene thin layer was tested using a battery of cellular, biochemical and genotoxicity markers in two model cell systems: human mesothelial MeT5A and C6 glioma cells.

2. Materials and Methods

2.1. Carbon nanomaterials.

Preparation of nitrogen-doped graphene by exfoliation of graphite rods with pulses of current Nitrogen-doped graphene was manufactured at the National Institute for Research and Development of Isotopic and Molecular Technologies (INCDTIM), Cluj-Napoca (Romania) as previously described (Baldea et., 2020). Briefly, samples have been obtained by exfoliation of graphite rods via pulses of current. Two graphite rods were employed as anode and cathode in an electrochemical cell, previously filled with 0.15 M NH_4OH + 0.15 M $(NH_4)_2SO_4$. The exfoliation has been realised through the application of an electrical voltage of 8 V, generating current around 0.5 A. To avoid overheating short current pulses have been applied between the electrodes with pulse duration of 0.8 s, intervals of 0.2 s,

total exfoliation length 4 h. At the end, the collected material has been washed with 10 L of distilled water. In the next steps the sample was dispersed by ultrasound in a water bath for 30 min in 125 mL of distilled water then filtered and finally dried by lyophilization. Elemental analysis of N-Graphene has shown that the sample contains a high number of hetero atoms: nitrogen (2.41 wt%) and sulfur (0.93 wt%). The full material characterization is available in Supplementary Information Section 1.

Carbon nanotubes (Nanothinx S.A. -Rio Patras, Greece) (Sweeney et al., 2015) and commercial carbon blacks Vulcan XC-72R™ (Fuel Cell, College Station, TX, USA) were used as reference control in some experiments.

2.2. Cultured cell models

MeT-5A cells were grown in Ham's F-10 medium with 10% foetal bovine serum and 1% penicillin-streptomycin, at 37 °C in 5% CO_2. C6 cells were grown in Dulbecco's Modified Eagle's Medium (DMEM) with 10% foetal bovine serum and 1% penicillin-streptomycin (Han et al. 2012), at 37 °C in 5% CO_2. The cultured cells were grown on 96 multi-well plates and seeded 24 hours before treatment to allow them to reach 40-50% confluence level. N-graphene concentrated (100X) stable dispersions were prepared in PBS / 2% foetal bovine serum, and sterilised in autoclave for 20 min at 121°C. Dilutions to each tested concentration were prepared in the full cell culture medium immediately before the start of the experiment. Four concentration levels were used: 4 µg/mL, 16 µg/mL, 64 µg/mL, 256 µg/mL

corresponding to 1.25; 5; 20; 80 µg / cm^2. Cells were incubated for 24 h (C6) and/or 72 hours (MeT5a and C6).

2.3. Cytotoxicity testing

For the Alamar Blue assay, resazurin (Calbiochem Research Biochemicals, Merck, Darmstadt, Germany) was prepared at 10 mg/mL concentration in sterile PBS and used as a 10X concentrated stock solution. Cells were prepared and treated as described in Section 2.2. After the addition of resazurin cells were incubated 2 h at 37 °C, 5% CO_2 and fluorescence read in a finale volume of 150 µl using a Infinite® 200 Pro (Tecan Sales AG, Mannedorf, Switzerland) plate reader using a 540- 570 nm excitation / 580-610 nm emission filter set. Data are presented as fluorescence arbitrary units.

Extracellular LDH enzyme levels were semiquantitatively determined using the CyQUANT LDH Cytotoxicity Assay (Thermofisher Scientific, Waltham, MA, USA) using 50 µl of cell culture supernatant. The intrinsic activity of N-graphene was subtracted to calculate the net extracellular LDH values. Data are presented as 490 nm absorbance units.

2.4. ROS formation assay

ROS formation was semiquantitatively evaluated using the cell-permeant 2',7'-dichlorodihydrofluorescein diacetate (H2DCFDA) dye (Thermofisher Scientific, Waltham, MA, USA). After cell exposure, cells were washed three times in sterile PBS and H2DCFDA dissolved in DMSO was added at a final concentration of 2.5 µM from a 100-

fold concentrated stock solution. After incubation at 37 °C for 30 min to allow dye penetration, cells were washed twice in PBS. Finally, 100 µl of PBS was added to each well and fluorescence was recorded for 30 min using a 485 nm excitation and 535 nm emission filter in a plate-reading fluorimeter (Tecan). ROS is shown as the slope of the linear curve obtained from the kinetic measurement.

2.5. Micronucleus Assay

The micronucleus assay was performed with cells grown on glass coverslips. The assay procedure and micronucleus frequency counting were performed according to Fenech (2007). After exposure, the cell medium was removed, the cells were washed three times in sterile PBS and left in air for 10 minutes. One (1) ml of methanol was added and incubated for 15 minutes for fixation. The methanol was discarded and the samples were allowed to air dry completely. The samples were rehydrated in Hank's balanced salt solution, and the coverslips were cleared of excess liquid and embedded in Floromount-G™ with DAPI (Invitrogen, Thermofisher Scientific, Waltham, MA, USA). Slides were evaluated under a fluorescence microscope at 400x magnification and analysed for micronucleus frequency using digital image analysis.

2.6. Statistical analysis

Data from at least four independent experiments were analysed using ANOVA after square root or logarithmic transformation and testing for homogeneity (Levene's test) and normality (Lilliefors K-S and Shapiro-Wilk test). When the criteria of ANOVA could not be met,

data were analysed using nonparametric statistics (Kruskal-Wallis and Kolmogorov-Smirnov two-sample tests) at $p \leq 0.05$. Further statistical details can be found in the text. The statistical software package Systat 12 (Systat Software, Inc, San Jose, CA, USA) was used for calculations.

3. Results

3.1. Cytotoxicity testing on MeT5A cells

Human pleural mesothelial cells -MeT5A- exposed to N-graphene at four increasing concentrations from 4 to 264 microg/mL for 72 hours were tested for cytotoxic effects using the Alamar Blue assay. In this assay, a statistically significant dose-dependent decrease in cell activity was detected, which was confirmed by the Kruskal-Wallis test at $p < 0.05$ (Figure 1). The concentrations showing a significant decrease in activity compared to the reference control were the two higher ones (64 and 264 microg/mL) (Kolmogorov-Smirnov Two Sample Test, $p < 0.05$)

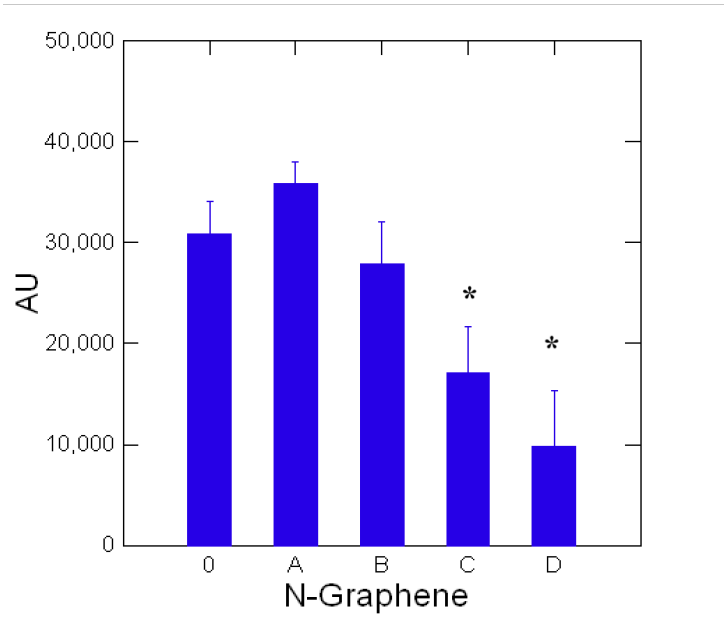

Figure 1. N-graphene cytotoxicity on mesothelial cells MeT5A (Alamar Blue assay). Shown are arbitrary fluorescence units (AU) -average +/- standard error from 4 independent experiments- obtained from the fluorimetric Alamar Blue assay evaluating the effects of N-graphene exposure on mitochondrial resazurin metabolization. Legend: 0 (reference control, not-exposed cells); A, 4 µg/ml; 16 µg/ml; C, 64 µg/ml; D, 256 µg/ml. * statistically different from reference control, $p < 0.05$ Kolmogorov-Smirnov Two Sample Test.

MeT5A cells were also tested for plasma membrane integrity by means of the LDH retention assay. After subtraction of the intrinsic activity of N-graphene, no statistically significant changes were observed in treated samples compared to not-exposed control cells controls (Supplemental Information Figure 1).

3.2. Cytotoxicity testing on C6 glioma cells

The cytotoxicity of N-graphene was studied in C6 glioma cells after 24- or 72-h exposure to the same concentration range (4-264 µg/mL) as MeT5A. Results showed a negligible effect on cellular metabolic activity after 24 hours and a scant decreasing trend (p=0.074, Kruskal-Wallis test) after 72 h which, however, is contained within 15% effect (Figure 2). The variable time, however, is highly significant (Kruskal-Wallis test, $p < 0.0001$).

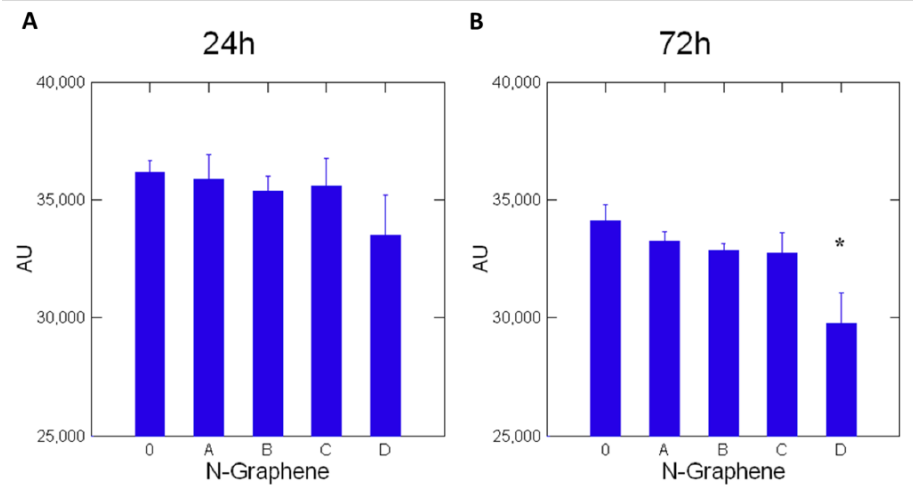

Figure 2. N-graphene cytotoxicity on C6 glioma cells(Alamar Blue). Panel A, 24 h exposure. Panel B, 72 h exposure. * Statistically different at $p < 0.05$ (Kolmogorov-Smirnov Two Sample Test); Legend as for Figure 1.

At 72 but not 24 h, net extracellular LDH activity showed a marked increase at all N-graphene values tested. Besides a threshold effect was

observed, this is clearly statistically significant at all exposure concentration with respect to reference control values ($p < 001$, Kolmogorov-Smirnov Two Sample Test). (Figure 3).

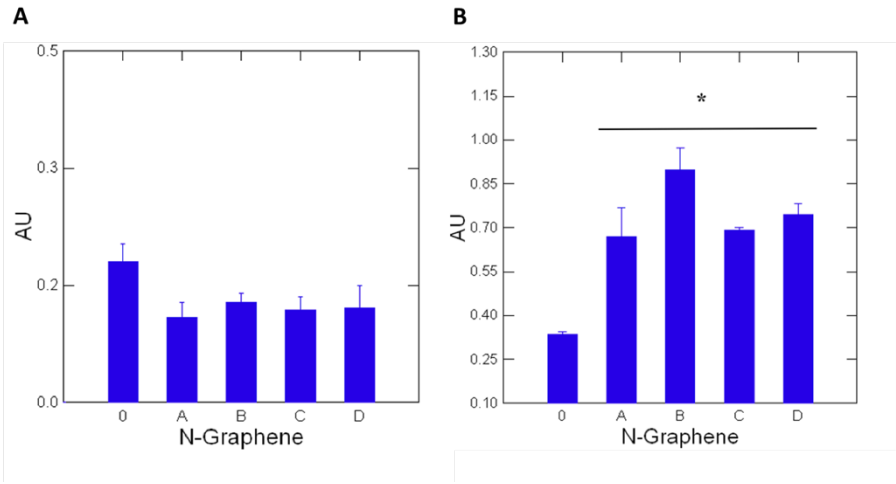

Figure 3. N-graphene cytotoxicity on C6 glioma cells (LDH assay). Caption as in Figure 2. * Statistically different at $p < 0.01$ (Kolmogorov-Smirnov Two Sample Test). Legend as in Figure 1.

3.3. ROS production and genotoxicity assessment of N-graphene

Both cell lines were exposed to N-graphene for 72 hours for ROS and micronuclei frequency evaluation (Figure 4 and Figure 5). Another two carbon nanomaterials, carbon black (CB) and carbon nanotubes (CNTs) were included in the analysis as reference materials. There was a statistically significant difference between the two cell models for both investigated variables (Kruskal-Wallis test, $p < 0.001$). In

particular, micronucleus frequency in MeT5A and C6 cells, basal level of micronuclei in the two cellular lines is different, C6 control showed an average of 0.42% vs 7.9% of MeT5A. N-graphene did not elicit any significant ROS increase in either cell models (Figure 4), but a trend of reduction in C6. At the same time, the frequency of micronuclei did not change significantly in MeT5A cells, while it actually decreased significantly by 25% in C6 glioma cells (Figure 5). Interestingly, CNT caused production of ROS and increased frequency of micronucleation (average value 19.8%) in MeT5A cells, and this was paralleled by CB in C6 cells (3.1%). In the latter, CNT is also positive for micronucleus (average value 1.26%), but not for triggering ROS formation.

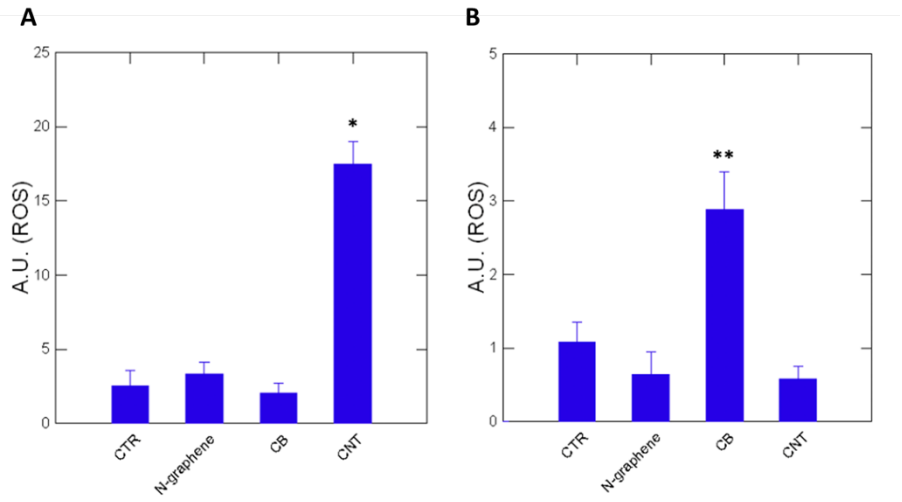

Figure 4. ROS production. ROS levels were evaluated in the two cell types after 72 h exposure at 4 µg/mL to N-graphene, along with carbon blacks nanoparticles and carbon nanotubes as reference materials. Legend: CTR, reference control (not-exposed cells); N-graphene, N-doped graphene; CB, carbon black nanoparticles; CNT, carbon nanotubes. Panel A, MeT5A cells; Panel B, C6 glioma cells. Shown are average ROS Arbitrary Units +/- standard error obtained from 4 independent experiments. * statistically different from reference control, p <0.001 Kolmogorov-

Smirnov Two Sample Test; ** p<0.05 One-way ANOVA, Tukey's post hoc test for pairwise comparison).

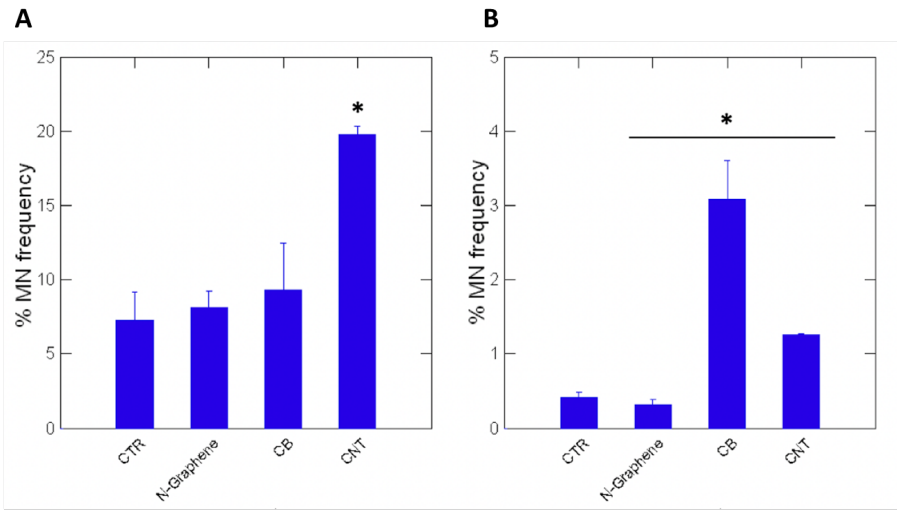

Figure 5 Micronucleus test. Figure caption as in Figure 4, except micronucleus frequencies +/- standard errors are indicated. * statistically different from reference control, $p < 0.0001$ Kolmogorov-Smirnov Two Sample Test.

4. Discussion

In this article, we have investigated the potential toxicological effects of N-graphene synthesized by electrochemical exfoliation of graphite rods using current pulses. Because of the important role that graphene-based nanomaterials play in many productive fields and in some relevant medical applications, it is essential to define the toxicity of graphene in a variety of models, and it is important to approach any new technological use of graphene with a safe-by-design approach (Guo et al., 2021).

It is important to note that this nanomaterial may enter the human body through inhalation, dermal adsorption, and ingestion during the manufacture and use of graphene-based products. Therefore, we decided to first investigate its potential toxicity in a mesothelial cell line (MeT5A) (Oberdorster, et al., 2005; Feedel, et al., 2018; Stone, et al., 2017). In addition, graphene has been used in various medical applications, including as a carrier for drugs or molecules. This material plays a really interesting role in cancer therapy. Some, et al., (2014), for example, described the use of another form of graphene for targeted delivery of anticancer drugs. Its use in brain disease therapy is also interesting. Many studies have highlighted the ability of graphene to cross the blood-brain barrier (BBB). Mendonca, et al., (2015) reported the ability of reduced graphene oxide to enter the brain and downregulate the junction proteins responsible for the tight connection between cells in the BBB. Su, et al., (2020) demonstrated the transport of graphene oxide (GO) and porphyrin-coupled GO -a form of N-graphene- through the BBB in an in vitro platform using human BBB microvascular endothelial cells. Similarly, Kim, et al., (2018) have demonstrated the ability of graphene quantum dots to cross the BBB for the treatment of Parkinson's disease and have shown that graphene quantum dots functionalized with α-syn fibrils exhibit neuroprotective properties. With this in mind, we decided to use C6 glioma cells as the second model of our study, which is also a good model for normal astrocyte cells (Galland, et al., 2019).

We coupled cytotoxicity assays-Alamar Blue and external LDH-with genotoxicity assays and included the production of ROS as a triggering

event for various pathological conditions such as genotoxicity itself and carcinogenesis. The Alamar Blue assay is an indicator of cell viability but also a marker of mitochondrial metabolism. In addition, the LDH retention assay was used as an indicator of plasma membrane damage/destabilisation. In terms of viability, our results showed a LOEC value of 64 μg/mL in MeT5A and 256 μg/mL in C6 glioma cells after 72 hours of exposure. It is important to note that shorter exposures to MeT5A are usually ineffective because mesothelial cells have little or no endocytosis (Nagai et al., 2011), but -unlike we expected- it was necessary to extend the exposure to 72 hours even in C6 cells. However, our results are comparable to those reported by other authors in human lung carcinoma A549 with chemically engineered N-graphene (Bhatt, et al., 2016) or primary human umbilical vein endothelial cells HUVEC (Shah, et al., 2021), the latter with chemically engineered N-carbon quantum dots. In another study using N-graphene preparations very similar to ours, Baldea, et al (2020) found a dose-dependent response but also reported very severe effects as low as 1 μg/mL. The same authors then reported weak N-graph effects in DLD-1 human colon cancer cells following a U-shape trend.

As for LDH and N-graphene exposure, it should be said that N-graphene showed a significant dose dependent intrinsic activity that can alter the test response. The enzyme activities we show in this work are net values from which intrinsic activity has been subtracted. Said that, MeT5A cells showed no significant effects (see Supplementary Information S1), but C6 glioma cells responded to the full range of N-graphene concentrations. It should be said, however, that the lack of loss of viability may indicate an increased rate of exocytosis rather than

membrane damage. Baldea, et al., (2020) reported some effects in both HUVECs and DLD1 cells.

The selected cell lines were tested for genotoxicity and ROS production as carbon nanomaterials are usual triggers.
N-graphene was not able to trigger the formation of ROS and at the same time did not elicit genotoxicity as evaluated by means of micronucleus frequency. In C6s, N-graphene showed a significant protective effect, which could be consistent with the slight reduction in the observed formation of ROS. Indeed, Baldea et al., (2020) obtained a statistically significant ROS scavenging effect with their three electrochemical graphite exfoliated N-graphenes, which we recall are similar to ours. Moreover, our results are confirmed by Deng, et al., (2019) in zebrafish embryos treated with N-GQD. By contrast, differential genotoxic effects were observed using other carbon nanomaterials, respectively CNT for MeT5A and CB for C6 cells whereby the more pronounced increases in ROS had a straightforward counterpart at the level of chromosomal damage (we do not dwell on these data because they are beyond the scope of the discussion).
The lack of genotoxic damage leaves less uncertainty that N-graphene poses no risk from accidental or occupational exposure. We believe that different levels of investigation should be considered in the risk assessment and that the inclusion of multiple cell lines and a genotoxicity test is mandatory to make a decision, especially if it is a "safe-by-design" approach procedure.

5. **Conclusions**

We have tested cytotoxicity and genotoxicity of N-graphene obtained by electrochemical exfoliation of graphite rods using current pulses. Scant cytotoxic effects and lack of impacts on micronucleus frequency were reported, suggesting this carbon nanomaterials as a safer alternative to e.g. graphene oxide, carbon nanotubes and carbon black.

Bibliography

1. Agnoli, S., Favaro, M., 2016. Doping graphene with boron: a review of synthesis methods, physicochemical characterization, and emerging applications. Journal of Materials Chemistry. 4, 5002.

2. Ahmed, F., Rodrigues, D.F., 2013. Investigation of acute effects of graphene oxide on wastewater microbial community: A case study. Journal of Hazardous Materials. 256-257, 33-39.

3. Akhavan, O., Ghaderi, E., 2012. *Escherichia Coli* Bacteria Reduce Graphene Oxide to Bactericidal Graphene in a Self-Limiting Manner. Carbon. 50, 1853-1860.

4. All-Boucetta, H., Bitounis, D., Raveendran-Nair, R., Servant, A., Van den Bossche, J., & Kostarelos, K., 2013. Purified Graphene Oxide Dispersions Lack *In Vitro* Cytotoxicity and *In*

Vivo Pathogenicity. Advanced Healthcare Materials. 2(3), 433-441.

5. Alwarappan, S., Erdem, A., Liu, C., Li, C., 2009. Probing the Electrochemical Properties of Graphene Nanosheets for Biosensing Applications. The Journal of Physical Chemistry. 113(20), 8853-8857.

6. Amiri, A., Zubir, M. N., Dimiev, A. M., Teng, K. H., Shanbedi, M., Kazi, S. N., & Rozali, S. B., 2017. Facile, environmentally friendly, cost effective and scalable production of few-layered graphene. Chemical Engineering Journal. 326, 1105-1115.

7. Baldea, I., Olteanu, D., Filip, G. A., Pogacean, F., Cros, M., Suciu, M., Tripon,S. C., Cenarius, M., Magerusan, L., Staden, R. S., Pruneanu, S., 2020. Cytotoxicity mechanisms of nitrogen-doped graphene obtained by electrochemical exfoliation of graphite rods, on human endothelial and colon cancer cells. Carbon. 158, 267-281.

8. Banni, M., Negri, A., Mignone, F., Bousetta, H., Viarengo, A., & Dondero, F. , 2011. Gene Expression Rhythms in the Mussel *Mytilus galloprovincialis* (Lam.) across an Annual Cycle. Plos One. 6(5), e18904.

9. Banerjee, A.N., 2018. Graphene and its derivatives as biomedical materials: future prospects and challenges.

Interface Focus. 6, 20170056. BCC Research, 2013. Graphene: Technologies, Applications and Markets. (https://www.bccresearch.com/market-research/advanced-materials/graphene-technologies-applications-markets-report.html)(accessed February 2016)

10. Benitez-Martinez, S., Lopez-Lorente, A.I., Valcarcel, M., 2016. Determination of TiO2 nanoparticles in sunscreen using N-doped graphene quantum dots as a fluorescent probe. Microchimica Acta. 183, 781-789.

11. Bhatt, J., Modal, D., Devkar, R.V., Prasad, K., 2016. Synthesis of functionalized N-doped graphene DNA hybrid material in a deep eutectic solvent. Green Chemistry. 18, 4297-4302.

12. Cai, M., Thorpe, D., Adamson, D.H., Schniepp, H.C., 2012. Methods of graphite exfoliation. Journal of Materials Chemistry. 22, 24992-25002.

13. Chen, G.Y., Yang, H.J., Lu, C.H., Chao, Y.C., Hwang, S.M., Chen, C.L., Lo, L.Y. Sung, K.W., Luo, W.Y., Tuan, H.Y., Hu, Y.C., 2012. Simultaneous Induction of Autophagy and Toll-like Receptor Signalling Pathways by Graphene Oxide. Biomaterials. 33, 6559-6569.

14. Choi, W., Lahiri, I., Seelaboyina, R., Kang, Y.S., 2010. Synthesis of Graphene and Its Applications: A Review. Critical Reviews in Solid State and Materials Sciences. 35, 52-71.

15. Cohen-Tanugi, D., Grossman, J.C., 2014. Water permeability of nanoporous graphene at realistic pressures for reverse osmosis desalination. The Journal of Chemical Physics. 141, 119901.

16. De Marchi, L., Pretti, C., Gabriel, B., Marques, P. A., Freitas, R., & Neto, V., 2018. An overview of graphene materials: Properties, applications and toxicity on aquatic environments. Science of the Total Environment. 631-632, 1440-1456.

17. De Silva, K.K.H., Huang, H.H., Joshi, R.K., Yoshimura, M., 2017. Chemical Reduction of Graphene Oxide Using Green Reductants. Carbon. 119, 190-199.

18. Deng, S., Fu, A., Junaid, M., Wang, Y., Yin, Q., Fu, C., L. Liu, Su, D., Bian, W. , Pei, D., 2019. Nitrogen-doped graphene quantum dots (N-GQDs) perturb redox-sensitive system via the selective inhibition of antioxidant enzyme activities in zebrafish. Biomaterials. 206, 61-72.

19. Feedel, B., Bussy, C., Merino, S., Varquez, E., Flahaut, E., Mouchet, F., Evariste, L., Gauthier, L., Koivisto, A.J., Vogel, U., Martin, C., Delogu, L.G., Buerki-Thurnherr, T. , Wick, P.,

Beloin-Saint-Pierre, D., Hischier, R., Pelin, M., Carniel, F.C., 2018. Safety Assessment of Graphene-Based www.acsnano.org Materials: Focus on Human Health and the Environment. ACS Nano. 12, 10582-10620.

20. Fenech, M., 2007. Cytokinesis-block micronucleus cytome assay. Nature Protocols. 2(5), 1084-1104.

21. Fernandez-Merino, M.J., Guardia, L., Paredes, J.I., Villar-Rodil, S., Solis-Fernandez, P., Martinez-Alonso, A., & Tascon, J.M., 2010. Vitamin C Is an Ideal Substitute for Hydrazine in the Reduction of Graphene Oxide Suspensions. The Journal of Physical Chemistry. 114(14), 6426-6432.

22. Ferrari, A.C., Bonaccorso, F., Fal'ko, V., Novoselov, K.S., Roche, S., Boggild, P., Borini, S., Koppens, F.H. L., Palermo, V., Pugno, N., Garrido, J.A., Sordan, R., Bianco, A., Ballerini, L., Prato, M., Lidorikis, E., Kivioja, J., Marinelli, C., Ryhan, 2015. Science and Technology Roadmap for Graphene, Related Two-Dimensional Crystals, and Hybrid Systems. Nanoscale. 7, 4598-4810.

23. Fowler, J.D., Allen, M.J., Tung, V.C., Yang, Y., Kaner, R.B., Weiller, B.H., 2009. Practical chemical sensors from chemically derived graphene. ACS Nano. 3, 201.

24. Galland, F., Seady, M., Taday, J., Smaili, S.S., Goncalves, C.A., Leite, M.C., 2019. Astrocyte culture models: Molecular and function characterization of T primary culture, immortalised astrocytes and C6 glioma cells. Neurochemistry International. 131, 104538.

25. Guo, Z., Chakraborty, S., Monikh, F.A., Varsou, D.D., Chetwynd, A.J., Afantitis, A., Lynch, I., Zhang, P., 2021. Surface Functionalization of Graphene-Based Materials: Biological Behaviour, Toxicology, and Safe By Design Aspects. Advanced Biology. 5(9), 2100637.

26. Gurunathan, S., Han, J.W., Abdal Daye, A., Eppakayala, V., Kim, J., 2012. Oxidative stress-mediated antibacterial activity of graphene oxide and reduced graphene oxide in *Pseudomonas aeruginosa*. International Journal of Nanomedicine. 7, 5901-5914.

27. He, K., Chen, G., Zeng, G., Peng, M., Huang, Z., Shi, J., Huang, T. , 2017. Stability, transport and ecosystem effects of graphene in water and soil environments. Nanoscale. 9(17), 5370-5388.

28. Hernandez-Sanchez, D., Scardamaglia, M., Saucedo-Anaya, S., Bittencourt, C., Quintana, M. , 2016. Exfoliation of graphite and graphite oxide in water by chlorin e6. RSC Advances. 6, 66634-66640.

29. Katsumiti, A., Tomovska, R., Cajaraville, M.P., 2017. Intracellular localization and toxicity of graphene oxide and reduced graphene oxide nanoplatelets to mussel hemocytes in vitro. Aquatic Toxicology. 188, 138-147.

30. Kim, J.K., Shin, J.H., Lee, J.S., Hwang, J.H., Lee, J.H., Baek, J.E., KIm, B.W., Kim,J. S., Lee, G.H., Ahn, K., Han, S.G., Bello, D., Yu, I.J., 2016. 28-Day Inhalation Toxicity of Graphene Nanoplatelets in Sprague-Dawley Rats. Nanotoxicology. 10, 891-901.

31. Kim, D., Yoo, J.M., Hwang, H., Lee, J., Lee, S.H., Yun, S. P., Park, M.J., Lee, M., Choi, S., Kwon, S.H., Lee, S., Kwon, S., Kim, S., Park,Y.J., Kinoshita, M., Lee, Y., Shin, S., Paik, S.R., Lee, S.J., Lee, S., Hong, B.H., Ko, H.S., 2018. Graphene quantum dots prevent α-synucleinopathy in Parkinson's disease. Nature Nanotechnology. 13, 812-818.

32. Konatham, D., Yu, J., Ho, T.A., Striolo, A., 2013. Simulation Insights for Graphene-Based Water Desalination Membranes. Langmuir. 29(38), 11884-11897.

33. Lee, C., Wei, X., Kysar, J.W., Hone, J., 2008. Measurement of the elastic properties and intrinsic strength of monolayer graphene. Science. 321, 385.

34. Lee, J.K., Jeong, A. Y., Bae, J., Seok, J.H., Yang, J.Y., Roh, H.S., Jeong, J., Han, Y., Jeong, J., Cho, W.S., 2017. The Role of Surface Functionalization on the Pulmonary Inflammogenicity and Trans- location into Mediastinal Lymph Nodes of Graphene Nanoplatelets in Rats. Archives of. Toxicology. 91, 667-676.

35. Li, X., Wang, X., Zhang, L., Lee, S., Dai, H., 2008. Chemically derived, ultrasmooth graphene nanoribbon semiconductors. Science. 319, 1229.

36. Li, J., Guo, S., Zhai, Y., Wang, E., 2009. Nafion–graphene nanocomposite film as enhanced sensing platform for ultrasensitive determination of cadmium. Electrochemistry Communications. 11(5), 1085-1088.

37. Maddi, C., Bourquard, F., Barnier, V., Avila, J., Asensio, M. C., Tite, T., Donnet, C.,Garrelie, F., 2018. Nano-architecture of nitrogen-doped graphene films synthesised from a solid CN source. Scientific Reports. 8, 3247.

38. Mendonca, M.C., Soares, E.S., De Jesus, M.B., Ceraglioli, H.J., Ferreira, M.S., Catharino, R.R., Da Cruz-Hofling, M.A., 2015. Reduced graphene oxide induces transient blood–brain barrier opening: an *in vivo* study. Journal of Nanobiotechnology. 13, 1-13.

39. Nazarpour, S., Waite, S.R., 2016. Graphene Technology: From Laboratory to Fabrication, first edition, Wiley-VCH Verlag GmbH & Co. KGaA, Weinheim, Germany.

40. Nicolai, A., Sumpter, B., Meunier, V., 2014. Tunable water desalination across graphene oxide framework membranes. Physical Chemistry Chemical Physics. 16(18), 8646-8654.

41. Nogueira, P.F., Nakabayashi, D., Zucolotto, V., 2015. The effects of graphene oxide on green algae *Raphidocelis subcapitata*. Aquatic Toxicology. 166, 29-35.

42. Oberdorster, G., Oberdorster, E., Oberdorster, J., 2005. DMCA Nanotoxicology: an emerging discipline evolving from studies of ultrafine particles. Environmental Health Perspectives, 113, 823-839.

43. Pattammattel, A., Pande, P., Kuttappan, D., Puglia, M., Basu, A. K., Amalaradjou, M. A., Kumar, C.V. , 2017. Controlling the Graphene−Bio Interface: Dispersions in Animal Sera for Enhanced Stability and Reduced Toxicity. Langmuir. 33, 14184-14194.

44. Pretti, C., Olivia, M., Di Pietro, R., Monni, G., Cevasco, G., Chiellini, F., Pomelli, C., Chiappe, C., 2014. Ecotoxicity of pristine graphene to marine organisms. Ecotoxicology and Environmental Safety. 101, 138-145.

45. Qui, Y., Wang, Z., Owen, A.C., Kulaots, I., Chen, Y., Kane, A.B., Hurt, R.H., 2012. Antioxidant chemistry of graphene-based materials and its role in oxidation protection technology. Nano. 6(20), 11744-11755.

46. Rauti, R., Lozano, N., Leon, V., Scaini, D., Musto, M., Rago, I., Ulloa Severino, F.P., Fabbro, A., Casalis, L., Vazquez, E., Kostarelos, K., Prato, M., Ballerini, L., 2016. Graphene Oxide Nanosheets Reshape Synaptic Function in Cultured Brain Networks. ACS Nano. 10, 4459-4471.

47. Rivera, L.M., Betancur, A.F., Zarate, D.G., Torres, D., Hoyos, L.M., Garcia, A., 2019. Reduction and Simultaneous Doping of Graphene Oxide to Repel LDL in Treatment of Atherosclerosis Disease. Chemical Physics. arXiv:1902.01850

48. Russier, J., Treossi, E., Scarsi, A., Perrozzi, F., Dumortier, H., Ottaviano, L.,Meneghetti, M., Palermo, V., Bianco, A. , 2013. Evidencing the Mask Effect of Graphene Oxide: A Comparative Study on Primary Human and Murine Phagocytic Cells. Nanoscale. 5, 11234-11247.

49. Scaini, D., Ballerini, L., 2018. Nanomaterials at the neural interface. Current Opinion in Neurobiology. 50, 50-55.

50. Schedin, F., Geim, A. K., Morozov, S. V., Hill, E. W., Blake, P., Katsnelson, M. I., & Novoselov, K. S., 2007. Detection of individual gas molecules adsorbed on graphene. Nature Materials. 6, 652.

51. Shah, H., Xie, W., Wang, Y., Jia, X., Nawaz, A., Xin, Q., Song, M., Gong, J. R., 2021. Preparation of blue- and green-emissive nitrogen-doped graphene quantum dots from graphite and their application in bioimaging. Materials Science & Engineering C. 119, 111642.

52. Soltani, T., Lee, B., 2017. A benign ultrasonic route to reduced graphene oxide from pristine graphite. Journal of Colloid and Interface Science. 486, 337-343.

53. Some, S., Gwon, A., Hwang, E., Bahn, G., Yoon, Y., Kim, Y., Kim, S., Bak, S., Yang, J., Jo, D., Lee, H., 2014. Cancer Therapy Using Ultrahigh Hydrophobic Drug-Loaded Graphene Derivatives. Scientific Report. 4, 6314.

54. Sophia, A.C., Lima, E.C., Allaudeen, N., Rajan, S., 2016. Application of graphene based materials for adsorption of pharmaceutical traces from water and wastewater- a review. Desalination and Water Treatment. 57, 27573-27586.

55. Stone, V., Miller, M.R., Clift, M.J., Elder, A., Mills, N.L., Moller, P., Schins, R.P.F., Vogel, U., Kreyling, W.G., Alstrup

Jensen, K., Kuhlbusch, T.A.J., Schwarze, P.E., Hoet, P., Pietroiusti, A., De Vizcaya-Ruiz, A., Baeza-Squiban, A. Teixe., 2017. Nanomaterials Versus Ambient Ultrafine Particles: An Opportunity to Exchange Toxicology Knowledge. Environmental Health Perspectives. 125, 106002.

56. Su, S., Wang, J., Qiu, J., Martinez-Zaguilan, R., Sennoune, S.R., Wang, S., 2020. In vitro study of transportation of porphyrin immobilised graphene oxide through blood brain barrier. Materials Science and Engineering C. 107, 110313.

57. Sweeney, C. J., Chen, Y., Carducci, M., Liu, G., Jarrad, D. F., Eisenberg, M., Wong, Y., Hahn, N., Kohli, M., Cooney, M. M., Dreicer, R., Vogelzang, N. J., Picus, J., Shevrin, D., Hussain, M., Jarcia, J. A., Di Paola, R.S., 2015. Chemohormonal therapy in metastatic hormone-sensitive prostate cancer. New England Journal of Medicine. 373, 737-746.

58. Tang, Y., Tian, J., Li, S., Xue, C., Xue, Z., Yin, D., Yu, S., 2015. Combined effects of graphene oxide and Cd on the photosynthetic capacity and survival of Microcystis aeruginosa. Science of The Total Environment. 532, 154-161.

59. Wang, Z., Gao, Y., Wang, S., Fang, H., Xu, D., Zhang, F. , 2016. Impacts of low-molecular-weight organic acids on aquatic behaviour of graphene nanoplatelets and their induced

algal toxicity and antioxidant capacity. Environmental Science and Pollution Research. 23, 10938-10945.

60. Zhu, C., Guo, S., Fang, Y., Dong, S., 2010. Reducing Sugar: New Functional Molecules for the Green Synthesis of Graphene Nano- sheets. ACS Nano. 4, 2429-2437.

61. Zurutuza, A., Marinelli, C., 2014. Challenges and opportunities in graphene commercialization. Nature Nanotechnology Volume. 9, 730-734.

Supplementary information: N-doped graphene toxicity assessment in human plural mesothelial cell MET5A and C6 glioma cells

1. Materials synthesis and characterization

1.1. Synthesis and characterization of N-doped graphene

Nitrogen-doped graphene (N-Graphene or N-Gr) has been manufactured and characterized at INCDTIM Cluj-Napoca during the end of first year and the start of second year of the PhD period.

The N-doped samples have been obtained by exfoliation of graphite rods via pulses of current (Figure 1). Two graphite rods were employed as anode and cathode in an electrochemical cell, previously filled with an appropriate electrolyte, 0.15 M NH_4OH + 0.15 M $(NH_4)_2SO_4$. The exfoliation has been realized through the application of an electrical voltage of 8 V, generating current around 0.5 A. To avoid over-heating short current pulses have been applied between the electrodes with pulse duration of 0.8 s, intervals of 0.2 s, total exfoliation length 4 h. At the end, the collected material has been washed with 10 L of distilled water. In the next steps the sample was dispersed by ultrasound in a water bath for 30 min in 125 mL of distilled water then filtered and finally dried by lyophilization. Elemental analysis of N-

Graphene has shown that the sample contains a high number of hetero atoms: nitrogen (2.41 wt%) and sulfur (0.93 wt%) (data not shown).

Figure 1. Apparatus for graphite exfoliation *via* pulses of current

1.2. XRD characterization of N-doped graphene

X-ray powder diffraction (XRD) pattern of N-graphene samples have been evaluated on a Bruker-D8 Advance Diffractometer with tube set at 40 kV and 40 mA. The DIFFRAC plus XRD Commander Package software has been used for data acquisition and analysis. Figure 2 shows the XRD pattern of a representative N-doped graphene sample, showing a majority of few-layer graphene (FLG), with some multi-layer graphene (MLG) and graphene oxide (GO).

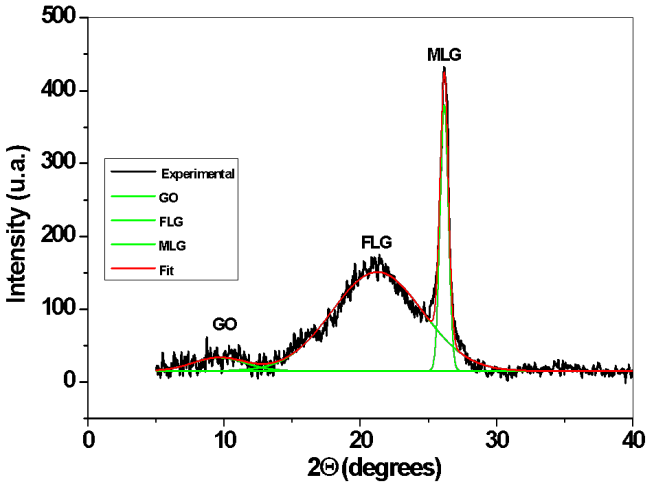

Figure 2. XRD pattern of N-Graphene sample

The XRD method is very attractive for structural characterization of N-graphene as it allows the determination of some critical parameters: the mean crystallite size (D), the interlayer distance (d), and the number of layers (n) within the crystallites. The D value has been determined from the full width at half maximum (FWHM) of the corresponding XRD peak using the Scherrer equation (Warren et al., 1969; 1990) while the interlayer distance has been found through the Bragg equation (Rashid bin et al., 2015). In addition, the average number of layers, n, has been calculated by equation $n=D/d$.

Table 1 reports the obtained parameters. Therefore, the crystallites size is ranging from 2.21 nm (GO) to 15.3 nm (MLG). As expected, the interlayer distance is very large for GO crystallites (0.93 nm) due to the presence of oxygen-containing groups and considerably smaller for MLG (0.34 nm). The largest amount of crystallites corresponds to FLG (75 %) while GO and MLG have been found in smaller amounts, 6% and 19% respectively.

Sample	*Peak position 2θ* (deg)	*D* (nm)	*d* (nm)	*n*	*Amount*
N-Gr	9.61 (GO)	2.21	0.93	~2	6 %
	21.23 (FLG)	1.29	0.42	~3	75 %
	26.16 (MLG)	15.3	0.34	~45	19 %

Table n1. The structural parameters obtained from XRD pattern for N-Gr sample

1.3. Scanning Electron Microscopy (SEM) analysis of N-graphene samples and other carbon (nano) materials

SEM analysis was performed using a SU8230 High-Resolution Scanning Electron Microscope (Hitachi, Tokyo, Japan) equipped with a cold field emission gun. Figure 3 shows representative SEM images of a N-Graphene sample. Both images reveal the thin layers of graphene with the lateral size below the micron scale.

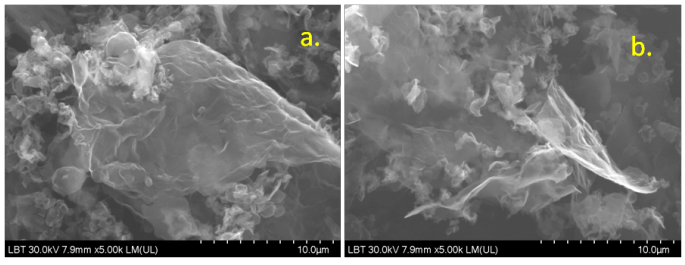

Figure 3. SEM images of N-Gr sample: horizontal(a) and lateral(b) view.

Figure 4 shows SEM imaging of Spent Coffee Ground carbon (biochar) that appear as a porous structure in the micron scale.

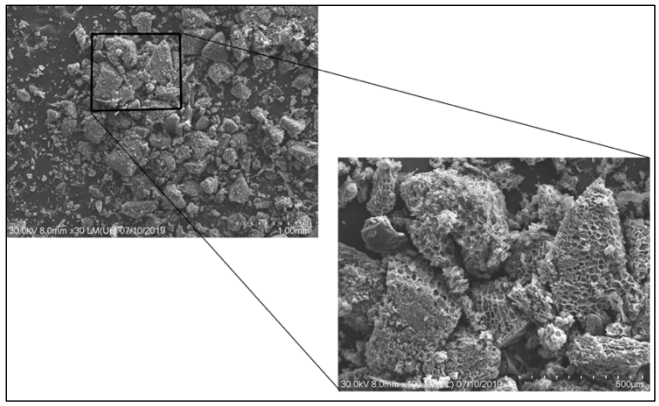

Figure 4. Representative SEM imaging of a biochar sample. The high magnification picture (left panel) shows a porous structure with pores in the micron scale.

Figure 5 shows SEM imaging of NTX-1 (< 1 μm), a CNT preparation made available in the framework of the H2020 project Nanogentools

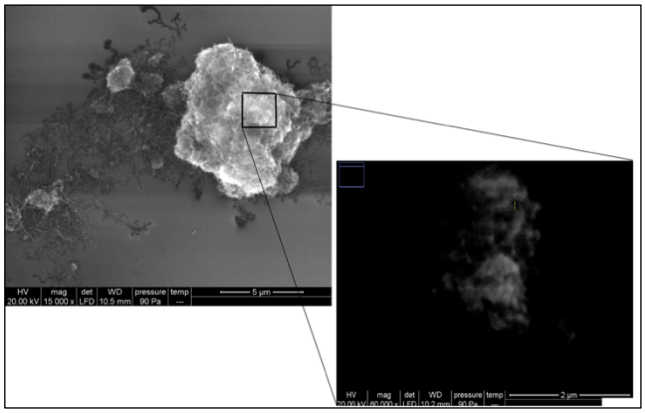

Figure 5. SEM image of NTX1 sample. The close-up frame (60000 x magnification) shows aggregated tangled nanotubes forming a sponge-like structure with 100-200 nm pores.

2. Supplementary Figure S1

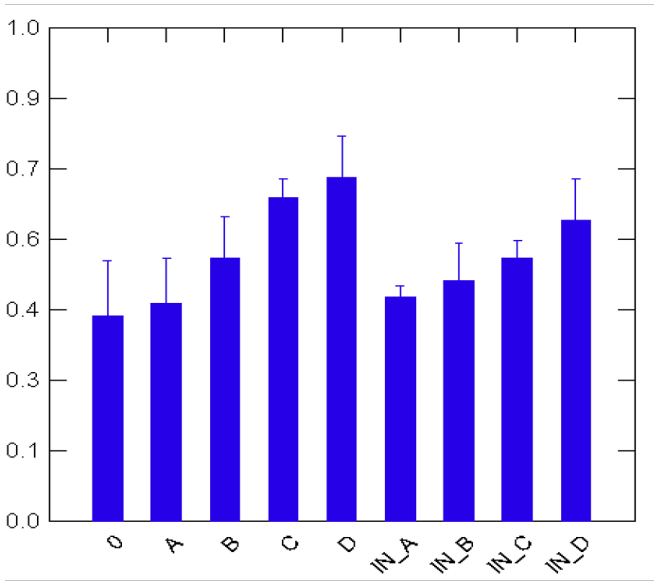

Supplementary Information Figure S1. LDH retention assay in MET5A exposed to N-Graphene.

Shown are arbitrary levels (average +- standard errors from at least 3 independent experiments) of LDH activity measured the cell culture medium (supernatant) after 72 h .

There were no statistically sigN-Graphene showed a dose dependent intrinsic enzymatic activity.

nificant differences in the presence / absence of cells (Kolmogorov-Smirnov Two Sample Test, $p > 0.05$). See Panel below

Legend: Legend: 0 (reference control, not-exposed cells); A, 4 µg/ml; 16 µg/ml; C, 64 µg/ml; D, 256 µg/ml. IN_A-D, intrinsic activity of N-Graphene.

Two-Sided Probabilities

	0	A	B	C	D	IN_A	IN_B	IN_C	IN_D
0	1.000								
A	1.000	1.000							
B	0.125	1.000	1.000						
C	0.125	0.000	0.125	1.000					
D	0.125	0.500	0.125	1.000	1.000				
IN_A	0.500	0.667	0.500	0.000	0.000	1.000			
IN_B	0.500	0.667	1.000	0.500	0.500	1.000	1.000		
IN_C	0.500	0.667	1.000	0.000	0.500	0.000	0.667	1.000	
IN_D	0.500	0.667	1.000	1.000	1.000	0.000	0.667	0.667	1.000

Chapter 6

Discussion

This work was developed within the European H2020- MSCA-RISE project NANOGENTOOLS (coordinator, University of Burgos, Spain; https://cordis.europa.eu/project/id/691095/it; GA number: 691095). The main aim of the project was to develop new methods to identify and control hazards and risks associated with nanomaterials (NMs), especially to ensure the safety of consumers and citizens. The project was carried out by a consortium composed of academic and industrial partners.

This work aimed to achieve two main objectives. First, to find and test a solution for a rapid and reliable assessment of the toxicity of carbon nanomaterials, using high-throughput screening and omics tools that can predict the toxicological properties of NMs; second, to develop the safe-by-design concept that demonstrates the safe use of NMs and carbon-based nanosensors.

The common denominator between these two important points was the approach to the question of safe by design. Therefore, we structured a work starting from a possible biotechnological application based on carbon nanomaterials and we evaluated the toxicity of these carbon nanomaterials.

The first step of the work was to evaluate the toxicity of carbon nanotubes (CNTs) provided by a NANOGENTOOL project partner (Nanothinx, Patras, Greece). This part of the work was part of the first of the two goals of the project, i.e., it allowed us to identify the least risky material for biotechnological application.

The second step of the work was to realize a biotechnological application based on carbon-based nanomaterials. The goal of this part of the project was to develop carbon-based nanomaterials functionalized with carboxylesterase enzymes capable of removing pesticides from water.

The rationale behind our NM toxicity tests was to develop a multi-tier assessment approach. It included multiple levels of complexity and biological organization, i.e., cytotoxicity, genotoxicity ROS formation, and toxicogenomics. This type of approach can provide mechanistic information on the mode of action of NMs and allow ranking of the hazard and risk of carbon NM according to the *weight of evidence*.

The multi-tier approach starts with a first stage of cytotoxicity assays (alamar blue, crystal violet, LDH assay). This rendered the effective concentration range of NM toxicity. The second tier is toxicogenomics. This provides information on the mode of action of carbon nanomaterials.

The third tier is variable depending on the results obtained in tier 2, but consists of functional validation of the toxicity mechanism. In the first work (Chapter 1), I tested carbon nanotubes-three different types in two different lengths-on human pleural mesothelial cells (MeT-5A) as a model for mesothelioma. After investigating the range of efficacy, we used toxicogenomics to identify the mechanism of action of CNTs

and also to classify their relative hazard in terms of similarity of molecular responses to that of crocidolite, a carcinogenic asbestos fiber. In the third step, we could confirm genomic instability emerging from Step 2 by the micronucleus frequency test. If toxicity analysis had been limited to Step 1, we would have lost any real ability to classify the hazardousness of materials. As a result of the expert's classification, it can be confirmed that NTX3 and NTX4 are more hazardous than NTX1 and that length reduction of nanofibers can attenuate their genotoxic effects. This is especially true for NTX4, the thinner fibers we tested, which have a large overlap with crocidolite. Length reduction prevented genotoxicity in two of the three cases studied, implying a lower risk of long-term toxicity. Additional statistical analysis of micronucleus data revealed that micronucleus formation was significantly higher in samples exposed to carbon fibers than amorphous carbon.

In the second work, thanks to a collaboration set up within the Nanogentools project, we looked at N-doped graphene exfoliated by current pulses. Here we used two cellular models, Met5A and C6 glioma cells, the latter as a proxy for cerebral astrocytes. We found that cellular responses to graphene can differ from each other. For example, external LDH release is completely absent in MET5A, whereas it is constitutive in C6. It is true that the absence of an effect on cellular viability suggests increased secretory activity rather than actual damage to cell membranes, yet the responses were very different. In both cases, there was no increase in micronucleation rate, indicating that there was no genotoxicity, which is an important consideration when evaluating potential long-term effects of materials.

Here we propose to always include ROS formation as an additional tier of investigation. It can be embedded in Tier 1 -cytotoxicity- or in any other position of the multi-level approach. This is probably the most important *initiating event* in the context of the Adverse Outcome Pathway (AOP) framework. An AOP depicts a coherent route to a disease, e.g. skin inflammation or lung fibrosis, from a triggering (initiating) event through a series of additional molecular events. ROS formation is linked to cancerogenesis and can be a hallmark of genotoxicity. In our study, the correlation between micronucleus frequency and ROS formation was clearly very evident, both in MeT5a cells, which have a bias for micronucleus, but also in C6 (which surprisingly responded to carbon nanotubes rather than CNT).

Indeed, the results of the first work highlighted a significant increase in ROS level in cells exposed to crocidolite, NTX1 (short), NTX3 and NTX4 long. These types of results suggest fibrous components trigger ROS formation and that size is not significant for ROS production. Based on these considerations, it could be argued that the combination -ROS formation + long fiber- is a dual characteristic associated with genotoxicity and thus with long-term effects. This leaves the exception of NTX1, which showed the opposite behavior, i.e., greater effects for short fiber, which will require further consideration.

Let's come back to Tier-2, toxicogenomics. RNA-seq high-throughput transcriptomics was fundamental to direct our attention to genotoxicity. Pathway analysis displayed several items related to DNA metabolism, DNA repair, p53, activation of ATR, etc. which is in agreement with genotoxicity. This kind of method to classify nanomaterials toxicity appeared to be faster and more reliable, and

allowed us to identify the risk from accidental or occupational exposure for carbon NMs, such as CNTs. On the other hand, while the lack of genotoxic damage in N-doped graphene exposed cells renders less uncertainty that N-doped graphene can pose a risk, indicating this can be a safer alternative in technological application. As regards the second objectives established in NANOGENTOOLS, -to improve the safe-by-design concept, I realized a carbon-based material functionalization with carboxylesterase enzyme to detoxify wastewater from pesticides. Three different carbon-based MNs were used (carbon black, CNTs, N-graphene) along with a biochar obtained from spent coffee grounds. We clearly showed that NMs outperformed biochar in many characteristics, from enzyme surface saturation to resistance to physicochemical stress (heat and pH), pesticide scavenging, etc. N-graphene often outperformed the other NMs, in particular in scavenging pesticides. Two different pesticides were used, a methyl carbamate (carbaryl) and an organo-phosphorus (dichlorvos). Besides the technological performance, N-graphene was also the least risky material. This evidence leads to select graphite exfoliated by current pulses N-doped graphene as a test bed for a biotechnological application of water clean-up from pesticide. We studied the role of carboxylesterase-functionalized N-graphene on survival of *Tetrahymena thermophila* from pesticide toxicity. *Tetrahymena thermophila*, a freshwater bioindicator, were exposed to two different pesticides at 10 or 5 times higher than the full lethal concentration of the two pesticides. The results are very promising since very short contact-time (1 min) of pesticide contaminated water with enzyme functionalized N-graphene could significantly protect *T. thermophila*

survival, and longer time (30 min) were 100% effective. Interestingly, we demonstrated that enzyme functionalization is responsible for pesticide toxicity scavenging in the case of dichlorvos exposure, while carbaryl seemed scavenged by bare N-graphene in a very similar fashion. This different response is mostly likely due to the different physicochemical property of the two pesticides, being dichlorvos very water soluble it does require enzyme catalysis to be scavenged. On the other hand carbaryl is hydrophobic enough to adsorb to N-graphene. As a future perspective, this applicative study will certainly require more investigation. In fact, it will be necessary to scale-up the readiness level of this application assessing more pesticide types, mixtures, real water effluents, and exploring the advantage of extremozymes with covalent functionalization for a longer durability.
In regards to toxicity assessment, future research should focus on a standardization of the multi-tier approach. A weight of evidence based on expert view should be changed to a fully systematic approach based on algorithm rules, in particular, for what concerns toxicogenomics, and hazard/risk classification using gene expression changes.

Conclusion

As a result of this research project, the objectives of the work were achieved to a good extent. Considering that carbon-based NMs have a great variability in terms of physicochemical properties, structure and functionalization, it becomes important to use an approach based on the use of different cell models and multi-level testing to evaluate hazard and risk of NMs. This study model used toxicogenomics, which could help define a new standard and guide to further in depth assessments. In the future, it will be necessary to define precisely the characterization of the materials and to adapt each test specifically to each single material. Adaptation of the test protocol was also necessary for our work due to the hyperreactivity of NMs. For the second goal, a safe application for carbon-based NMs, several steps are still needed in a future perspective, as mentioned before. First, the robustness of the functionalization has to be improved and then the application has to be actually deployable at a high technological readiness level.

List of publications

Lorusso, C., Calisi, A., Sarà, G., Dondero, F., 2022. In-Gel Assay to Evaluate Antioxidant Enzyme Response to Silver Nitrate and Silver Nanoparticles in Marine Bivalve Tissues. Applied sciences, 12, 2760.

Calisi, A., Lorusso, C., Gallego-Urrea, J. A., Hassellöv, M., & Dondero, F., 2021. Ecotoxicological effects of silver nanoparticles in marine mussels. Science of the total environment, 851,1581113.

Lorusso, C., Sanchez-Hernandez, J. C., Varodi, C., Pogăcean, F., Pruneanu, S., & Dondero, F. Carbon Nanomaterial Functionalization with Pesticide-Detoxifying Carboxylesterase Enzyme. Accepted for publication.